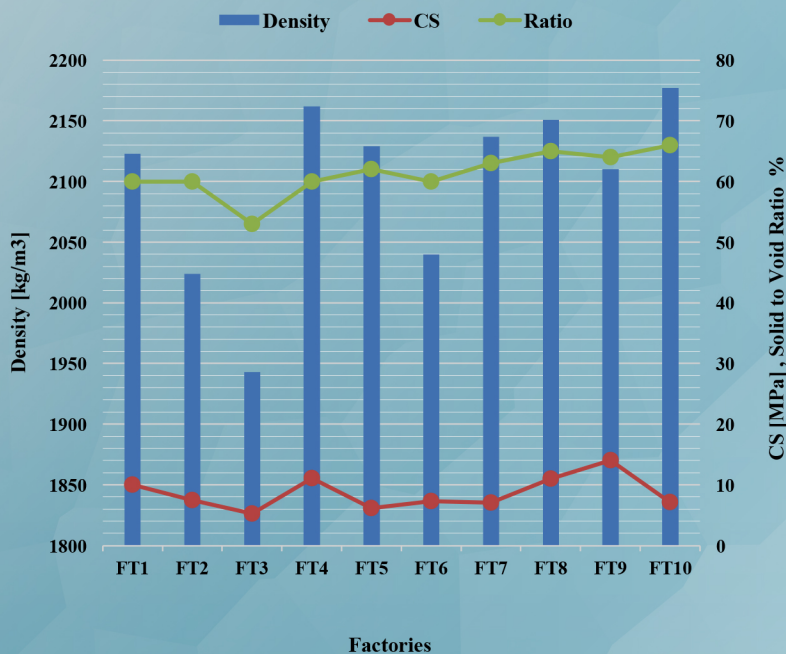


ARO

The Scientific Journal of Koya University



Issue Highlights

- ◊ Economical and Structural Feasibility of Concrete Cellular and Solid Blocks in Kurdistan Region
- ◊ Optical Design of Dilute Nitride Quantum Wells Vertical Cavity Semiconductor Optical Amplifiers for Communication Systems
- ◊ Male Rat Susceptibility for Liver and Kidney Injury
- ◊ The Plant Regulator Soaking Seeds and its Reflections on Growth and Yield Quality of Wheat
- ◊ Non-destructive Method of Leaf Area Estimation for Oleander (*Nerium oleander* L.) Cultivated in the Iraqi Kurdistan Region
- ◊ Taguchi Method for Investigating the Performance Parameters and Exergy of a Diesel Engine Using Four Types of Diesel Fuels
- ◊ Tissue-like P system for Segmentation of 2D Hexagonal Images
- ◊ Hemodynamic, Thyroid and Immunomodulatory Effects of Heroin in Rats

ARO-The Scientific Journal of Koya University

The Aro (“Today” in Hewramí Kurdish), is an international scientific journal published by the Koya University with p-ISSN: 2410-9355, e-ISSN: 2307-549X and DOI: 10.14500/2307-549X. Aro is a journal of original scientific research, global news, and commentary. The Aro Scientific Journal is a peer-reviewed, open access journal that publishes original research articles as well as review articles in all areas of Science.



Aro Executive Publisher

Dr. Wali M. Hamad; is the President of Koya University and the Executive Publisher of Aro.

Aro Editorial Board

The editorial board of Aro includes a five-member Senior Executive Editorial Board and a nine-member Associate Editorial Board that help in setting journal policy; a Board of Reviewing Editors consisting of more than 180 leading scientists.

Aro Editorial Group

Senior Executive Editors: Dilan M. Rostam, Shwan K. Rachid, Salah I. Yahya and Sarkawt S. Abdulrahman.

Associate Editors: Basim M. Fadhil, Fahmi F. Muhammad, Hamed M. Jassim, Husein A.H. Shekhbzainy, Iqbal M.G.Tahir, Saddon T. Ahmad, Taha J. Omar, Tara F. Tahir and Yazen A. Khaleel.

This issue reviewers: Abd Elmoniem A. Elzain, Akram O. Esmail, Bisan Alslibi, Fouad A. Mohammad, Gailan I. Hasan, Hawri O. Majeed, Hiwa Kh. Saeed, Ismail S. Kakey, Kawa A. Ali, Loay E. George, Nawroz A. Tahir, Omar Q. Aziz, Parekhan M.Abdulrahman, Sarkawt R. Hassan, Sarmad R. Kareem and Shaheen A. Mustafa.

Aro Editorial Web and New Media: Dilan M. Rostam and Salah I. Yahya

Secretarial Office of the Journal: Jwan T. Rawuf and Shakar H. Kareem

Journal Designer: Dashti A. Ali

Journal Copyeditor: Harith I. Turki

Journal Proofreader: Salah I. Yahya

Aro, the International journal of original scientific research and commentary is an online and published twice a year, as well, by Koya University. The published articles are free and online open access distributed under the Creative Commons Attribution License (CC BY-NC-SA 4.0: <https://creativecommons.org/licenses/by-nc-sa/4.0/>). Responsibility of the content rests upon the authors and not upon Aro or Koya University.

ARO the Scientific Journal Office

Koya University
University Park
Danielle Mitterrand Boulevard, Koya KOY45
Kurdistan Region - F.R. Iraq

Tel.: +964 (0) 748 0127423

Mobile: +964 (0) 7502257080

E-mail: aro.journal@koyauniversity.org

url: aro.koyauniversity.org

May - 2016 | Cozerdan - 2716

ARO

The Scientific Journal of Koya University

Vol IV, No 1(2016)

Contents

Aro Editorial Words	iii
Dilan M. Rostam and Taghreed K.M. Ali and Dawood S.S. Atrushi	01
Economical and Structural Feasibility of Concrete Cellular and Solid Blocks in Kurdistan Region	
Faten A. Chaqmaqchee	08
Optical Design of Dilute Nitride Quantum Wells Vertical Cavity Semiconductor Optical Amplifiers for Communication Systems	
Sarkawt H. Hamad, Karwan I. Othman, Karwan J. Hamad, Balkes H. Rasul, Shorsh M. Abdulla and Ismael A. Ismael	13
Male Rat Susceptibility for Liver and Kidney Injury	
Mohammed Q. Khursheed, Trifa Z. Saber and Tara M. Hassan	17
The Plant Regulator Soaking Seeds and its Reflections on Growth and Yield Quality of Wheat	
Ikbal M. Al-Barzinji and Barham M. Amin	22
Non-destructive Method of Leaf Area Estimation for Oleander (<i>Nerium oleander</i> L.) Cultivated in the Iraqi Kurdistan Region	
Dara K. Khidir and Soorkeu A. Atrooshi	27
Taguchi Method for Investigating the Performance Parameters and Exergy of a Diesel Engine Using Four Types of Diesel Fuels	
Rafaa I. Yahya, Siti Mariyam Shamsuddin, Shafaatunnur Hasan and Salah I. Yahya	35
Tissue-like P system for Segmentation of 2D Hexagonal Images	
Ismail M. Maulood	43
Hemodynamic, Thyroid and Immunomodulatory Effects of Heroin in Rats	
General Information	48
Guide to Author	49
Aro Reviewer/Associate Editor Application Form	51



Aro Editorial Words

Dear readers, you are holding the sixth issue (Vol IV, No 1) of Aro-The Scientific Journal of Koya University in your hand. With this issue Aro is starting a new era as the first ever internationally listed Scientific Journal in Kurdistan Region/Iraq history. Aro has been accepted for indexing in the Emerging Sources Citation Index (ESCI), a new edition of Web of Science™ as of Feb 2016. Content in this index is under consideration by Thomson Reuters to be accepted in the Science Citation Index Expanded™ (SCIE). This is a great achievement that we share with our academic communities. Aro is starting its fourth year journey in leading the quality of regional scientific publications with global impact. The editorial team is determined to keep the path of such a mission and sustain the future publications of Aro with quality and reliability in mind.

Despite the continuous financial crises which has had a great impact on scientific research and particularly universities in our region, Aro is lasting to receive good numbers of well-motivated quality papers that shows its steadily growing trust among researchers in the region. With increasing demands by volume of submission, The Associate Editorial of Aro has grown larger, well dedicated and our meetings are richer. Our colleagues with great passion are contributing to the long-term visions of Aro.

Aro was created with long-term visions to become accessible to all researchers in Kurdistan and beyond, covering a wide range of scholarly disciplines in sciences. The focus of the journal is to reflect that of Koya University, namely promoting scientific knowledge and research in Kurdistan and secure a brighter future in education with global representation. Aro aspires to become a channel for exchanging scholarly research by establishing academic connections between scholars globally.

Aro is a journal of original scientific research, global news, review paper, letters and commentary. The Aro Scientific Journal is a peer-reviewed, open access journal that publishes original research articles as well as review articles in areas of natural sciences and technology. In this issue you will have access to genuine research paper in variety of areas such as; Petroleum, Physics, Chemical Engineering, biochemistry, engineering and material.

The warm response from researchers, academics and professionals in the last four years has made us to create a wider Editorial Board which serves the wider submitted scientific manuscripts. However, it is clear that to have a dedicated and well organized editorial board for the journal is only one side of the coin. The other is the ability to attract submissions of quality research and scholarly work. We are thankful to all of those who put their trust in Aro and presented their original research work for publication in Vol IV, No 1 of the journal, as well as, our thanks are extended to the 16 peer-reviewers from the Universities worldwide for their efforts in reviewing and enabling this issue of Aro.

Your support and feedback are invited and appreciated.

Dilan M. Rostam
Editor-in-Chief

Wali M Hamad
Executive Publisher

Dilan M. Rostam, Shwan K. Rachid, Salah I. Yahya, Sarkawt S. Abdulrahman
Executive Editorial Board

Economical and Structural Feasibility of Concrete Cellular and Solid Blocks in Kurdistan Region

Dilan M. Rostam¹, Taghreed K.M. Ali¹ and Dawood S.S. Atrushi²

¹Department of Architectural Engineering, Koya University
Daniel Mitterrand Boulevard, Koya KOY45 AB64, Kurdistan Region – F.R. Iraq

²Department of Civil Engineering, Duhok University
Zaxo Street 38, 1006AJ, Duhok, Kurdistan Region – F.R. Iraq

Abstract—Cellular concrete blocks are the major building materials in Kurdistan Region in Iraq. This study is carried out to check the economical and structural feasibility. The integrity of the blocks as well as its industrial production process compared with local and international standards. Recommendations for the concrete block production have been given in this paper. Samples from 10 local factories of total 60 blocks have been collected and tested at Koya University Laboratory. The carried out tests covered the dimensions, compression strength and water absorption of the samples. The results of this research study were compared with the requirements of the Iraqi and European specifications. They showed that the products of all factories do not fulfil the specified requirements. The dimensions of specimens exhibited relatively high deviations with no recommended tolerances for dimensions of the blocks. The results analysis showed that the weight of the 400x200x200mm block size was about 20-23 kg and the size of the represented voids was about 60% of the volume. This study made some regulatory recommendations to standardise the concrete block production in the region.

Index Terms—Building standard codes, cellular concrete block, eurocode, structural feasibility.

I. INTRODUCTION

“Concrete is one of the most basic building blocks of modern life that most people take for granted” (Neville, 1996). Historical records show that concrete mortar as a building product was used by the Romans as early as 200 B.C. to erect

stone walls in the construction of buildings. By fall of the Romans Empire in 5th century much of the learned concrete technology was lost. It was not until 1824 that the English stonemason Joseph Aspdin developed Portland cement, which became a major component of today's concrete products (GOI, 2012).

To In 1890 the first hollow concrete block was designed by Harmon S. Palmer in the United States. After 10 years of experimenting, Palmer patented the design in 1900. Palmer's blocks were produced in $203 \times 254 \times 762 \text{ mm}^3$. The blocks were so heavy they had to be lifted with a small crane (Hornbostel, 1991). “By 1905, an estimated 1,500 companies were manufacturing concrete blocks in the United States. These early blocks were usually cast by hand, and the average output was about 10 blocks per person per hour. Today, concrete block manufacturing is a highly automated process that can produce up to 2,000 blocks per hour” (Cavette, 2007).

The Kurdistan Region in Iraq has been going through a rapid building boom since 2004. Due to geopolitical situation of the region commercial building materials have largely been limited to concrete products in particular concrete blocks. The use of concrete blocks is found suitable in region where other building elements are costly, and not available (Barbosa, et al., 2010). These blocks are being widely used in construction of residential, factories and multi-storied buildings (see Fig. 1). Despite these facts, the composite strength of hollow and cellular block concrete block masonry still represents a real challenge in the region.

In general the concrete blocks as precast masonry units such as Hollow and Solid normal and lightweight concrete blocks of different sizes are used for erecting walls in various conditions. Depending upon the structural requirements of masonry unit, concrete mixtures are prepared using components available locally or most economical distance (Chandra and Bhise, 1994).

ARO-The Scientific Journal of Koya University
Volume IV, No 1(2016), Article ID: ARO.10113, 07 pages
DOI: 10.14500/aro.10113

Received 23 November 2015; Accepted 07 January 2016

Regular research paper: Published 08 February 2016

Corresponding author's e-mail: dilan.rostam@koyauniversity.org

Copyright © 2016 Dilan M. Rostam, Taghreed K.M. Ali and Dawood S.S. Atrushi. This is an open access article distributed under the Creative Commons Attribution License.





Fig. 1. Concrete structure erected with diaphragm Cellular Concrete Block (Photo by Authors)

The most common concrete block type in Kurdistan Region is Cellular block In-line Void type. “Cellular blocks are masonry units that contain one or more formed voids that do not fully penetrate the block. The selection of cellular blocks can have significant advantages over solid blocks where weight is a prime consideration. The reduced unit weight makes for ease of handling, reduced floor/foundation loading, economic and efficient productivity. The Cellular blocks do not require special laying techniques and can be laid on a full bed of standard or general purpose mortar for most applications” (CBA, 2007).

In Kurdistan region the cellular blocks are used also as a replacement for solid blocks. According to the UK based Concrete Block Association (CBA) by selecting the correct specification, cellular blocks can be used in the following common applications (CBA, 2007): Infill in framed structures, providing improved insulation as the inner leaf to external cavity walls, Outer leaves of cavity walls when protected e.g. render, tiling etc., Single leaf external walls when protected e.g. render, tiling etc., Internal partitions, and sound separating walls when supported by acoustic test evidence

In the regional building market there are several face sizes (length \times width \times height) of $400 \times 200 \times 200 \text{ mm}^3$, $400 \times 200 \times 150 \text{ mm}^3$ and $300 \times 300 \times 300 \text{ mm}^3$ cellular aggregate concrete blocks are available. These are the most common sizes used in construction of domestic dwellings. CBA specifies that based on the UK industrial standards, cellular blocks are normally available in compressive strengths from 2.90 MPa to 22.50 MPa. Common strengths are 3.60 MPa and 7.30 MPa (CBA, 2008).

This study examined product of 10 different local factories which supply the region with concrete cellular blocks. The specimens were tested and analysed against available standards, where some practical recommendations have been provided accordingly.

II. MAKING OF CONCRETE BLOCK

Most people who work with blocks probably don't give much thought to how it is produced. Koski (1992) emphasised that people's main concerns are that the block's colour and dimensions are uniform, and that it meets other appropriate specifications (Koski, 1992). Basic knowledge across the

industry needed to understand that concrete mixture can be turned into precast masonry elements such as different type of concrete blocks of suitable sizes which are used for load and non-load bearing units for masonry walls. The concrete mix used for normal hollow and solid blocks shall not be richer than one part by volume of cement to 6 parts by volume of combined room dry aggregates before mixing (Kaushal, 2011). Normal weight blocks are made with cement, sand, gravel, crushed stone and air-cooled slag.

The old Iraqi specification standard (ISS) from 1987 gives directions on how to produce the concrete blocks. ISS was created based on American Society for Testing and Materials (ASTM) Specification of materials Part 16 of year 1986, the British Specification (BS) No. 1364 and No. 2028 of year 1968 and Japanese specification A No. 5406 of year 1976. The load-bearing concrete masonry units part of ISS covers resolutions for Dimensions, Categories and Physical requirements in details. The requirements provide instructions for class (A) block as general use in the internal or external walls which are exposed to moisture or climate changes under or above ground level with variation of any dimension must be no more than $\pm 3 \text{ mm}$. The physical requirements of cellular concrete blocks with an extraction of average value provided for solid and hollow blocks recommended as a minimum compressive strength of 10 N/mm^2 and maximum water absorption of 12.5%, (Siram, 2012). It is also advised that concrete blocks must not be used before 14 days of their production. Factories which failed complying with these ISS recommendations were fined and their product were removed from the market (ISS, 1987). However, since the release of ISS in 1987 Iraq has gone through two wars and ongoing sectarian war therefore follows up regulation has not been a priority for the market in this country.

The study of this paper required collection of specimens from local concrete production factories. None of the visited factories applied any standard regulations for their production but rules of thumbs. In general at the visited factories they put cement in vertical silos, the sand and gravel are placed nearby as fill (No-stock). Then, they put gravel, sand, cement and water in conic mobile mixing to mix. The quantity of material is measured by using spade and naked eyes. The water for the mixture is added based on pure thumb rules without any measurements. The quantity of water is depending on the temperature at the mixing time. Finally, the mobile mixing is driven to the location of casting.

The casting of the cellular blocks includes following stages, a) placing the molds on a clean plane ground, b) putting the concrete mixture in the molds, and c) compacting the mixture the steel sticks unit, which is available in the mobile mixing machine. The number of compaction blows is determined manually. Immediately the molds are removed and the process is repeated. The curing is started when all castings are completed. The curing process is done directly by using water sprinkle machine. The curing is continued for three days and then, concrete blocks are stored for immediate delivery to the building sites.

III. SPECIMENS

To conduct this research study 60 specimens from 10 different local factories were collected and transferred to laboratory for testing, see Fig 2. All specimens were measured for length, width and height, as well as minimum thickness of face, shells and webs. These blocks were tested for water absorption, block density and compressive strength.



Fig. 2. Factory site where specimens have been taken (Photo: Authors)

The specimens were tested within 72 hours after delivery to the laboratory, where they were kept under laboratory temperature and humidity. For the purpose of this study the specimens were all aged for 28 days and cured normally. All factories have given their consent to anonymously use their specimens for the purpose of this study. All data related to the specimens are available by request for future studies.

A. The Blocks' Density

The dimensions of each block were measured in millimetre and the overall volume calculated in cubic meters. The blocks were then weighted in kilograms to the nearest 10 gm. The density of each block is calculated as follows:

$$\text{Density} = \text{Mass of block} / \text{Solid Vol of block} \quad (1)$$

where; the density is measured in $[\text{kg}/\text{m}^3]$, mass in $[\text{kg}]$, solid volume in $[\text{m}^3]$.

The blocks of all factories have dry density more than recommended $2000 \text{ kg}/\text{m}^3$ (ISS, 1987), where the maximum dry density was $2483 \text{ kg}/\text{m}^3$, see Fig 3 for more details.

The recommendation by standard specifications suggests an allowed tolerance on the declared density value of $\pm 10\%$ but closer tolerances may be declared on both gross and net density (CBA, 2008). The gross density of aggregate concrete masonry units ranges from about $1700 \text{ kg}/\text{m}^3$ to $2400 \text{ kg}/\text{m}^3$. According to modern building standard codes such as Eurocode EN 772-13 manufacturers are required to provide data relevant to the density of their products, which allow for

calculation of dead load forces, sound insulation or thermal performance and the surface mass of a given section of masonry can be determined (DeVekey, 2001).

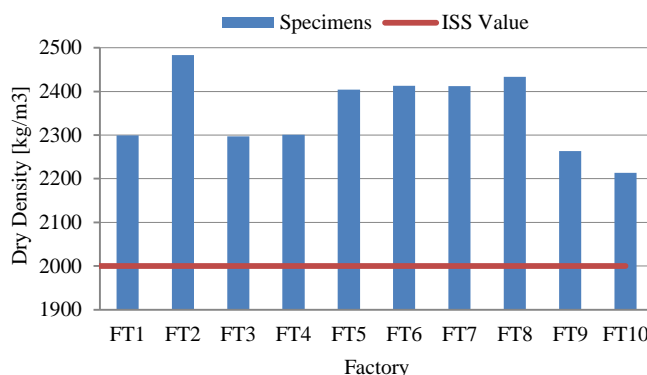


Fig. 3. Dry density of the blocks for different factories

The solid to void ratio of tested specimens indicated 10% to 12% below 75% recommended ratio by ISS as illustrated in Fig 4. This means that the amount of mixture used to produce these blocks are lower than recommended ISS guidelines.

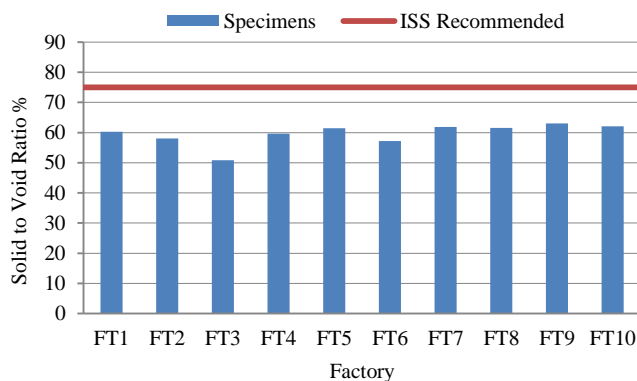


Fig. 4. Solid to void ratio of the blocks for different factories.

B. The Blocks' Water Absorption

It is recommended by CBA to consider water absorption only in the case of CBA units with no applied finishing (CBA, 2008). Most of the units tested in this study are used with applied finishing but this does not take place immediately. However, based on recommendations from CBA, the specimens were tested for water absorption level. The water absorption calculates as $\text{Water Absorption \%} = (A - B) / B * 100$, where (A) is wet mass of unit in kg and (B) dry mass of unit in kg (Kaushal, 2011). The collected specimens from factories were proven to have water absorption level less than 12.5%, a maximum recommended level for water absorption by ISS which is indicated in Fig 5. The Sieve Analysis of specimens revealed that the use of good grading quality of sand and gravel which is available locally to these factories causing lower water absorption level. Also, it is

widely believed that curing conditions can greatly affect the water absorption of concrete. Based on the curing conditions Zang (2014) stated that the concrete which was exposed to air curing exhibited low water absorption. (Zhang and Zong, 2014).

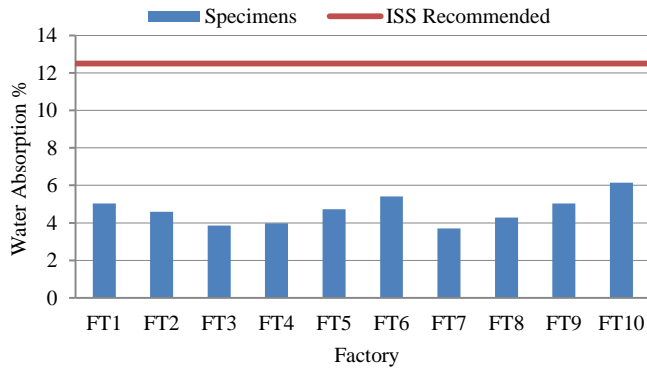


Fig. 5. Water absorption of the blocks for different factories.

C. Testing Procedure

The comprehensive testing process was carried out in the Laboratory of Civil and Structural Engineering at Koya University. Specimens were tested with the centroid of their bearing surfaces aligned vertically with the centre of thrust of the spherically seated steel bearing blocks of the testing machine, see Fig 6. The load up to one-half of the expected maximum load was applied at any convenient rate, after which the control of the machine was adjusted as required to give a uniform rate of travel of the moving head such that the remaining load was applied about two minutes.



Fig. 6. The Compression Testing Machine (CTM) (Photo: Authors)

The compressive strength of the concrete blocks units were measured by Compression Testing Machine (CTM) as the maximum load in Newton divided by the gross cross sectional area of the unit in square millimetres which is the total area occupied by a block on its bedding face, including areas of the cavities and end recesses. It is round up to the nearest 0.1 N/mm² for each tested specimen and then an average value is

calculated for 6 blocks from the same factory.

The following graph shows the average value of compressive strength of 6 blocks from each examined factory. The distributed value shows that most of the strength are over the minimum acceptable on average 10 MPa based on Iraqi specifications (CBA, 2008). The specification gives standard values for solid and hollow concrete blocks. For this study we have taken an average advised values for class A of Solid and Hollow Concrete blocks as a reference value for compressive strength of Cellular Concrete Blocks. Just 4 out of 10 factories satisfied ISS requirements, which mean more than half of factories failed to satisfy ISS as indicated Fig 7.

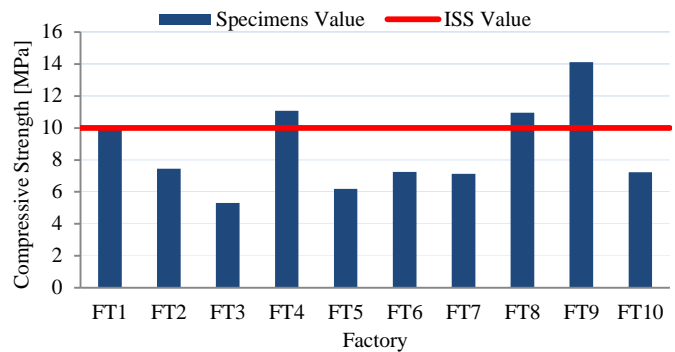


Fig. 7. Compressive strength of the blocks for different factories.

The average compressive strength of only four factories (FT1, FT4, FT8 and FT9) are satisfactory as compared with ISS guidelines. Fig. 8 shows that the lower limit of the average compressive strength is much lower than the minimum value recommended by ISS of 10 MPa (ISS, 1987). The combo graph of Fig. 8 clearly shows that the mixture proportion of the concrete block is irregular in various factories. They use more sand and gravel with higher density than cement, which leads to lower compressive strength and higher density with less solid material (Sturgeon, 2013). By mixing the right quantities of various sizes of gravel and sand and appropriate degree of compaction it is possible to achieve a dense and strong concrete (Johannessen, 2008).

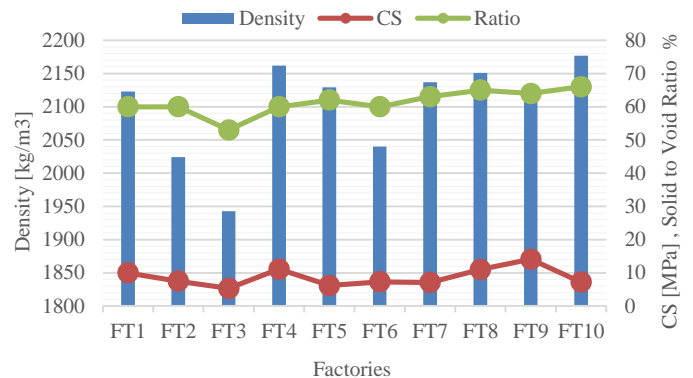


Fig. 8. Relational comparison among compressive strength, solid ratio and density of specimens.

Fig. 9 and Fig. 10 show the length, width and height of blocks for different factories. The actual measurement of tested specimens indicates huge variations in sizes compared with recommended values by ISS. Nevertheless, the latest recommendation by Eurocode BS EN 771-3 gives tolerance of +3, -5mm on all dimensions for all classes of concrete blocks (CBA, 2008).

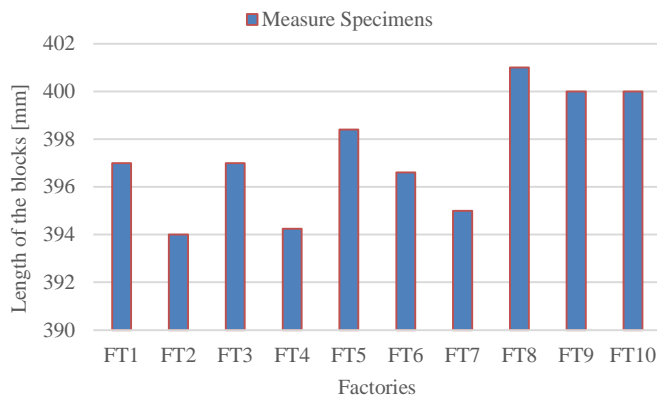


Fig. 9. Length of the blocks for different factories.

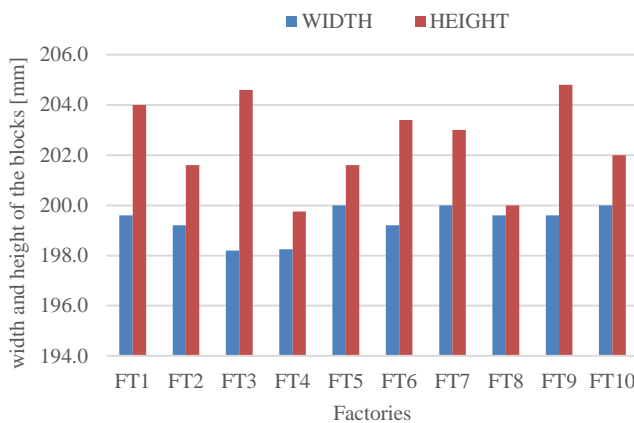


Fig. 10. Width and Height of the blocks for different factories.

IV. ECONOMIC FEASIBILITY

Stability, resistance, serviceability, durability and economic feasibility of structure are the primary requirements for market evaluation of any building project. In fact, the best viable construction is the one which shows an optimise balance among these primary factors. The comparative research studies have been the focus of finding an optimum way of selecting various concrete blocks or bricks for erecting the building. Ahmad and et al., (2014) in their research study claimed that the compressive strength of hollow concrete block masonry wall was lower than brick masonry wall but block masonry is economical than brick masonry (Ahmad et al., 2014).

The building materials' market in Kurdistan region has been

limited to few units such as concrete blocks, Bricks, and stones. The cost of using these building materials is measured by production and transportation costs as well as time used to erecting the building. A market survey of price, availability of craftsmen and locality of these materials show that cellular blocks are most popular amongst consumers, see Table I.

TABLE I
ESTIMATE MARKET VALUE OF COMPARABLE BUILDING MATERIALS

Material	Cellular Block	Brick	Natural Stone
Weight {kg/m ³ }	2110	1890	2900
Price {per m ² }	\$48	\$96	\$143
Craftsmen {Cost/m ² }	\$20	\$28	\$55
Craftsmen availability	Common	Moderate	Rare

The building construction market is booming by first time homeowners and private investors (Duhoki, 2015, pers. comm., 3 Sep). Both categories are trying to build with least costs. In the lack of effective building regulators the market is dominated with irregular building practices which make cellular concrete block as a fast and least costly erecting building material an attractive product in the market of Kurdistan Region. The traditional craftsmanship for erecting natural stone wall is very rare and normally hired from East Kurdistan says Faruk a local traditional builder from Tewelle Town (Dawood, 2015, pers. comm., 8 Oct).

V. RESULT ANALYSIS

This research study shows that most of the blocks produced by the local factories are non-bearing blocks and are used to build internal and external walls of buildings.

There are clear issues with standard dimensions of all tested blocks especially in the height of the blocks. This will create issues during application process, such as erecting walls. Normally the blocks are casted on uneven unprepared industrial ground in open space which results in uneven bases for the blocks; therefore there will be need for more mortar during erection of the walls. However the curing of the concrete blocks in the factory remains an issue which was observed during collection of the specimens. Curing is the process of maintaining satisfactory moisture content and a favourable temperature in the blocks to ensure hydration of the cement and development of optimum strength (CCI, 2011) something which was ignored in all visited factories.

Lack of proper industrial production expertise by factories has led to series of shortcoming in relevant to former Iraqi Standard ISS of 1987 and modern international standards such as Eurocode. This study has shown shortcomings in density, dimensions, mixtures and comprehensive strength, as well as nonstandard production methods which all related to lack of knowledge, expertise, quality checks, and market responsibilities and accountability.

VI. STUDY RECOMMENDATIONS

This study is conducted on the basis of information and operation available in the production of concrete blocks market and factories. The aim is to provide information to the prospective investors and consumers of regional concrete block factories. It is advised that prior to making a firm decision for investment in the project the investors must verify the various feasibility aspects together along with the requirements relevant to industrial standard of concrete masonry unit production. This needs to become a legal framework for the procurement of plant and machinery and raw materials before they establish a factory.

This is the first research study on cellular concrete blocks conducted in the region. The study shows that none of the monitored factories actually undergone any training or industrial regulatory monitoring system. Their products do not follow any known standards and the product mixtures are prepared using rules of thumbs and trial and error process. None of the factories indicated unannounced visits to collect random sampling of block from their plants. Regulating the concrete block manufacturer via standard production method, quality control, and imposed national building standard building code can promote the following objectives:

1. Increasing the quality of building products.
2. Reducing the cost and waste of materials.
3. Increasing structural safety.
4. Increasing the chances of producing and marketing.
5. Increasing the life space of building.

In the visited factories, the blocks were in open air and not kept in shelters from sun and drying winds therefore the curing process were not controlled. Normally it is recommended that after 24 hours the blocks watered and kept damp for several days to allow the cement to hydrate completely (Steven et al., 2003). The longer the curing process the better is the strength. The blocks should thereafter be completely dried prior delivery to the market for application.

This study strongly recommends the implementation of Eurocode in general and Eurocode 6 (Pluijm, 2009) in particular to regulate the concert block market in the region. Guidelines such as Aggregate Concrete Blocks, A Guide to Selection & Specification (CBA, 2007) are simply available to standardise the production method and ensure the stability, resistance, serviceability, durability and economic feasibility of structure based on long global experience and well-studied standards. All factories need to provide full product description that follows the recommended standard for production process (Collins, 2015). To maintain the validity of regulations in line with changes and developments in the field of industry and science, these recommended national standards will be revised when necessary. A professional and governmental entity needs to ensure that manufacturers have valid professional certificates before they are permitted to operate in the market.

VII. CONCLUSIONS

Laboratory tests using cellular concrete blocks permitted to adequately characterise the block specific market value

properties by specimen testing. Tests on these blocks indicate that the non-standard production methods are associated with irregular market and lack of education and specific requirements to establish and operate concrete block production factories. This paper has made a series of recommendations to tackle the shortcomings and regulate the market in section VI.

This paper concluded that three aspects should be monitored to ensure quality masonry units namely strength, dimensions and water absorption. Ideally, blocks should be regularly tested for strength and mixes and production processes modified if necessary. This needs to randomly be observed and quality checked for safety and improvement of building construction materials which consequently raise the quality and structural safety in the construction industry of the region.

ACKNOWLEDGMENT

We would like to thank all the factories which allowed us to carry on with our laboratory test using their products. We also thank lab assistance at the Faculty of Engineering who facilitated the testing procedures.

REFERENCES

- Ahmad, R., Malik, M.I., Jan, M.U., Ahmad, P., Seth, H. and Ahmad, J., 2014. Brick Masonry and Hollow Concrete Block Masonry – A Comparative Study, *International Journal of Civil and Structural Engineering Research (IJCSER)*, 1(1), pp.14-21.
- Barbosa, C., Lourenço, P. and Hanai, J., 2010. On the compressive strength prediction for concrete masonry prisms. *Materials and Structures*, 43(3), pp.331-344.
- Cavette, C., 2007. *How concrete block is made - material, manufacture, used, components, structure, steps, machine*. [Online] Available at: <http://www.madehow.com/Volume-3/Concrete-Block.html> [Accessed 17 Nov. 2015].
- CBA UK, 2007. *Aggregate Concrete Blocks, A Guide to Selection & Specification; Cellular Blocks, Concrete Block Association*, [online] Available at: <http://www.thakeham.co.uk/images/upload/docum/Block%20Selector.pdf> [Accessed 2 Nov. 2015].
- CBA UK, 2008. Understanding BS EN 771-3: *Aggregate concrete masonry units*, [online] Available at: <http://www.cba-blocks.org.uk/downloads/CBA%20Understanding%20EN%20771%202009.pdf> [Accessed 17 Nov. 2015].
- CCI, 2011. *How to make concrete bricks and blocks, midrand, South Africa*, [online] Available at: http://www.afrisam.co.za/media/13734/how_to_make_concrete_bricks_and_blocks.pdf [Accessed 20 Sep. 2015].
- Chandra, D. and Bhise, N., 1994. *Solid concrete block masonry scheme. Roorkee*, India: Central Building Research Institute, [online] Available at: <http://krc.cbri.res.in/dspace/bitstream/123456789/264/1/BRN69.pdf> [Accessed 17 Nov. 2015].
- Collins, M., 2015. *Concrete Technology & Construction, The Concrete Society*, [online] ict.concrete.org.uk. Available at: <http://ict.concrete.org.uk/exams/qualifications.asp> [Accessed 17 Nov. 2015].
- DeVekey, R.C., 2001. Bricks, blocks and masonry made from aggregate concrete: performance requirements, BRE Centre for Whole Life Construction and Conservation, BRE Digest 460 Part 1.

GOI (Government of India), 2012. Techno economic feasibility report on concrete hollow & solid block, Building Materials and Technology Promotion

- Council Ministry of Housing & Urban Poverty Alleviation Government of India, New Delhi
- Hornbostel, C., 1991. *Construction Materials*, 2nd Edition, John Wiley and Sons, Inc.
- Iraqi Standard Specification (ISS), 1987. ISS No. 1077, Load-Bearing Concrete Masonry Units,
- Johannessen, B., 2008. *Building rural roads*, chapter 12, 1st ed., Bangkok, Thailand: ILO.
- Kishore, E.K., 2011. *Testing of Concrete Blocks*. [Online] Available at: <http://www.engineeringcivil.com/testing-of-concrete-blocks.html> [Accessed 2 Nov. 2015].
- Koski, J.A., 1992. *How Concrete Block Are Made*, Masonry Construction, pp.374-377.
- Kosmatka, S.H., Kerkhoff, B., and Panarese, W.C., 2003. *Design and control of concrete mixtures EB001*, 14 edn., Skokie, Illinois, USA: Portland Cement Association.
- Neville, A.M., 1996. *Properties of Concrete*. (4th ed.). England: Wiley.
- Pluijm, R.V.D., 2009. EUROCODE 6 Design of masonry structures, Dissemination of information for training – Brussels, 2-3 April 2009 [online] Available at: http://eurocodes.jrc.ec.europa.eu/doc/WS2009/2_6_Pluijm.pdf [Accessed 17 Aug. 2015].
- Siram, K.K.B., 2012. Cellular Lightweight Concrete Blocks as a Replacement of Burnt Clay Bricks, *International Journal of Engineering and Advanced Technology (IJEAT)*, ISSN: 2249–8958, 2(2).
- Sturgeon, G., 2013. *Metric Technical Manual*. 16th ed. [ebook] CCMPA, Region 6 of the National Concrete Masonry Association, p.Chapter 4. Available at: <http://www.ccmpa.ca/wp-content/uploads/2012/02/Final2013Sec4.pdf> [Accessed 1 Jul. 2015].
- Zhang, S. and Zong, L., 2014. Evaluation of Relationship between Water Absorption and Durability of Concrete Materials. *Advances in Materials Science and Engineering*, 2014, pp.1-8.

Optical Design of Dilute Nitride Quantum Wells Vertical Cavity Semiconductor Optical Amplifiers for Communication Systems

Faten A. Chaqmaqchee

Department of Physics, Faculty of Science and Health, Koya University
Daniel Mitterrand Boulevard, Koya KOY45, Kurdistan Region – F.R. Iraq

Abstract—III-V semiconductors components such as Gallium Arsenic (GaAs), Indium Antimony (InSb), Aluminum Arsenic (AlAs) and Indium Arsenic (InAs) have high carrier mobilities and direct energy gaps. This is making them indispensable for today's optoelectronic devices such as semiconductor lasers and optical amplifiers at 1.3 μm wavelength operation. In fact, these elements are led to the invention of the Gallium Indium Nitride Arsenic (GaInNAs), where the lattice is matched to GaAs for such applications. This article is aimed to design dilute nitride GaInNAs quantum wells (QWs) enclosed between top and bottom of Aluminum (Gallium) Arsenic Al(Ga)As distributed Bragg mirrors (DBRs) using MATLAB® program. Vertical cavity semiconductor optical amplifiers (VCSOAs) structures are based on Fabry Perot (FP) method to design optical gain and bandwidth gain to be operated in reflection and transmission modes. The optical model gives access to the contact layer of epitaxial structure and the reflectivity for successive radiative modes, their lasing thresholds, emission wavelengths and optical field distributions in the laser cavity.

Index Terms—Amplifier, Al(Ga)As, gain, GaInNAs, VCSEA.

I. INTRODUCTION

Dilute nitride III-V alloys are essential for today's optoelectronic devices applications, such as lasers modulators, photodetectors and optical fibre communication systems. One potentially important material for such applications is the quaternary alloy GaInNAs (Kondow, et al. 1996; Buyanova, Chen and Monemar 2001). GaInNAs/GaAs quantum well (QW) based devices were originally proposed as replacements for GaInAs/InP QW based devices due to their reduced temperature sensitivity (Sun, et al., 2009). GaInNAs may be grown on GaAs, allowing the use of high quality

Al(Ga)As/GaAs distributed Bragg reflectors (DBRs) for the long wavelength optical communications window. GaInNAs have potential cost advantages compared to indium phosphide (InP)-based approaches. It can be used to fabricate several devices, such as high performance laser diodes among which are vertical cavity surface emitting lasers (VCSELs) emitting in 1.3 μm window. The massive interest in VCSEL devices has focused on semiconductor optical amplifier (SOA) based VCSEL technology. Vertical cavity semiconductor optical amplifiers (VCSOAs) are important components in optical fiber networks. These devices have advantages over edge emitting lasers (EEL) and in plane- semiconductor optical amplifiers (SOAs) of various amplifier lengths. The vertical cavity geometry for such devices yields high coupling efficiency to optical fiber, which is useful for achieving a low noise figure with better performance. It also allows for single wavelength amplification, and two dimensional array fabrication; hence lowering the power consumption and manufacturing cost. The narrower bandwidth of the vertical cavity structures makes the devices also good for filtering applications (Piprek, Björilin and Bowers, 2001).

GaInNAs material has attracted attention by virtue of its unusual physical properties compared to conventional III-V compounds. By adding small amounts of nitrogen and Indium to GaAs, the whole wavelength range between 1.3 μm and 1.6 μm is reachable in principle. However as this material system has been explored the unique nature of the nitrogen (N) interaction with the GaInAs system has become apparent. This arises because the nitrogen is very electronegative and pushing the conduction band energy down as modeled successfully by the band anti-crossing (BAC) model (Shan, et al., 1999). When small amounts of nitrogen are introduced into (In)GaAs, a strong interaction occurs between the conduction band and a narrow resonant band formed by the highly localized nitrogen states E_N , as shown clearly in Fig.1 The nitrogen level is treated as a perturbation on the host material conduction band E_M ; the effect of this is a splitting of the conduction band into two non-parabolic subbands, E_+ and E_- . The E_- is pushed downwards relative to E_M level, while the E_+ is pushed upwards relative to E_N level. The reduction in the energy of the E_- level is responsible for the observed decrease in emission energy (Skierbiszewski, et al., 2000).

ARO-The Scientific Journal of Koya University
Volume IV, No 1(2016), Article ID: ARO.10076, 05 pages
DOI: 10.14500/aro.10076

Received 29 March 2015; Accepted 02 March 2016

Regular research paper: Published 06 April 2016

Correspond. author's e-mail: faten.chaqmaqchee@koyauniversity.org

Copyright © 2016 Faten A. Chaqmaqchee. This is an open access article distributed under the Creative Commons Attribution License.



The mathematical expression for the upper and lower conduction subbands in the BAC approach can be expressed by the following determinant (Shan, et al., 2000):

$$\begin{vmatrix} E_N - E(k) & V_{MN} \\ V_{MN} & E_M - E(k) \end{vmatrix} = 0 \quad (1)$$

The matrix element V_{MN} is dependent on the nitrogen concentration with fraction y using following expression:

$$V_{MN} = C_{MN}\sqrt{y} \quad (2)$$

where C_{MN} is the coupling parameter that illustrates the combination between conduction bands and valance bands of extended heavy hole (HH) states, light hole (LH) states, and spin-orbit split-off (SO) states, respectively (Lindsay and O'Reilly, 1999).

$$E_{\mp}(k) = \frac{1}{2} \left(E_N + E_M(k) \mp \sqrt{(E_N - E_M(k))^2 + 4V_{MN}^2} \right) \quad (3)$$

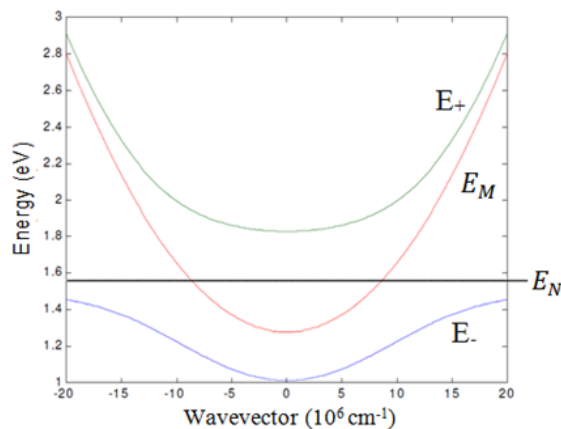


Fig. 1. Schematic of the band structure of GaInNAs, using the BAC model. The splitting of the conduction band into E_- and E_+ bands is clearly shown (Aissat, et al. 2007).

In this article, the cavity of VCSCOA device consists of multi quantum wells (MQWs) distributed equally in three stacks forming a cavity of $3\lambda/2n_c$ long. Holes and electrons are injected through the un-doped top and bottom mirrors, respectively, pass through the QWs, recombine and generate photons. The reflectivities of the top and the bottom DBR mirrors VCSCOA are designed using Fabry Perot models. The model includes optical gain and amplifier bandwidth in both reflection and transmission modes.

II. MATERIAL AND METHOD

VCSCOAs can be operated in reflection and transmission modes, depending on the reflectivity from the DBR mirrors.

The reflected and transmitted light can be determined by applying the boundary conditions to Maxwell's equation of electromagnetism. The active region of GaInNAs/GaAs is enclosed between two dielectric mirrors of front and back reflectivities. Electrons and holes are injected into the active region uniformly through the surface of the confinement layers.

VCSCOA designs need to fit a large number of QWs into more than two stacks to achieve a high gain that is matched to the standing wave pattern in the cavity. However, incorporating a large number of QWs makes it difficult to achieve uniform carrier distribution by using electrical injection, where the gain in QWs is no longer homogenous. The QWs should be pumped as close to full inversion as possible, in order to achieve the lowest noise figure. The standing wave effect (gain enhancement) increases with decreased number of QWs per standing wave peak. When the spacer layers are doped as in an electrically pumped device, there will be a trade-off between gain enhancement and absorption loss. If higher gain is desired, the maximum number of QWs is limited by the pumping process and it is difficult to pump uniformly using electrical injection. Accordingly, the amplification process takes place in an active region.

Gain models have been used to determine the gain spectra, which is based on the Fabry-Perot (FP) for gain calculations. The signal intensity gain of a VCSCOA in reflection mode G_r and transmission mode G_t can be considered as a total of the reflection on the top DBR and the reflected part from the cavity (Adems, Collins and Henning, 1985).

$$G_r = \frac{(\sqrt{R_t} - \sqrt{R_b}g_s)^2 + 4\sqrt{R_t R_b}g_s \sin^2 \theta_s}{(1 - \sqrt{R_t R_b}g_s)^2 + 4\sqrt{R_t R_b}g_s \sin^2 \theta_s} \quad (4)$$

$$G_t = \frac{(1 - R_t)(1 - R_b)g_s}{(1 - \sqrt{R_t R_b}g_s)^2 + 4\sqrt{R_t R_b}g_s \sin^2 \theta_s} \quad (5)$$

Where, R_t is the reflectivity of the top DBR mirror, R_b is the reflectivity of the bottom DBR mirror, and g_s is the single pass gain. As mentioned before, DBRs can be calculated using the transfer matrix method, but can be also simulated as a fixed mirror positioned from the boundary with the incident medium and having effective reflectivity (Coldren and Corzime, 1995) of:

$$R_{DBR} = R_{t,b} = \left(\frac{1 - qp^{N-1}a}{1 + qp^{N-1}a} \right)^2 \quad (6)$$

where $q = \frac{n_{low}}{n_{high}}$, $p = \frac{n_{low}}{n_{high}}$, and $a = \frac{n_{low}E}{n_{high}E}$ are low and high refractive index ratios at the incident, internal and exit interfaces.

The gain is limited by either the lasing action or by the maximum material gain available. The gain of a reflection-format VCSCOA and the resonance θ_s (Björlin, Kimura and Bowers, 2003) are given by:

$$G_R = \frac{(\sqrt{R_t} - \sqrt{R_b}g_s)^2}{(1 - \sqrt{R_t R_b}g_s)^2} \quad (7)$$

$$\phi_s = 2\pi n_c L_c \left(\frac{1}{\lambda} - \frac{1}{\lambda_R} \right) \quad (8)$$

Where ϕ_s , n_c , L_c , are the single pass phase detuning, the refractive index of the optical cavity and the total cavity length, respectively. λ , λ_R are a signal wavelength and the resonant wavelength of the cavity.

The single pass gain in a VC SOA can be calculated from the active region of material gain g using:

$$g_s = \exp[\xi g L_a - \alpha_i L_c] \quad (9)$$

where L_a , α_i , ξ are referred to as the thickness of the QWs, the average cavity loss coefficient and the gain enhancement factor, respectively. In our calculation we assume that the single pass gain g_s is varying from $(R_b)^{-0.5}$ to $(R_f R_b)^{-0.5}$, in which the laser threshold is reached when $(R_f R_b)^{-0.5} = 1$.

The optical gain depends on the QW carrier density (N), the signal wavelength (λ), the temperature (T), and the photon density (S), at room temperature and low photon densities. The QW material gain g can be approximated by (Coldren and Corzine, 1995).

$$g = g_0 \ln \left[\frac{N + N_s}{N_{tr} + N_s} \right] \quad (10)$$

where g_0 , N_{tr} and N_s are the gain coefficient, the carrier density concentration at transparency and the fitting parameters, respectively.

The gain bandwidth can also describe the amplifier. The gain bandwidth in reflection and transmission mode is restricted by the line width of the Fabry-Perot modes and can be obtained by (Piprek, Björlin and Bowers, 2001).

$$\Delta f_R = \frac{c}{\pi n_c L_c} \times \arcsin \left\{ 4\sqrt{R_f R_b} G_s \left[(1 - \sqrt{R_f R_b} G_s)^{-2} - 2(\sqrt{R_f} - \sqrt{R_b} G_s)^{-2} \right]^{-1/2} \right\} \quad (11)$$

$$\Delta f_T =$$

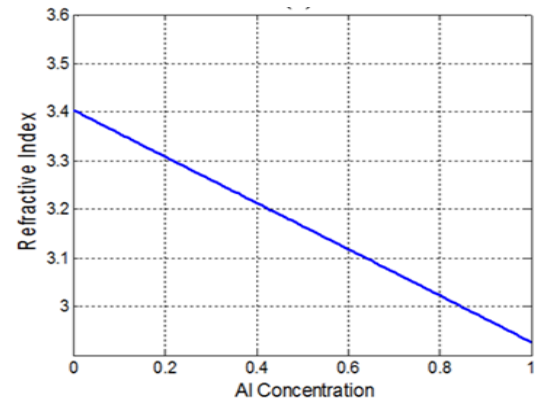
$$\frac{c}{\pi n_c L_c} \times \arcsin \left\{ (4\sqrt{R_f R_b} G_s)^{-1} \times (1 - \sqrt{R_f R_b} G_s)^2 \right\}^{1/2} \quad (12)$$

where R_f and R_b are referred to in-front and back reflectivities in both reflection and transmission modes, respectively.

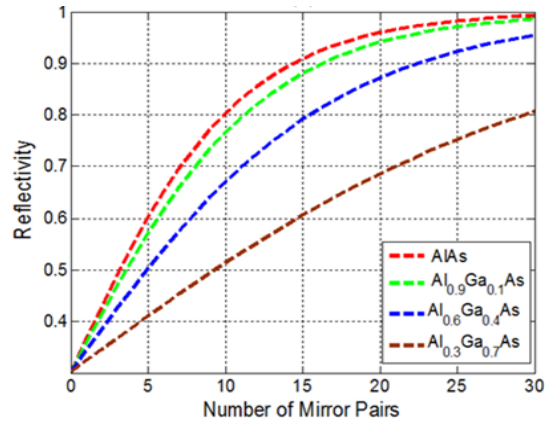
III. RESULTS AND DISCUSSION

There is a useful simulation steps used to design the structure of VC SOA at 1.3 μm wavelength. A comprehensive model of a VC SOA includes the optical model and the optical gain. In this article, an optical design relies on the determination of the epitaxial layer contrast, layer thickness and the reflectivity dependence upon wavelength. The

refractive index versus aluminum (Al) concentration for $\text{Al}_x\text{Ga}_{1-x}\text{As}$ mirrors and the influence of the index contrast ratio are given in Fig. 2-a and Fig. 2-b. It is clear with high index contrast ratio, only a small number of pairs are required to achieve a given reflectivity. The peak reflectivity depends on the number of quarter wavelength layers, the refractive indices of the incident and exit media, and the high and low refractive index materials. Increasing the number of DBR layers increases the mirror reflectivity, while increasing the refractive index contrast between the materials in DBRs increases both reflectivity and the bandwidth. Thus, Bragg Reflectivities have significant consequence on the amplifier results including gain, amplifier bandwidth, figure noise and saturation output power.



(a)



(b)

Fig. 2. Distributed Bragg Reflector illustrates: (a) the reflective index versus different Al concentration for $\text{Al}_x\text{Ga}_{1-x}\text{As}$ mirrors, and (b) the influence of the refractive index contrast ratio.

Fig. 3 shows the front mirror versus bottom mirror reflectivities as a function of single pass gain G_s . The lines indicated to the lasing threshold, where the lowest excitation level is dominated by stimulated emission rather than by spontaneous emission. Below threshold, the laser's output power increases slowly with increasing excitation. A VC SOA is required to operate below threshold according to the

equation of $G_s\sqrt{R_f}\sqrt{R_b} < 1$ to avoid lasing. The small G_s requires relatively high Bragg mirror reflectivities to increase the total signal gain.

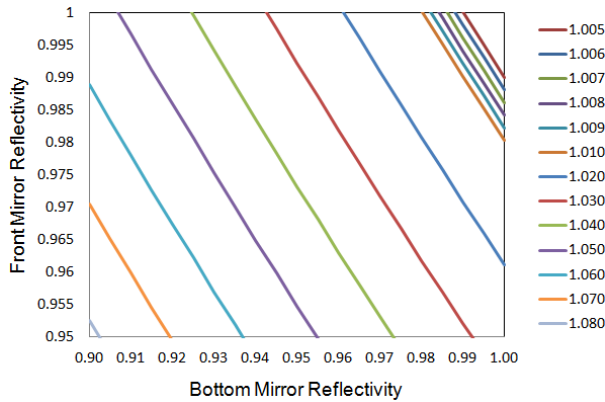


Fig. 3. The lasing threshold lines, in which the amplifier needs to operate at $G_s\sqrt{R_f}\sqrt{R_b} < 1$ to avoid lasing.

The relation between material gain and carrier density is calculated by MATLAB® program as illustrated in Fig. 4. To show general trends using an established model, material gain value can be estimated according to the parameter approximation (Lanurand, et al., 2005) using (10). The material gain has a logarithmic tendency but it is almost linear below and above the carrier transparency of $1.18 \times 10^{18} \text{ cm}^{-3}$ and $6.4 \times 10^{18} \text{ cm}^{-3}$, respectively.

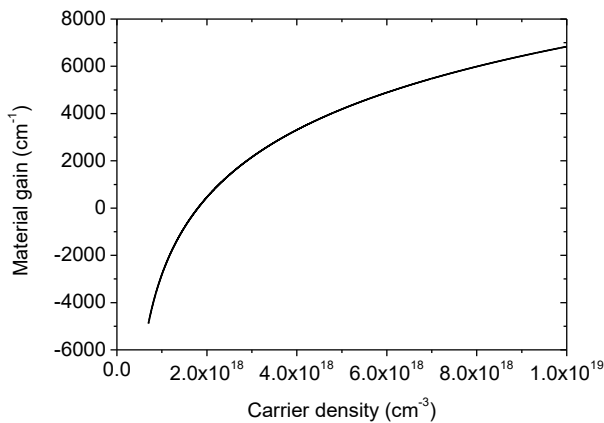


Fig. 4. Material gain versus carrier density curve for GaInNAs/GaAs QW active region.

In order to show the gain effect of the VCSEA, (4) and (5) can be used to calculate the peak gain. The peak gain of the device (or chip) depends on three parameters of the top mirrors, the bottom mirrors and the single pass gains. Fig.5 and Fig.6 presents the gain spectra in reflection and transmission modes using different single pass gains. By increasing the gain spectrum, the VCSEA bandwidth is became narrower for signal amplifying optical filter.

To illustrate the relation between VCSEA gain and its bandwidth, (4) and (5) were used to obtain the gain bandwidth using different top Bragg mirrors. The equation is mainly restricted by the line-width of the Fabry-Perot modes and it used to understand the amplifier properties of the VCSEA device in reflection mode. In high reflectivities, a net gain is demonstrated where the device start lasing, while in low reflectivities, a higher carrier density and wider gain amplifier bandwidth is obtained. However if the reflectivity is too low, there will not be enough signal pass gain. The amplifier gain bandwidth is usually measured from the optical width of the gain spectrum at the full-width half-maximum (FWHM). Amplifier bandwidth versus peak reflection gain for 24-period bottom mirrors and various top mirrors reflectivities are shown in Fig. 7 It's clear from the figure that the amplifier bandwidth in reflection mode decreases as the peak reflection gain increases. The higher reflectivity allows for high gain and lower amplifier bandwidth. The small bandwidths are advantageous for optical filter to reduce the signal noise, while the larger bandwidths are desirable for devices used in applications with multiple channels.

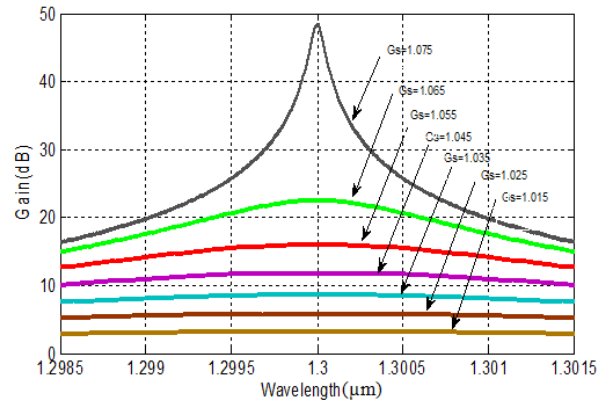


Fig. 5. Reflection VCSEA gains spectra for different G_s value, where $R_f = 0.867\%$, $R_b = 0.997\%$ and $L_c = 3\lambda/2nc$.

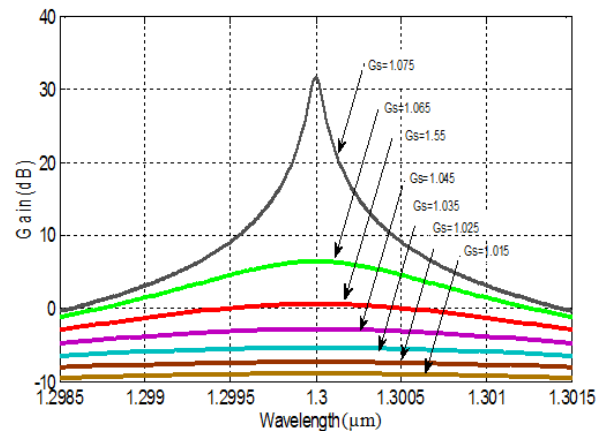


Fig. 6. Transmission VCSEA gains spectra for different G_s value, where $R_f = 0.867\%$, $R_b = 0.997\%$ and $L_c = 3\lambda/2nc$.

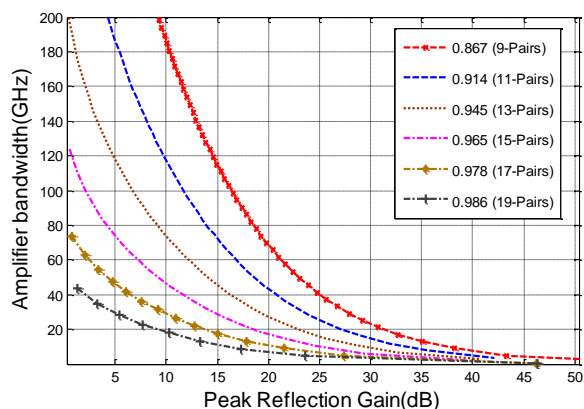


Fig. 7. Amplifier bandwidth in reflection mode versus peak reflection gain for 0.997 (24-Pairs bottom mirror) and top mirror's reflectivity for different numbers of pairs.

IV. CONCLUSION

In conclusions, vertical cavity semiconductor optical amplifiers VCISOAs based GaInNAs/GaAs quantum wells have been designed using MATLAB® program. Device analyses are based on the theory of the Fabry-Perot semiconductor optical amplifier (SOA). VCISOAs are usually made by sandwiching a thin layer of high optical gain between two epitaxial growths of distributed Bragg mirrors (DBRs). Once the correct composition of material is selected for operating at 1.3 μm emission wavelength, the design is moved to the Bragg mirrors with different Al composition and into dilute nitride QWs in an active region. In VCISOAs, mirror with high reflectivity are necessary to reduce the resonant cavity losses and to achieve stimulated emission process. In VCISOAs, the decreased top mirror reflectivity allows for the higher pump power to achieve a higher saturation output power without losing gain.

ACKNOWLEDGMENT

F.A.I. Chaqmaqchee is gratefully acknowledges the financial support of the ministry of higher education and scientific

research in Baghdad/Iraq during her study at University of Essex in UK.

REFERENCES

- Adams, M.J., Collins, J.V. and Henning, I.D., 1985. Analysis of semiconductor laser optical amplifiers. *IEE Proc. J.*, 132(1), pp.58-63.
- Aissat, A., Nacer, S., El-Bey, M., Guessoum, A., Ferdjani, K., Berkani, D. and Vilcot, J.P., 2007. The effect of nitrogen on the energy gap of a structure with strained quantum well containing GaInNAs/GaAs. *Iranian J. of Elect. and Comp. Eng.*, 6(2), pp.169-161.
- Buyanova, I.A., Chen, W.M. and Monemar, B., 2001. Electronic properties of Ga(In)NAs alloys. *MRS Internet J. Nitride Semicond. Res.*, 6(2), pp.2.
- Björlin, E.S., Kimura, T. and Bowers, J.E., 2003. Carrier-confined vertical cavity semiconductor optical amplifiers for higher gain and efficiency. *IEEE J. Select. Topics Quant. Elect.*, 9(5), pp.1374-1385.
- Coldren, L.A., Corzine, S.W. 1995. Diode lasers and photonic integrated circuits, *NY: Wiley, New York*.
- Kondow, M., Uomi, K., Niwa, A., Kitatani, T., Watahiki, S. and Yazawa, Y., 1996. GaInNAs: A novel material for long-wavelength-range laser diodes with excellent high-temperature performance. *Jpn. J. Appl. Phys.*, 35(1), pp.1273-1275.
- Laurand, N., Calvez, S., Dawson, M.D., Bryce, A.C., Jouhti, T., Konttinen, J. and Pessa, M., 2005. Performance comparison of GaInNAs vertical cavity semiconductor optical amplifiers. *IEEE J. Quant. Elect.*, 41(5), pp.642-649.
- Lindsay, A. and O'Reilly, E.P., 1999. Theory of enhanced bandgap non parabolicity in $\text{GaN}_x\text{As}_{1-x}$ and related alloys. *Solid State Communication*. 112(8), pp.443-447.
- Piprek, J., Björlin, E.S. and Bowers, J.E., 2001. Design and analysis of vertical-cavity semiconductor optical amplifiers. *IEEE J. Quant. Elect.*, 37(1), pp.127-134.
- Piprek, J., Björlin, E.S. and Bowers, J.E., 2001. Optical gain-bandwidth product of vertical cavity laser amplifiers. *Elect. Letts.*, 37(5), pp.298-299.
- Shan, W., Walukiewicz, W., Ager, J.W., Haller, E.E., Geisz, J.F., Friedman, D.J., Olson J.M. and Kurtz, S.R., 1999. Band anticrossing in GaInNAs alloys. *Phys. Rev. Lett.*, 82(6), pp.1221.
- Skierbiszewski, C., Perlin, P., Wiśniewski, P., Knap, W., Suski, T., Walukiewicz, W., Shan, W., Yu, K.M., Ager, J.W., Haller, E.E., Geisz, J.F. and Olson, J.M., 2000. Large, nitrogen-induced increase of the electron effective mass in $\text{In}_y\text{Ga}_{1-y}\text{N}_x\text{As}_{1-x}$. *Appl. Phys. Lett.* 76(17), pp.2409-2411.
- Sun, Y., Balkan, N., Erol, A. and Arikian, M.C., 2009. Electronic transport in n- and p-type modulation-doped GaInNAs/GaAs quantum wells. *Microelect. J.*, 40(30), pp.403-405.

Male Rat Susceptibility for Liver and Kidney Injury

Sarkawt H. Hamad¹, Karwan I. Othman², Karwan J. Hamad¹, Balkes H. Rasul¹,
Shorsh M. Abdulla¹ and Ismael A. Ismael¹

¹Department of Biology, Faculty of Science, Soran University
Kurdistan Region - F.R. Iraq

²Ashti Hospital, Soran, Erbil, Ministry of Health, Kurdistan Region - F.R. Iraq

Abstract—The experimental study of this paper was designed to investigate male rat susceptibility to liver injury. A combination of two experimental animal models (Lead acetate for tissue injury (80 mg/L) and castration) had been used on twenty male rats, they were divided into two groups sham ($n = 10$); castrated ($n = 10$). Results revealed that; liver weight reduced significantly ($P < 0.05$) in sham group in comparison with castrated rats, but kidney weight changed slightly. Also, serum aminotransferase (AST) was significantly higher in sham versus castrated rats. Neither alanine aminotransferase (ALT) and alkaline phosphatase (ALP) nor malondialdehyde (MDA) changed. In conclusion, the absence of male sex hormone would delay tissue injury of male rat organs especially liver organ.

Index Terms—Alanine aminotransferase, liver injury, testosterone.

I. INTRODUCTION

Lead acetate is widely used in experimental animals for pathophysiological studies (Venkareddy and Muralidhara, 2015), because it plays an important role in hepatotoxicity and lipid peroxidation (Sharma, et al., 2015). Castration is a process involves removing male tests (Fan, et al., 2014), and Lead acetate causes liver injury, a combination between them generates changes in liver and kidney weights, lipid peroxidation, and liver enzymatic activity.

Although, liver is the site of production most of the antioxidant enzymes and purifies body from all toxins and body waste substances (Shymans'kyi, et al., 2014), kidney also has a crucial role in purification and regulation of body fluid balance (Gueutin, et al., 2013), their size and weight of organs

are reflection of their physiological actions, a minor change of them is taken in medical consideration. Either an increase or decrease in anatomy and physiology of liver and kidneys produce problem for the whole body (Block, et al., 2015; Vilar-Gomez, et al., 2015).

On the other hand, lipid such as cholesterol is a precursor for many steroidal hormones such as testosterone, which contributes in male sex organ development and liver cell proliferation (Kelly, et al., 2014). Also, lipid reacts with free radicals to produce lipid peroxide (Perez-Rodriguez, et al., 2015); malondialdehyde is a byproduct lipid oxidation, usually it is used to detect free radical injury indirectly through reaction with thiobarbituric acid, commonly named TBA-MDA reaction (Papastergiadis, et al., 2012).

Measurement of serum liver enzymatic activity changes, called liver function tests (LFT) includes (AST), (ALT), and (ALP) (Mikolasevic, et al., 2015), their concentration in the plasma fluctuate in proportion to physiological events of liver and heart, either in normal or in abnormal situations (Naik, et al., 2011). Therefore, in most experimental animal models especially inducing liver injury, the LFT is the well-known parameter to measure activity of liver enzyme (Wang, et al., 2008).

The fluctuation of hormonal concentration has negative consequences on the liver tissue architecture, lipid oxidation, and enzymatic activity (Naik, et al., 2011; Kelly, et al., 2014; Pertsov, et al., 2014), but until now the reason behind male vulnerability to liver injury is not fully understood. So the present study was designed to investigate mysterious effects of male sex hormone on liver and kidney damage, by using a combination animal model, lead acetate to produce organ injury and castration to inhibit testosterone effects on the body.

ARO-The Scientific Journal of Koya University
Volume IV, No 1(2016), Article ID: ARO.10087, 04 pages
DOI: 10.14500/aro.10087

Received 14 May 2015; Accepted 01 September 2015

Regular research paper: Published 06 April 2016

Corresponding author's e-mail: sarkawt.hamad@soran.edu.iq

Copyright © 2016 Sarkawt H. Hamad, Karwan I. Othman, Karwan J. Hamad, Balkes H. Rasul, Shorsh M. Abdulla and Ismael A. Ismael. This is an open access article distributed under the Creative Commons Attribution License.



II. MATERIALS AND METHODS

A. Animals

The present study was conducted in the animal house of Biology department, Faculty of Science, Soran University; under supervision and approval of local scientific committee and animal care rules. Twenty male albino rats their body weights rang between (250 - 370) gram were used, each five

in one plastic cage with free access for standard rat diet, the house temperature about 25 ± 2 °C and 12/12 hour photoperiod dark and light cycle.

B. Experimental Design

An experiment was designed to investigate that, whether male rats are more sensitive to liver and kidney damage. Animals were divide into two groups, each group contain 10 rats as follow;

Group sham (Not castrated) their scrotum opened and sewed without touching the tests and given lead acetated (Spain) 80 mg/L distal water (D.W) by drinking for 15 days.

Group castrated their testes removed surgically and given lead acetate 80 mg/L D.W by drinking for 15 days.

C. Castration

Rat were anaesthetized by injection a mixture of Ketamine hydrochloride (80 mg/Kg) and Xylazine (12 mg/Kg) intraperitoneally; a small incision (1 – 2 cm) was done on the frontal aspect of scrotum, then testes pulled out gently without bleeding, near abdomen the blood vessels and ducts tightly ligated by absorbable suture (DemTech, England), then after cutting the testes sterilized with Hibitane (5%), and scrotum sewed by Nylon mono filament; all steps were performed for sham group without touching the testes.

D. Blood Sample Collection, Liver and Kidney Organ Weight

Under anaesthetized condition by (Ketamine) (80 mg/Kg)/ Xylazine (12 mg/Kg), the blood was taken (8 – 10 mL) by cardiac puncture, and transferred into gel tube (Fl medical, Italy), left standing for 30 minutes, then centrifuged at 2000 rpm /15 minutes, the sera were stored in 3 eppedrof tubes at – 20 °C till the assay day. The skin and abdominal muscle were removed, then immediately both kidneys and liver had been cut and weighted.

E. Liver Function Tests

Serum levels of liver enzymes (AST, ALT, and ALP) were measured by automated chemical analyzer (BioTech, Uk).

F. Determination of MDA

Serum concentration MDA was determined according to TBA-MDA method; 0.150 μ L added into clean glass test tube, then 1 ml thiobarbituric acid (TBA) (0.66%) and trichloroacetic acid (TCA) (17%) were added respectively, after boiling at 95 °C for 45 minutes another 1 mL TCA (70%) would be added; cooled and centrifuged at 2000 rpm for 15 minutes; and the supernatant was read at 532 nm.

G. Statistical Analysis

Statistical Package for Social Science (SPSS) version 16 was used for analysis of data. Results were expressed as Mean \pm Standard error. Student t-Test was applied to compare between groups. Figures had been drawn by GraphPad Prism software.

III. RESULTS

This study showed that, giving lead acetate (80 mg/L)

through drinking, for fifteen days could decrease significantly ($P < 0.05$) liver weight of sham group in comparison with castrated rats (Fig. 1).

While, the toxic effect of lead acetate reduced the right kidney weight (3.890 ± 0.077) gram in sham group as compared castrated group, but was none statistically significant ($P > 0.05$) consideration. The left kidney weight (3.766 ± 0.075) none significantly diminished in sham versus castrated group (3.858 ± 0.099) (Table I).

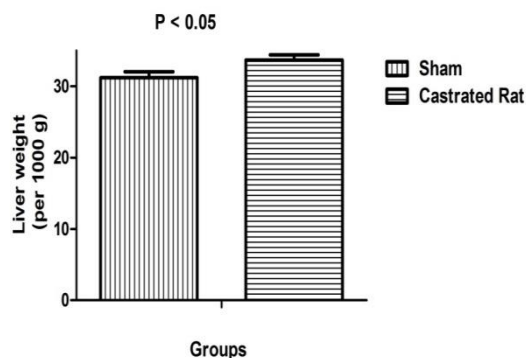


Fig. 1. Liver weight of male rat treated by lead acetate (80 mg/L).

Parameters	Groups		(P Value)
	Sham	Castrated Rat	
Right kidney weight (Per 1000 gram)	3.890 ± 0.077	3.977 ± 0.115	0.540
Left kidney weight (Per 1000 gram)	3.766 ± 0.075	3.858 ± 0.099	0.476

Sham; Rat's with intact testes, castrated rat; Rat's without testes

Furthermore, the serum level of AST was measured by automated chemical analyzer instrument; it showed that, there was significant ($P < 0.05$) increased in AST as compared to castrated groups (Fig. 2). Whereas, minor in ATL and ALP level, it means that, neither ATL (64.42 ± 10.70) nor ALP (873.8 ± 90.09) concentration in both groups significantly different (Table II).

On the other hand, serum MDA determination would helpful to identified liver injury, but despite harmful effects of lead as a model to liver injury there was not significant ($P > 0.05$) changes between castrated rats (14.34 ± 0.548) and sham rats (15.08 ± 0.229) (Table II).

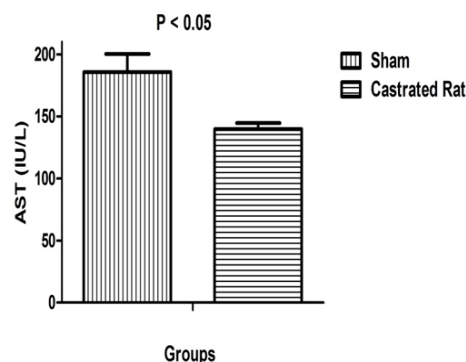


Fig. 2. Serum AST (IU/L) of male rat as treated by lead acetate.

TABLE II
SERUM ALT, ALP, AND MDA OF MALE RAT AS TREATED BY LEAD
ACETATE

Parameters	Groups		(P Value)
	Sham	Castrated Rat	
ALT (IU/L)	64.42 ± 10.70	62.66 ± 4.862	0.786
ALP (IU/L)	873.8 ± 90.09	752.1 ± 32.00	0.232
MDA (µ/L)	14.34 ± 0.548	15.08 ± 0.229	0.243

Sham; rat's with intact testes, castrated rat; rat's without testes

IV. DISCUSSION

The two experimental animal models have been used to investigate male vulnerability for liver injury. Lead acetate administration through drinking water would produce whole body injury, specifically liver and kidney (Waseem, et al., 2014), also castration is surgical procedure to block androgen hormones, diminishing their concentration inside body fluids such as blood plasma (Duran-Pasten, et al., 2013). The present study tries to explain the role of androgens (Testosterone) in enhancement of many physiological processes in liver and kidney injury, such serum enzymatic activities, and lipid peroxidation.

The weight of liver fallen ($P < 0.05$) in the sham rats (Fig. 1), while the kidney weight did not decreased significantly according to castrated animals (Table I). Many mechanisms contributes in that phenomenon such as, the testosterone hormone stimulate and enhance liver injury (Hoedebecke, et al., 2013). Much more levels of androgen signaling, reflected by higher testosterone levels may associated with the risen risk of many hepatic disease (Yu, et al., 2000). The induces toxic hepatitis testosterone's character, also may lead to reduce liver weight and enhances liver cell damage (Timcheh-Hariri, et al., 2012). Beside male sex hormones which has typical effects on liver tissue, administration of high dose of testosterone caused increase kidney tissue damage and kidney weight fallen (Rostami, et al., 2014), but it needs sufficient time, for that reason kidney weight not decrease significantly in sham group, as induces organ injury by lead acetate (Table I).

The activity of AST in castrated rats is significantly ($P < 0.05$) lower than sham (Fig. 2). Neither ALT nor ALP was decreased significantly (Table I). Consideration of enzyme activity in this investigation, due to testosterone dose dependent risk effects on liver organ, such as enhancing liver fibrosis (Vieira, et al., 2008), "hepatocellular necrosis instead of intrahepatic cholestasis" (Stimac, et al., 2002), androgenic hepatotoxicity includes "genetic cholestatic syndromes" (El Sherrif, et al., 2013), and the varieties physiological action of androgen hormones effects on the body, through wide spread of their receptors on the organ tissues (Coss, et al., 2012).

Furthermore, TBA-MDA showed that there was not significant ($P > 0.05$) variation between castrated and uncastrated rats (Table II). When, there was obvious relation or interactions between Leydic cell testosterone production and increasing oxidative stress (Chen, et al., 2015). Believed that, this free radical proportional effect on testicular cells and risen lipid peroxidation dependent on time, because the time to produce tissue injury was short, it was 15 days.

V. CONCLUSION

It was clearly demonstrated that, the availability of testosterone would lead to increase liver injury; also the vulnerability of male to liver disease was time dependent, beside that kidney injury was delayed for harmful substance.

ACKNOWLEDGMENT

We appreciate laboratory manager of Ashti hospital (Mr. Fakhri) for his patience and support, while we were worked with his staff. We thank Mr. Ardalan Ali Nabi for his gift (Lead acetate).

REFERENCES

- Block, D.B., Mesquita, F.F., de Lima, I.P., Boer, P.A. and Gontijo, J.A., 2015. Fetal kidney programming by maternal smoking exposure: Effects on kidney structure, blood pressure and urinary sodium excretion in adult offspring. *Nephron*, 129(4), pp.283-392.
- Chen, H., Jin, S., Guo, J., Kombairaju, P., Biswal, S. and Zirkin, B.R., 2015. Knockout of the transcription factor Nrf2: Effects on testosterone production by aging mouse Leydig cells. *Mol Cell Endocrinol*, 409, pp.113-120.
- Coss, C.C., Bauler, M., Narayanan, R., Miller, D.D. and Dalton, J.T., 2012. Alanine aminotransferase regulation by androgens in non-hepatic tissues. *Pharm Res*, 29, pp.1046-1056.
- Duran-Pasten, M.L., Fiordeliso-Coll, T. and Hernandez-Cruz, A., 2013. Castration-induced modifications of GnRH-elicited [Ca²⁺]_i signaling patterns in male mouse pituitary gonadotrophs in situ: studies in the acute pituitary slice preparation. *Biol Reprod*, 88(2), pp.32.
- El Sherrif, Y., Potts, J.R., Howard, M.R., Barnardo, A., Cairns, S., Knisely, A.S. and Verma, S., 2013. Hepatotoxicity from anabolic androgenic steroids marketed as dietary supplements: contribution from ATP8B1/ABCB11 mutations?. *Liver Int*, 33(8), pp.1266-1270.
- Fan, S., Hao, Z.Y., Zhang, L., Chen, X.G., Zhou, J., Zang, Y.F., Tai, S. and Liang, C.Z., 2014. Increased chromogranin A and neuron-specific enolase in rats with chronic nonbacterial prostatitis induced by 17-beta estradiol combined with castration. *Int J Clin Exp Pathol*, 7(7), pp.3992-3999.
- Gueutin, V., Vallet M, Jayat M, Peti-Peterdi J, Corniere N, Leviel F, Sohet F, Wagner CA, Eladari D, Chambrey R, 2013. Renal beta-intercalated cells maintain body fluid and electrolyte balance. *J Clin Invest*, 123, pp.4219-4231.
- Hoedebecke, K., Rerucha, C., Maxwell, K. and Butler, J., 2013. Drug-induced liver injury secondary to testosterone prohormone dietary supplement use. *J Spec Oper Med*, 13(4), pp.1-5.
- Kelly, D.M., Nettleship, J.E., Akhtar, S., Muraleedharan, V., Sellers, D.J., Brooke, J.C., McLaren, D.S., Channer, K.S. and Jones, T.H., 2014. Testosterone suppresses the expression of regulatory enzymes of fatty acid synthesis and protects against hepatic steatosis in cholesterol-fed androgen deficient mice. *Life Sci*, 109(2), pp.95-103.
- Mikolasevic, I., Orlic, L., Zaputovic, L., Racki, S., Cubranic, Z., Anic, K., Devcic, B. and Stimac, D., 2015. Usefulness of liver test and controlled attenuation parameter in detection of nonalcoholic fatty liver disease in patients with chronic renal failure and coronary heart disease. *Wien Klin Wochenschr*, 127(11), pp.451-458.
- Naik, S.R., Thakare, V.N. and Patil, S.R., 2011. Protective effect of curcumin on experimentally induced inflammation, hepatotoxicity and cardiotoxicity in rats: evidence of its antioxidant property. *Exp Toxicol Pathol*, 63(5), pp.419-431.
- Papastergiadis, A., Mubiru, E., Van Langenhove, H. and De Meulenaer, B., 2012. Malondialdehyde measurement in oxidized foods: evaluation of the spectrophotometric thiobarbituric acid reactive substances (TBARS) test in various foods. *J Agric Food Chem*, 60(38), pp.9589-9594.

- Perez-Rodriguez, L., Romero-Haro, A.A., Sternalski, A., Muriel, J., Mougeot, F., Gil, D. and Alonso-Alvarez, C., 2015. Measuring oxidative stress: the confounding effect of lipid concentration in measures of lipid peroxidation. *Physiol Biochem Zool*, 88(3), pp.345-351.
- Pertsov, S.S., Koplik, E.V., Kalinichenko, L.S. and Alekseeva, IV, 2014. Effect of melatonin on lipid peroxidation in the blood of rats with various behavioral characteristics during acute emotional stress]. *Ross Fiziol Zh Im I M Sechenova*, 100(6), pp.759-766.
- Rostami, B., Nematbakhsh, M., Pezeshki, Z., Talebi, A., Sharifi, M.R., Moslemi, F., Eshraghi-Jazi, F. and Ashrafi, F., 2014. Effect of testosterone on Cisplatin-induced nephrotoxicity in surgically castrated rats. *Nephrourol Mon*, 6(5), pp.7.
- Sharma, S., Raghuvanshi, S., Jaswal, A., Shrivastava, S. and Shukla, S., 2015. Lead acetate-induced hepatotoxicity in wistar rats: possible protective role of combination therapy. *J Environ Pathol Toxicol Oncol*, 34(1), pp.23-34.
- Shymans'kyi, I.O., Khomenko, A.V., Lisakovs'ka, O.O., Labudzyns'kyi, D.O., Apukhovs'ka, L.I. and Velykyi, M.M., 2014. The ROS-generating and antioxidant systems in the liver of rats treated with prednisolone and vitamin D3]. *Ukr Biokhim Zh*, 86(5), pp.111-125.
- Stimac, D., Milic, S., Dintinjana, R.D., Kovac, D. and Ristic, S., 2002. Androgenic/Anabolic steroid-induced toxic hepatitis. *J Clin Gastroenterol*, 35(4), pp.350-352.
- Timcheh-Hariri, A., Balali-Mood, M., Aryan, E., Sadeghi, M. and Riahi-Zanjani, B., 2012. Toxic hepatitis in a group of 20 male body-builders taking dietary supplements. *Food Chem Toxicol*, 50(10), pp.3826-3832.
- Venkareddy, L.K. and Muralidhara, 2015. Potential of casein as a nutrient intervention to alleviate lead (Pb) acetate-mediated oxidative stress and neurotoxicity: First evidence in *Drosophila melanogaster*. *Neurotoxicology*, 48, pp.142-151.
- Vieira, R.P., Franca, R.F., Damaceno-Rodrigues, N.R., Dolhnikoff, M., Caldini, E.G., Carvalho, C.R. and Ribeiro, W., 2008. Dose-dependent hepatic response to subchronic administration of nandrolone decanoate. *Med Sci Sports Exerc*, 40(9), pp.842-847.
- Vilar-Gomez, E., Martinez-Perez, Y., Calzadilla-Bertot, L., Torres-Gonzalez, A., Gra-Oramas, B., Gonzalez-Fabian, L., Friedman, S.L., Diago, M. and Romero-Gomez, M., 2015. Weight Loss via Lifestyle Modification Significantly Reduces Features of Nonalcoholic Steatohepatitis. *Gastroenterology*, 149(2), pp.367-378.
- Wang, M.Y., Anderson, G., Nowicki, D. and Jensen, J., 2008. Hepatic protection by noni fruit juice against CCl(4)-induced chronic liver damage in female SD rats. *Plant Foods Hum Nutr*, 63(3), pp.141-145.
- Waseem, N., Butt, S.A. and Hamid, S., 2014. Amelioration of lead induced changes in ovary of mice, by garlic extract. *J Pak Med Assoc*, 64(7), pp.798-801.
- Yu, M.W., Cheng, S.W. and Lin, M.W., 2000. Androgen-receptor gene CAG repeats, plasma testosterone levels, and risk of hepatitis B-related hepatocellular carcinoma. *J Natl Cancer Inst*, 92(24), pp.2023-2028.

The Plant Regulator Soaking Seeds and its Reflections on Growth and Yield Quality of Wheat

Mohammed Q. Khursheed, Trifa Z. Saber and Tara M. Hassan

Department of Biology, College of Education, Salahaddin University
Erbil, Kurdistan Region - F.R. Iraq

Abstract—A greenhouse pot experiment was carried out during November 2013 to May 2014. Winter wheat grains (*Triticum aestivum* L.), cultivars Abu-Ghureb and Cham6 were used to investigate the effect of soaking seeds in 300ppm of benzyl adenine (BA) or daminozide solutions for 6 hours before sowing vegetative, yield components, leaf chlorophylls and some chemical constituents of seeds. BA treatment led to significant increases in tiller number plant⁻¹, chlorophyll b, P, dry gluten, N and protein contents of seeds. It also led to significant decreases in number of leaves plant⁻¹. In addition, the number of tillers plant⁻¹, shoots dry weight plant⁻¹, P, N and protein contents of seeds were increased by daminozide treatment, but this caused a significant decrease in the plant height, number of leaves plant⁻¹ and flag leaf area. Number of grains plant⁻¹, weight of 1000 grains and grains yield were significantly increased by both treatments. Cultivar variability was noted for some tested parameters. The tall, N, P content and protein content of Abu-Ghureb cultivar were higher significantly than Sham6. The case was opposite with number of leaves plant⁻¹, flag leaf area, shoots dry weight plant⁻¹, spike length and grain number plant⁻¹.

Index Terms—BA, Daminozide, wheat (*Triticumaestivum* L.).

I. INTRODUCTION

Cereals are one of the most important sources of food for the world's population, providing energy, protein, vitamins, minerals and fiber (Craig, et al., 2009). Common wheat or Bread wheat (*Triticum aestivum* L.) is one of the world's most important food crops along with rice and maize. It is a staple food crop for many countries in the world. Bread wheat is a part of the grass family Poaceae. The flour from soft wheat contains a high percentage of gluten and is generally used for

making bread and cakes. White- and soft-wheat varieties are paler and have starchy kernels and their flour is preferred for piecrust, biscuits, and breakfast foods. The grain, the bran (the residue from milling) and the vegetative plant parts make valuable livestock feed.

Plant growth regulators (PGRs), either produced naturally by the plant or synthetically by a chemist, are small organic molecules that act inside the plant cells and alter the growth and development of plants. PGRs can be broadly divided into two groups: plant growth promoters and bioinhibitors. Growth promoters are involved in cell division, cell enlargement, pattern formation, tropic growth, flowering, fruiting and seed formation. Bioinhibitors play an important role in plant responses to wounds and stresses of biotic and abiotic origin and they are also involved in various growth inhibiting activities such as dormancy and abscission (Giannakoula, et al., 2012). Cytokinins are essential hormones for plant growth and development (Moke, et al., 2000). Cytokinin are required for cell division, proliferation and differentiation of plant cells, and also controls various processes in plant growth and development, such as delay of senescence, control of shoot/root balance transduction of nutritional signals and increased crop productivity (Sakakibara, 2006). Daminozide is a growth retardant with proven effects and practical application on many plant species, as it inhibits the biosynthesis of certain plant hormones like gibberellins and generally induces shortening of internodes of higher plants and has some additional effects such as reduction in leaf size (Hazarika, 2003).

Pre-treatment sowing for seeds is consider as one of the best practices that used for improving plant growth and yield. Many studies were conducted by soaking seeds, such as chicory *Cichorium intybus* L. (Tzortzakis, 2009), wheat *Triticum aestivum* L. (Yari, et al., 2011) and shisham *Dalbergia sissoo* (Roxb.) (Al-Barzinji, et al., 2015)

The goal of this research is to study the effects of soaking seeds in CK or Daminzide solutions on some vegetative characteristics, yield characteristics and some chemical contents of leaves and seeds of two wheat cultivars.

ARO-The Scientific Journal of Koya University
Volume IV, No 1(2016), Article ID: ARO.10084, 05 pages
DOI: 10.14500/aro.10084

Received 29 April 2015; Accepted 16 November 2015

Regular research paper: Published 30 April 2016

Corresponding author's e-mail: trifa.saber@su.edu.krd

Copyright © 2016 Mohammed Q. Khursheed, Trifa Z. Saber and Tara M. Hassan. This is an open access article distributed under the Creative Commons Attribution License.



II. PROCEDURE FOR PAPER SUBMISSION

The experiment was conducted at the Glasshouse of Biology Department, College of Education, University of Salahaddin-Erbil, during December 20, 2013 to April 20, 2014. Two winter wheat (*Triticum aestivum* L.) cultivars (Abu-Ghureb and Sham6) were used, which were obtained from the Agricultural Research Center in Erbil. The plastic pots were used in the experiment. Each pot contains 7Kg of sandy loam soil. Diammonium Phosphate (DAP) fertilizers containing 18% N and 46% P were added to the pots as solutions, at the rate of (472mg) per each pot which is equivalent to 270Kg ha⁻¹. The experimental treatments consisted of soaking seeds in benzyl adenine (BA) or daminozide for 6 hours before sowing at concentration of 300ppm. In each pot, seven grains were sown; two week after seed germination the seedling were thinned to two per pot. The experiment has been conducted in completely randomized design, included (6) treatments with 3 replicates. Plant height (cm), tiller numbers plant⁻¹, leaf numbers plant⁻¹, flag leaf area, shoot dry weight plant⁻¹, leaf chlorophylls, spike length (cm), spike number plant⁻¹, spikelet spike⁻¹, grain number plant⁻¹, weight of 1000 grains, grains yield plant⁻¹, total nitrogen (mg g⁻¹), protein (mg g⁻¹), phosphorus (mg g⁻¹), potassium (mg g⁻¹), wet and dry gluten (%) of seeds were measured. The flag leaf area was calculated according to Hunts formula (leaf area = leaf length x leaf widthx0.905) (Hunt, 1982). Plant shoots were dried in oven at 75 °C for 72h. Total nitrogen was determined by Kjeldahl method (Ryan et al.,2001) and total phosphorus was determined using spectrophotometer method as described by (Ryan et al.,2001). Total potassium was determined, using Flame – photometer method as described by (Kalra, 1998). The total protein was calculated by multiplying the value of total nitrogen by 5.7 (Dalaly and Al-Hakim, 1987). The gluten was determined according to hand washing method (Williams et al.,1988). The wet gluten was then oven-dried to weight constancy.

The chlorophyll *a* and *b* were measured according to the methods applied by Wintermand and Demote (1965); chlorophyll *a* and Chlorophyll *b* were spectrophotometrically estimated on two wave length 665nm and 649nm as follow:
 $\mu\text{g Chlorophyll } a/\text{ml solution} = (13.70) (665\text{nm}) - (5.76) (A649\text{nm})$
 $\mu\text{g Chlorophyll } b/\text{ml solution} = (25.80) (A649\text{nm}) - (7.60) (A665\text{nm})$

Total Chlorophyll = Chlorophyll *a* + Chlorophyll *b*

The comparisons between means were made using least significant difference test (L.S.D.) at significant level of 5% for pot experiment parameters and 1% for chemical characteristics. SPSS version 16 was used for data analysis.

III. RESULTS AND DISCUSSION

Table I shows the effects of soaking seeds in BA or daminzide solutions on some vegetative characteristics. It was

observed that BA treatment led to significant decreases in number of leaves plant⁻¹ and increases in tiller number plant⁻¹ as compared with controls. On the other hand, daminozide treatment caused significant decreases in the plant height, number of leaves plant⁻¹ and flag leaf area. In addition, the number of tillers and shoot dry weight of plant were increased by daminozide treatment. These results disagree with (Gumani, et al., 2007) concerning wheat plants. While partially agreed with those obtained by by (Sorte, et al., 1991) concerning wheat plants. The increase in the number of tillers could be due to the suppression of apical dominance by BA, thereby diverting the polar transport of auxins towards the basal nodes leading to increased branching (Hopkins, 1999). The significant decrease of plant height, leaves number plant⁻¹ and flag leaf area by daminozide treatments and significant increases of tiller number plant⁻¹ and shoot dry weight by such treatment may be explained that the growth of many stems can be reduced or inhibited by synthetic chemicals that block gibberellin biosynthesis. This so-called growth retardant or antigibberellins, they reducing endogenous gibberellins levels, suppressing internodes elongation and promoting root formation (Simas, et al., 2007). It has been suggested that, daminozide is anti-gibberellins dwarfing agents, leading to a deficiency of gibberellins in the plant consequently reducing the growth by blocking the conversion of geranyl pyrophosphate to copalyl pyrophosphate which is the first step of gibberellins synthesis (Hazarika, 2003).

TABLE I
EFFECT OF BENZYL ADENINE (BA) OR DAMINOZIDE ON SOME VEGETATIVE CHARACTERISTICS

Treatments (ppm)	Plant height (cm)	Number of tillers plant ⁻¹	Number of leaves plant ⁻¹	Flag leaf area(cm) ²	Shoot dry weight (g)
Control	70.85	4.67	15.50	40.44	9.86
BA300	70.08	6.58	13.00	42.41	10.77
Daminozide300	66.94	6.50	9.67	29.34	11.52
L.S.D. (0.05)	3.55	1.48	2.13	5.18	1.56

Fig. 1 shows that plant height of Abu-Ghureb cultivar was significantly higher than that of Sham6 cultivar. The number of leaves, flag leaf area and shoot dry weight of Sham6 cultivar plant were significantly higher than that of Abu-Ghureb cultivar. Probably, this was due to genetic potential variation of the species.

According to results represented in Table II, it is found that chlorophyll *b* was increased significantly by BA. Other treatments showed no significant effects on leaf chlorophyll content. This results partially agree with those obtained by (Mehrotra, et al., 1983) and (Yang, et al., 2003) concerning wheat plants. The increase in chlorophyll content of BA treated plants could be referred to hormonal effects as it has been noted earlier that BA stimulate chlorophyll biosynthesis through acceleration of chloroplasts differentiation and stimulating photosynthetic enzymes and retard chlorophyll degradation (Abdul and Mohamad, 1986). On the other hand,

Fig. 2 shows that no significant differences were observed on chlorophyll content between both cultivars and the highest values of chlorophyll found with Abu-Ghureb cultivar.

TABLE II
EFFECTS OF BENZYL ADENINE (BA) OR DAMINOZIDE ON LEAF CHLOROPHYLL CONTENT

Treatment (ppm)	Chlorophyll a (mg g ⁻¹)	Chlorophyll b (mg g ⁻¹)	Total Chlorophyll (mg g ⁻¹)
Control	0.65	0.19	0.83
BA300	0.92	0.46	1.38
Daminozide300	0.63	0.13	0.76
L.S.D. (0.01)	n.s.	0.22	0.57

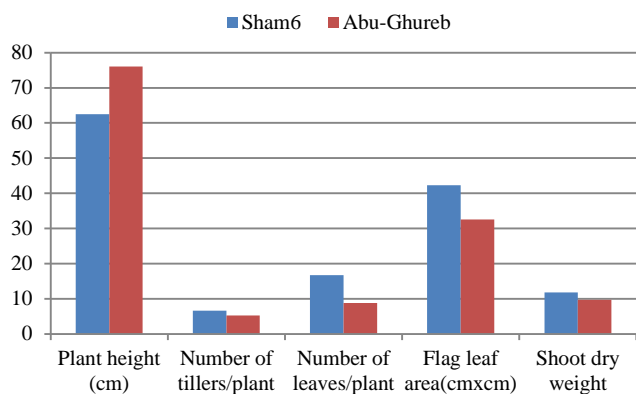


Fig. 1. Effect of cultivars on some vegetative characteristics.

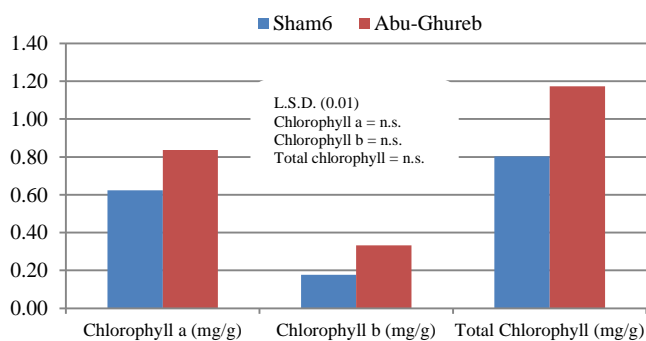


Fig. 2. Effects of wheat cultivars on leaf chlorophyll content.

The results indicated that the number of grains plant⁻¹, weight of 1000 grains and grains yield were significantly increased by both treatments as compared with controls (Table III). This results partially agree with those obtained by (Gurmani, et al., 2007) and (Sorte, et al.,1991) concerning wheat plants. The significant increases in grain number plant⁻¹ and weight of 1000 grains by BA treatments may be due to the essential role of this plant growth regulator in the regulation of different physiological processes including plant growth and development, increased cell division and high assimilate

demand in the growing embryonic tissue and it was suggested that BA is required for early embryo growth (Crosby et al., 1981).

TABLE III
EFFECTS OF BENZYL ADENINE (BA) OR DAMINOZIDE ON SOME YIELD CHARACTERISTICS

Treatment (ppm)	Spike length (cm)	Number of spikes plant ⁻¹	Number of spikelets spike ⁻¹	Number of grains plant ⁻¹	Weight of 1000 grains (g)	Grains yield (g plant ⁻¹)
Control	14.18	4.00	12.06	100.17	33.12	3.31
BA300	13.71	3.67	13.04	120.84	34.68	4.19
Daminozide300	13.71	3.33	11.10	122.34	35.08	4.29
L.S.D. (0.05)	n.s.	n.s.	n.s.	9.39	1.46	0.71

The increased of grain number plant⁻¹ and weight of 1000 grains by daminozide treatments may be attributed to the retarded vegetative growth because growth inhibition in one plant part may enhance growth in other plant parts ordaminozide treatments increased nutrient supplies and metabolites for reproductive growth such as water soluble carbohydrates, sucrose, proteins, gliadin, glutenin, enzymes and plant hormones (Scott et al., 1967).

Cultivar variability was noted for some tested parameters Fig. 3, it shows that spike length and grain number of Sham6 cultivar were significantly higher than Abu-Ghurebcultivar. This means they are differing in their response to the studied treatments and this may be due to genetic factor.

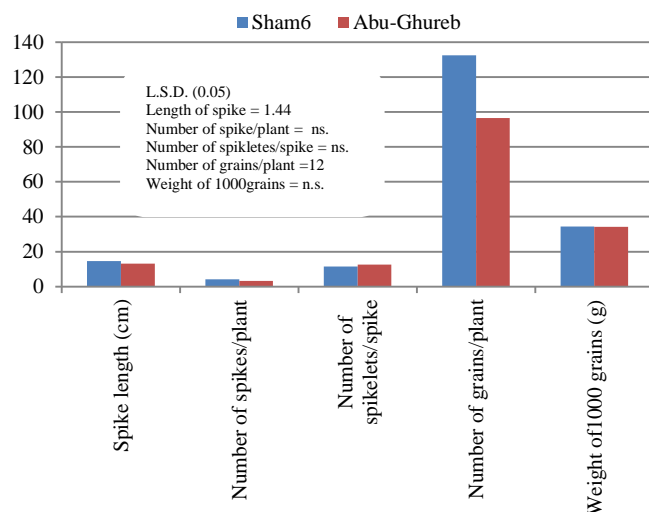


Fig. 3. Effects of wheat cultivars on some yield characteristics.

Table IV showed BA treatment significantly increased the P, dry gluten, N and protein contents of the seeds. Also daminozide treatment led to significant increases in the P, N and protein contents of the seeds. There were no previous studies concerning these parameters, it may be explained

through role of daminozide in increasing osmotolerance metabolites include a variety of proteins, sugars (trehalose, sucrose, mannitol, etc.), amino acids (proline, glycinebetaine), glycerol, polyols and /or through regulating various processes including absorption of nutrients from soil solution might be the cause for increase root growth increases the hydraulic conductivity of the root or the increasing of nutrient content of the seeds may be due to the role of daminozide in reducing the vegetative growth, which led to decrease the competition between vegetative and reproductive organs for nutrients (Rathod, et al., 2015).

TABLE IV
EFFECTS OF BENZYL ADENINE (BA) OR DAMINOZIDE ON SOME SEED NUTRIENTS CONTENT

Treatment (ppm)	Phosphorus (mg g ⁻¹)	Potassium (mg g ⁻¹)	Wet Gluten (%)	Dry Gluten (%)	Nitrogen (mg g ⁻¹)
Control	3.24	3.82	26.95	10.39	11.24
BA300	4.80	4.04	31.89	14.00	20.98
Daminozide300	5.08	3.86	33.45	12.91	20.26
L.S.D. (0.01)	0.60	n.s.	n.s.	3.44	3.09

The increase in nutrients content of BA treated plants could be referred to hormonal act as sink for mobilization of nutrients like amino acids, hormones and mineral nutrients (Hopkins, 1999). There were high significant differences among cultivars. Moreover, it was found that Abu-Ghureb cultivar had high significant more P, N and protein than that of Sham6 cultivar (Fig. 4). However, non-significant differences were observed between Abu-Ghureb and Sham6 with regarding to K, wet and dry gluten seed content.

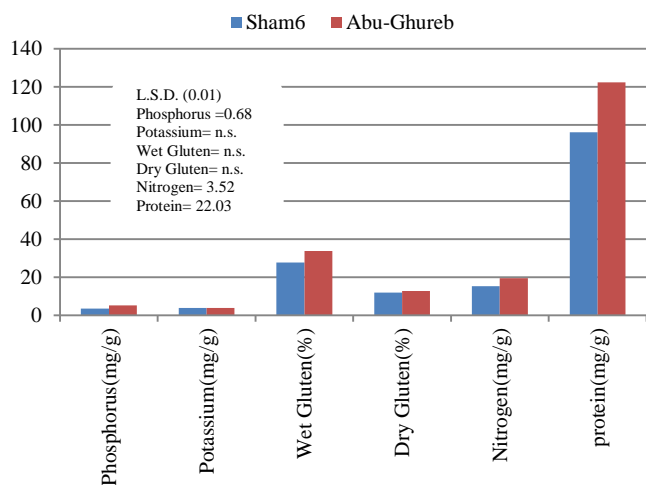


Fig. 4. Effect of wheat cultivars on some seed nutrients content.

IV. CONCLUSION

From the study, it might be concluded that both plant growth regulators (BA and daminozide) had the positive effect. In this respect, the impact of BA on quantitative and qualitative characteristics of wheat plant was greater than daminozide. The highest value of some vegetative characteristics and yield characteristics was obtained from Cham6, whereas, the highest value of plant height and some nutrient contents of seed was recorded from Abu-Ghureb.

REFERENCES

- Abdul, K.S. and Mohamad, A.K., 1986. *Vege شمالي Physiology. Directorate of Dar- Ell-Kutub for Printing and Publishing, University of Mosul, pp.282 (In Arabic).*
- Al-Barzinji, I.M., Khudhur, S.A. and Abdulrahman, N.M., 2015. Effects of Some Dates, Pre-treatment Sowing, Soil Texture and Foliar Spraying of Zinc on Seedling of *Dalbergia sissoo* (Roxb.). *ARO-The Scientific Journal of Koya University*, 3(1), pp.14-22. Retrieved from <http://dx.doi.org/10.14500/aro.10050>.
- Craig, B. F., Juge, N. and Svensson B., 2009. Enzymes in grain processing. *Journal of Cereal Science*, 50(3), pp.305-414.
- Crosby, K.E., L.H. Aung and G.L. Buss, 1981. Influence of 6-Benzyl aminopurine on fruit-set and seed development in two soybean (*Glycinemax* L.) merr. genotypes. *Plant Physiology*, 68(5), pp.985-988.
- Giannakoula, A.E., Jelena, I.I. and Maksimovic, J.D., 2012. The effects of plant growth regulators on growth, yield, and phenolic profile of lentil plants. *Journal of Food Composition and Analysis*, 28(1), pp.46-53.
- Gumani, A.R., Bano, A. and Salim, M., 2007. Effect of abscisic acid and benzyladenine on growth and iron accumulation of wheat under salinity stress. *Pakistan J. of Botany*, 39(1), pp.141-149.
- Hazarika, B.N., 2003. Acclimatization of tissue culture plants. *Current Science*, 85(12), pp.1704-1712.
- Hopkins, W.G., 1999. Introduction to Plant Physiology, 2nd edition, *John Wiley and Sons, Inc., U.S.A.*
- Hunt, R., 1982. Plant Growth Curves the Functional Approach to Plant Growth Analysis. *First published by Edward Arnold L.T.D.* London. pp.172-173.
- Kalra, Y.P., 1998. Reference Method for Plant Analysis. Taylor and Francis Group, LLC., pp.153-155.
- Mehrotra, O.N., R.K. Mathur and R.S. Tripathi, 1983. Effect of growth regulators on wheat. *Indian Journal of Agricultural Research*, 17(1-2), pp.57-61.
- Mok, M.C., Martin, R. C. and Mok, D.W.S., 2000. Cytokinins: Biosynthesis, Metabolism and Perception. *In Vitro Cell. Dev. Biol.Plant*, 36, pp.102-107.
- Rayan, J., Estefan, G. and Rashid, A., 2001. Soil and Plant Analysis Laboratory Manual. 2nd Edition. National Agriculture Research Center (NARC) Islamabad, Pakistan. pp.231-234.
- Rathod, R.R., Gore, R.V. and Bothikar, P.A., 2015. Effect of Growth Regulators on Growth and Yield of French bean (*Phaseolus vulgaris* L.) Var. Arka Komal. *Journal of Agriculture and Veterinary Science*, 8(5), pp.36-39.
- Sakakibra, H., 2006. Cytokinins: activity, biosynthesis, and translocation. *Annual Review of Plant Biology*, 57, pp.431-49.
- Schmulling, T., 2004. Cytokinin. *In Encyclopedia of Biological Chemistry (Eds. Lennarz, W., Lane, M.D.) Academic Press/Elsevier Science*. pp.27-29.
- Scott, T.K., Case, D.B. and Jaccobs, W.P., 1967. Auxin and gibberellin interactions in apical dominance. *Plant Physiology*, 42(10), pp.1329-1333.

- Simas, G., Tamosiunas, A. and Stuopytr, L., 2007. Effect of some growth regulators on chlorophyll fluorescence in *Viola x wittrockiana* 'Wesel Ice.' *Biologia*, 53(2), pp.24-27.
- Sorte, N.V., Deotale, R.D., Gajbhiye, D.T. and Kene, D.R., 1991. Effect of growth retardant (Alar) on morpho-physiological characters and yield wheat. *Journal of Social and Crop*, 1(1), pp.40-46.
- Tzortzakis, N.G., 2009. Effect of pre-sowing treatment on seed germination and seedling vigour in endive and chicory. *Hort. Sci.*, 36(3), pp.117-125.
- Williams, P., El-Haramein, F.J., Nakkoul, H. and Rihawi, S., 1988. *Crop Quality Evolution Methods and Guidelines*, 2nd edition, (ICARDA), Aleppo, Syria. pp.367-369.
- Wintermans, J.F. and Demote, A., 1965. Spectrophotometry characteristics of chlorophyll (a) and (b) and their phytylins in ethanol. *Biochimica et Biophysica Acta (BBA) - Biophysics including Photosynthesis*, 109, pp.448-453.
- Yang, J.S., Zhang, J.H., Wang, Z.Q., Zhu, Q.S. and Liu, L.J., 2003. Involvement of abscisic acid and cytokinins in the senescence and remobilization of carbon reserves in wheat subjected to water stress during grain filling. *Plant Cell and Environment*, 26(10), pp.1621-1631.
- Yanhai, Z., Xu, X., Simmons, M., Zhang, C., Gao, F. and Li, Z., 2010. Responses of physiological parameters, grain yield, and grain quality to foliar application of potassium nitrate in two contrasting winter wheat cultivars under salinity stress. *Journal of Plant Nutrition and Soil Science*, 173(3), pp.444-452.
- Yari, L., Abbasian, A., Oskouei, B. and Sadeghi, H., 2011. Effect of seed priming on dry matter, seed size and morphological characters in wheat cultivar. *Agriculture Biology Journal of North America*, 2(2), pp.232-238.

Non-destructive Method of Leaf Area Estimation for Oleander (*Nerium oleander* L.) Cultivated in the Iraqi Kurdistan Region

Ikbal M. Al-Barzinji and Barham M. Amin

Department of Biology, Faculty of Science and Health, Koya University
Daniel Mitterrand Boulevard, Koya KOY45, Kurdistan Region – F.R. Iraq

Abstract—This study was conducted in the Iraqi Kurdistan region in January 2014 to determine the individual leaf area of oleander (*Nerium oleander* L.) by easy, accurate, inexpensive, and nondestructive method. Simple, multiple and exponential regression analyses were used by length (L) and width (W) and their combinations as independent variables and with leaf area as dependent variable to determine more accurate models (high coefficient of determination and less MSE). The results showed that the best fitting models that show more accurate estimation of oleander leaf area, compared to other models, were the simple linear regression that depends on length multiple width for Koya and Erbil cities and the total leaves of the two cities plants. On the other hand, the best fitting multiple linear equations were those which depend on square length and square width for Koya city and the total leaves of the two cities plants, whereas for Erbil city the best model was that depends on leaves with square length and width. Multiple linear regressions were the more accurate among the models, followed by simple linear regression, whereas the exponential model had the lowest accuracy. All coefficients of regressions values were found to be significant at the $P < 0.0001$ level.

Index Terms— Leaf area estimation, *Nerium oleander* L., non-destructive methods, regression equations.

I. INTRODUCTION

Nerium oleander L. (Apocynaceae) is an evergreen shrub, distributed in the Mediterranean region and subtropical Asia. It is an urbanite plant widely used for ornamental purposes in streets, gardens, and hospitals (Rasul, Abbas and Abdul, 1986). Plant Leaf Area (LA) is an essential component to

estimate plant growth through its incidence on crop physiology mechanisms (Bhatt and Chanda, 2003), also it is an important determinant of light interception and consequently of transpiration, photosynthesis and plant productivity (Rosatia, Badeck and Dejong, 2001; Blanco and Folegatti, 2005). Leaf area production is essential for energy transference and dry matter accumulation processes in crop canopies. It is also useful in the analysis of canopy architecture (Mohammad, et al., 2011).

Measurement of leaf area divided to destructive and non-destructive methods. Usually destructive methods almost used by means of leaf area meter, this instrument may not available or expensive and very sensitive for calibration, while the non-destructive method is very simple and need to expensive instrument like portable scanning planimeter (Daughtry, 1990), but it is used for plants with a few small leaves (Nyakwende, Paull and Atherton, 1997). The measurement of LA, expressed per tree or as Leaf Area Index (LAI), can be a time consuming process and requires sophisticated electronic instruments, which are expensive especially for developing countries (Bhatt and Chanda, 2003). Moreover, destructive methods may cause inconvenient for some investigations, therefore, alternatives to estimate LA on the field may be provided by practical and non-destructive methods (Gutierrez and Lavín, 2000). For example, a rapid and non-destructive method to estimate LA is the use of equations that needs leaf dimensions (length and width) as inputs. Accurate non-destructive measurements permit repeated sampling of the same plants over time and have the advantage that biological variation can be avoided, especially when using unique plants (Schwarz and Klaring, 2001).

Various combinations of measurements and various models relating length and width to area have been utilized in, for example, grapevine (Gutierrez and Lavín, 2000; Williams and Martinson, 2003), dracaena *Dracaena sandariana* L. (Srikrishnah, Peiris and Sutharsan, 2012), rose *Rosa hybrida* L. (Fascella and Roupheal, 2013), *Crytorchid monteiroae* (Olosunde, Dauda and Aiyelaagbe, 2010) common bean *Phaseolus vulgaris* L. (Bhatt and Chanda, 2003), pepper *Capsicum annum* L. (De Swart, et al., 2004), radish

ARO-The Scientific Journal of Koya University
Volume IV, No 1(2016), Article ID: ARO.10088, 05 pages
DOI: 10.14500/aro.10088

Received 17 May 2015; Accepted 22 February 2016

Regular research paper: Published 30 April 2016

Corresponding author's e-mail: ikbal.tahir@koyauniversity.org

Copyright © 2016 Ikbal M. Al-Barzinji and Barham M. Amin. This is an open access article distributed under the Creative Commons Attribution License.



Raphanus sativus L.(Salerno, et al., 2005), cucumber *Cucumis sativus* L.(Cho, Oh and Son, 2007), cauliflower and cabbage *Brassica oleracea* (Olfati, et al., 2010) and elephant's ears *Bergenian purpuracense* (Zhang and Liu, 2010). Such equations allow growers and researchers to estimate LA in relation to other factors like crop load, drought stress and insect damage (Williams and Martinson, 2003).

The objective of this study was to develop an accurate, simple, non-destructive and time saving model for estimation leaf area for oleander shrubs.

II. MATERIALS AND METHODS

A. Sample Collection

The research was conducted in both of Koya (clayey soil with pH 7.45 and EC 9.15, located at 44°39'E, 36°05'N, and 618 m of altitude) and Erbil (sandy clay soil with pH 8.1 and EC 0.5, located at 44°03'E, 36°16'N, and 436 m of altitude) cities, Iraq-Kurdistan. Sampling of leaves of oleander shrubs was conducted at January 2014. Ten shrubs from each location were selected and leaves from 4 branches (one branch for each site of North, South, East and West) per shrub were chosen as samples (leaves number were 210 for each city). Table I shows the temperature, relative humidity and the amount of rain fall during the last 13 months of conducting the study, as it prepared in Agro-Meteorological Station in Koya city/ Ministry of Agriculture/ Iraq- Kurdistan Region for Koya city and Directorate of Weather and Earthquakes/ Erbil/ Iraq-Kurdistan Region for Erbil city.

B. Measurement Parameters

The measurements parameters comprise of leaf length (L) from lamina tip to the connected place petiole to lamina and width (W) from tip to tip at the widest of the lamina. The length and maximum width of leaves were measured to the

nearest 0.01 cm and the area to the nearest 0.01 cm².

C. Leaf Area Estimation

Leaf area is determined by spreading each leaf over a paper, and the outline of the leaf was drawn. By using a scissor, the area of the paper covered by the outline was cut and weighed on an electronic balance. One cm² of the same paper was also cut and weighed. The following equation was used to calculate the leaf area:

$Leaf\ area\ (cm^2) = x/y$, where x is the weight of the paper covered by the leaf outline (g) and y is the weight (g), of the cm² area of the paper (Pandey and Singh, 2011).

Simple linear, multiple linear and exponential regression equations were utilized by using length (L), width (W) and their products (L+W), (L²+W), (L+W²), (L²+W²) and (LW) as independent variables. These analyses were performed on each location individually, and also on the two locations together. The best and more accurate predicted equation for the leaf area (LA) was the equation with high coefficient of determination and less mean square of error (MSE).

D. Statistical Analysis

Analyses of the data were done by using SPSS program. ANOVA analysis was carried out to detect the significantly of the different regression models (Reza, 2006).

III. RESULTS AND DISCUSSIONS

A. Simple Linear Regression

Table II show simple linear regression models that used for determine the predicated leaf area regarding to leaf length (L), square length (L²), width (W), square width (W²), length plus width (L+W) and length multiple width (LW). The results show that in both Koya and Erbil cities and also about total leaves of the two cities, the equation numbered 16, 17 and 18

TABLE I
MAXIMUM, MINIMUM AND AVERAGE OF TEMPERATURE, AVERAGE RELATIVE HUMIDITY AND THE AMOUNT OF RAIN FALL DURING
JANUARY 2013 TO JANUARY 2014

Jan. 2013 to Jan. 2014	Koya				Erbil					
	Temperature (C°)			Average Relative Humidity (%)	Fall (mm)	Temperature (C°)			Average Relative Humidity (%)	Fall (mm)
	Min.	Max.	Average			Min	Max.	Average		
Jan.	5.87	10.90	8.21	72	254.5	5.3	12.7	9.0	74	174.4
Feb.	8.21	13.75	10.98	72	95.7	7.7	16.4	12.1	76	55.8
Mar.	10.10	17.52	13.97	66	10.9	10.0	19.9	15.0	62	17.7
Apr.	15.87	23.23	19.55	60	10.6	14.5	26.2	20.4	54	37.4
May	21.48	29.16	25.47	57	16.4	19.4	31.2	25.3	48	40.6
June	27.43	36.87	32.15	42	0.0	24.8	38.0	31.4	31	0.0
July	26.10	33.81	29.97	36	0.0	27.3	41.3	34.3	29	0.0
Aug.	16.71	25.87	21.29	36	0.0	27.1	41.0	34.1	29	0.0
Sep.	20.60	29.40	25.00	30	0.0	22.0	35.6	28.8	38	T.R *
Oct.	18.77	28.32	23.40	30	1.5	17.5	28.9	23.2	39	0.2
Nov.	20.47	17.65	14.20	60	69.5	12.8	21.9	17.4	68	19.1
Dec.	5.81	10.26	8.00	61	117.7	5.6	13.6	9.6	66	86.6
Jan.	6.23	11.97	9.10	65	330.5	1.9	18.0	9.8	66.0	47.8
Average	15.7	22.2	18.6	52.8	69.8	15.1	26.5	20.8	52.3	36.9

* T. R means that rain fall was less than 1 mm

TABLE II
INTERCEPT (a) AND REGRESSION COEFFICIENT (b) FOR SIMPLE LINEAR REGRESSION USED FOR ESTIMATING *Nerium oleander* L. LEAF AREA FROM LENGTH (L), WIDTH (W) AND SOME COMPATIBLES

Location	Treatment No.	Equation type	Intercept (a)	Coefficient (b)	Coefficient of Determination (R ²)	Coefficient of Correlation (R)	MSE	Significant (P<0.0001)
Koya	1	$LA = a + bL$	-21.464	3.336	0.841	0.917	14.368	**
Erbil	2		-7.149	1.771	0.772	0.879	4.433	**
Total	3		-19.162	3.042	0.817	0.904	15.940	**
Koya	4	$LA = a + bL^2$	-0.160	0.126	0.857	0.926	12.852	**
Erbil	5		1.073	0.090	0.827	0.909	3.363	**
Total	6		-2.191	0.129	0.870	0.933	11.310	**
Koya	7	$LA = a + bW$	-12.223	15.194	0.889	0.940	10.516	**
Erbil	8		-4.492	11.229	0.837	0.915	3.176	**
Total	9		-8.606	13.532	0.914	0.956	7.526	**
Koya	10	$LA = a + bw^2$	5.287	3.102	0.882	0.939	10.703	**
Erbil	11		3.538	3.698	0.825	0.908	3.435	**
Total	12		4.678	3.198	0.919	0.959	7.046	**
Koya	13	$LA = a + b(L + W)$	-21.853	2.866	0.889	0.943	10.027	**
Erbil	14		-8.163	1.643	0.839	0.916	3.131	**
Total	15		-18.785	2.611	0.778	0.937	10.652	**
Koya	16	$LA = a + b(LW)$	1.037	0.681	0.951	0.975	4.432	**
Erbil	17		1.222	0.659	0.956	0.978	0.865	**
Total	18		.915	0.683	0.970	0.985	2.574	**

that using leaf length multiple width (LW) had the strongest relationship ($p < 0.0001$) with LA, manifested in high coefficients of determination (R^2) of the equations and low mean square of error (MSE), whereas, regarding the equations that used only one leaf dimension, the equation using leaf width (W) had the strongest relationship ($p < 0.0001$) with LA, compare to equations depend on leaf length (L), square length (L^2) and square width (W^2).

Kumar and Sharma (2010) found that linear model ($LA = -3.44 + 0.729 LW$) which depending length multiple width (LW) as independent variable gave more accurate estimation for saffron (*Salvia sclarea* L.) leaf area compared to other models. Many other researchers also reported that leaf area can be estimated by linear measurement such as leaf width and leaf length in plants, such as Cristofori, et al. (2007), Mendoza-de Gyves, et al. (2007), Peksen (2007) and Rivera, et al. (2007) for developing simple and non-destructive models for estimating plant leaf area by using simple linear regression measurement. Also each of Lakshmanan and Pugazhendi found that the best fitting equations for oleander was $LA = -22.562 + 21.209W$ and $LA = -22.226 + 2.978L$ with $R^2 = 0.847$ and 0.893 respectively. The results in Table II show high significant correlation relationship ($P < 0.0001$) between independent variables used in the study with the leaf area which consider as dependent variable.

B. Multiple Linear Regression

The advantage of multiple regressions over simple regression analysis is in its enhancing our ability to use more available information in estimating the dependant variable (Reza, 2006). When the models change from simple to multiple linear regression by using length and width and some combinations as independent variables as it shown in Table III, the leaf area estimation became more accurate through increasing coefficient of determination and decreasing mean

square experimental error (MSE). The results of this Table show that the equation numbered 22 that using leaf square length and square width (L^2 and W^2) had the strongest relationship ($p < 0.0001$) with LA in Koya city, manifested in high coefficients of determination (R^2) of the equations and low mean square of error (MSE). In Erbil city the equation numbered 26 that depends square length and the width (L^2 and W) had the strongest relationship ($p < 0.0001$) with LA. About total leaves of the two cities, the equation No. 24 had the strongest relationship with LA, which were (L^2 and W^2) respectively.

This results agree with Cirak, et al. (2005) who found that multiple regression analysis used for determination of the best fitting equation for estimation of leaf area in seven medicinal plants (*Calamintha nepeta*, *Datura stromonium*, *Melissa officinalis*, *Mentha piperita*, *Nerium oleander*, *Origanum onites* and *Urtica dioica*) showed that most of the variation in leaf area values was explained by the basic parameters (length and width) and reached to 91%. The more accurate fitting in multiple linear regression is due to multiple linear regression model can be set more beside leaves length or width, when other variables that not measured in simple linear regression are responsible for the variation in the leaf area (Clewer and Scarisbrick, 2001).

C. Exponential Regression

Table IV show exponential regression models that used for determine the predicated leaf area regarding to leaf length (L), square length (L^2), width (W), square width (W^2), length plus width (L+W) and length multiple width (LW). The results show that equations 43 and 45 which use leaf length plus width (L+W) had the strongest relationship ($p < 0.0001$) with LA, manifested in high coefficients of determination (R^2) of the equations and low mean square of error (MSE) for Koya city and total leaves of Koya and Erbil cities. For leaves of Erbil city plants the equation number 47 that depends on leaf

TABLE III

INTERCEPT (a) AND REGRESSION COEFFICIENTS (b1 AND b2) FOR MULTIPLE LINEAR REGRESSION WITH TWO INDEPENDENT VARIABLES USED FOR ESTIMATING *Nerium oleander* L. LEAF AREA FROM LENGTH (L), WIDTH (W) AND SOME COMPATIBLES.

Location	Treatment No.	Equation type	Intercept (a)	Coefficient (b ₁)	Coefficient (b ₂)	Coefficient of Determination (R ²)	Coefficient of Correlation (R)	MSE	Significant (P<0.0001)
Koya	19	$LA = a + b_1L + b_2W$	-19.359	1.551	9.435	0.934	0.987	5.959	**
Erbil	20		-8.536	0.926	7.195	0.940	0.970	1.170	**
Total	21		-13.98	1.291	8.052	0.939	0.969	4.701	**
Koya	22	$LA = a + b_1L^2 + b_2W^2$	0.784	0.064	1.808	0.953	0.976	4.261	**
Erbil	23		0.831	0.052	2.131	0.955	0.977	0.871	**
Total	24		0.523	0.058	1.991	0.971	0.985	2.573	**
Koya	25	$LA = a + b_1L^2 + b_2W$	-9.209	0.062	8.896	0.945	0.972	4.961	**
Erbil	26		-3.770	0.050	6.562	0.957	0.978	0.846	**
Total	27		-7.244	0.058	8.348	0.961	0.980	3.398	**
Koya	28	$LA = a + b_1L + b_2W^2$	-9.667	1.641	1.884	0.949	0.974	4.609	**
Erbil	29		-3.729	0.964	2.343	0.943	0.971	1.114	**
Total	30		-6.186	1.234	2.203	0.965	0.982	3.085	**

TABLE IV

INTERCEPT (a) AND REGRESSION COEFFICIENT (b) FOR EXPONENTIAL REGRESSION USED FOR ESTIMATING *Nerium oleander* L. LEAF AREA FROM LENGTH (L), WIDTH (W) AND SOME COMPATIBLES.

Location	Treatment No.	Equation type	Intercept (a)	Coefficient (b)	Coefficient of Determination (R ²)	Coefficient of Correlation (R)	MSE	Significant (P<0.0001)
Koya	31	$LA = ae^{bL}$	2.569	0.157	0.881	0.938	0.022	**
Erbil	32		1.888	0.164	0.810	0.900	0.030	**
Total	33		1.707	0.181	0.873	0.934	0.036	**
Koya	34	$LA = ae^{bL^2}$	7.318	0.005	0.835	0.914	0.031	**
Erbil	35		4.172	0.008	0.816	0.903	0.029	**
Total	36		4.955	0.007	0.847	0.920	0.044	**
Koya	37	$LA = ae^{bW}$	4.210	0.693	0.864	0.929	0.026	**
Erbil	38		2.566	1.000	0.808	0.899	0.030	**
Total	39		3.557	0.769	0.886	0.941	0.032	**
Koya	40	$LA = ae^{bW^2}$	9.695	0.135	0.791	0.889	0.040	**
Erbil	41		5.361	0.319	0.751	0.866	0.039	**
Total	42		7.631	0.171	0.796	0.892	0.059	**
Koya	43	$LA = ae^{b(L+W)}$	2.556	0.134	0.919	0.950	0.015	**
Erbil	44		1.737	0.151	0.870	0.932	0.020	**
Total	45		1.770	0.154	0.921	0.959	0.022	**
Koya	46	$LA = ae^{b(LW)}$	7.962	0.030	0.886	0.941	0.021	**
Erbil	47		4.326	0.057	0.897	0.947	0.016	**
Total	48		6.092	0.037	0.885	0.941	0.033	**

length multiple widths (LW) had the strongest relationship with LA. Whereas, regarding the equations that used only one leaf dimension, the equation using leaf length (L), square leaf length (L²) and leaf width (W) had the strongest relationship with LA in each of Koya city, Erbil city and total leaves of Koya and Erbil cities respectively. These results agree with Kumar (2009) whom found that exponential model that depending length as independent variable gave more accurate estimation for saffron (*Crocus sativus* L.) leaf area compared to other models as a result of higher value of R².

From the results shows in Tables II, III and IV the equations using leaf length (L), maximum leaf width (W) or their products had strong relationships with LA, manifested in high coefficients of determination (R²) of the equations and low mean square error (MSE). Single variable equations would be preferred because they avoid problems of co-linearity between L and W, and require measurement of only one leaf

dimension.

However, the best fitting simple linear equations for oleander was $LA = 1.037 + 0.681(LW)$ for Koya city, $LA = 1.222 + 0.659(LW)$ for Erbil city and $LA = 0.915 + 0.683(LW)$ for the leaves of the two cities, while, the best fitting multiple linear equations was $LA = 0.784 + 0.064L^2 + 1.808W^2$ for Koya city, $LA = -3.77 + 0.05L^2 + 6.562W$ for Erbil city and $LA = 0.523 + 0.058L + 1.991W$ for the leaves of the two cities. The variation between independent variables included in simple linear, multiple linear and exponential regressions between Koya and Erbil cities may due to the differences between the environmental conditions, and its effects on leaves growth, where the climactic condition in Erbil city is characterizes by more temperature degrees and low relative humidity and rain fall (Table I), in addition to the differences between the soil texture (clayey in Koya city and sandy clay in Erbil city) which has a role in

determining the leaf growth and area, this result agree with Al-Barzinji, Khudhur and Abdulrahman (2015) whom found significant differences in *Dalbergia sissoo* (Roxb.) leaf area for plants grow in clayey and sandy clayey soils.

IV. CONCLUSIONS

In this study the models for predicting leaf area for the oleander plants were developed, and the multiple linear regression models were more accurate than simple linear regression models. Also simple linear regression model was more accurate than exponential regression model. We can estimate oleander leaf area on the plant without destroying them anywhere in a field or pot and continue with taking data for long time. The highest regression correlation between L and W and actual leaf area belonged to $LA = 0.784 + 0.064L^2 + 1.808W^2$ for Koya city, $LA = -3.77 + 0.05L^2 + 6.562W$ for Erbil city and $LA = 0.523 + 0.058L^2 + 1.991W^2$ for the leaves of the two cities

REFERENCES

- Al-Barzinji, I.M., Khudhur, S.A. and Abdulrahman, N.M., 2015. Effect of some date, pre-treatment sowing, soil texture and foliar spraying of zinc on seedling of *Dalbergia sissoo* (Roxb.). *ARO-The Scientific Journal of Koya University*, 3(1), pp.14-22. Retrieved from <http://dx.doi.org/10.14500/aro.10050>.
- Bhatt, M. and Chanda, S.V., 2003. Prediction of leaf area in *Phaseolus vulgaris* by non-destructive method. *Bulg. J. Plant Physiol.*, 29(2), pp.96-100.
- Blanco, F.F. and Folegatti, M.V., 2005. Estimation of leaf area for greenhouse cucumber by linear measurements under salinity and grafting." *Agricultural Science*, 62(4), pp.305-309.
- Cho, Y.Y., Oh, S., Oh, M.M. and Son, J.E., 2007. Estimation of individual leaf area, fresh weight, and dry weight of hydroponically grown cucumbers (*Cucumis sativus* L.) using leaf length, width, and SPAD value. *Sci. Hort.*, 111(4), pp.330-334.
- Cirak, C., Odabas, M.S., Saglam, B. and Ayan, A.K., 2005. Relation between leaf area and dimensions of selected medicinal plants. *Res. Agr. Eng.*, 51(1), pp.13-19.
- Clewer, G.A. and Scarisbrick, D.H., 2001. *Practical Statistics and Experimental Design for Plant and Crop Science*. England, John Wiley & Sons, Ltd.
- Cristofori, V., Roupael, Y., Mendoza-de Gyves, E. and Bignami, C., 2007. A simple model for estimating leaf area of hazelnut from linear measurements. *Scientia Horticulturae*, 113(2), pp.221-225.
- Daughtry, C., 1990. Direct measurements of canopy structure. *Remote Sensing Reviews*, 5(1), pp.45-60.
- De-Swart, E.A.M., Groenold, R., Kannne, H.J., Stam, P., Marceis, L.F.M. and Voorrips, R.E., 2004. Non-destructive estimation of leaf area for different plant ages and accessions of *Capsicum annum* L. *Journal of Horticultural Science & Biotechnology*, 79(5), pp.764-770.
- Fascella, G., Darwich, S. and Roupael, Y., 2013. Validation of a leaf area prediction model proposed for rose. *Chilean J. Agric.*, 73(1), pp.73-76.
- Gutierrez, T. and Lavin, A., 2000. Linear measurements for non-destructive estimation of leaf area in 'Chardonnay' vines. *Agricultura Técnica*, 60(1), pp.69-73.
- Kumar, R., 2009. Calibration and validation of regression model for non-destructive leaf area estimation of saffron (*Crocus sativus* L.). *Scientia Horticulturae*, 122(1), pp.142-145.
- Kumar, R. and Sharma, S., 2010. Allometric model for nondestructive leaf area estimation in clary sage (*Salvia sclarea* L.). *Photosynthetica*, 48(2), pp.313-316.
- Lakshmanan, C. and Pugazhendi, N., 2013. Leaf area prediction models through leaf morphometry. *OUTREACH. A multi-Disciplinary Refereed Journal*, 6, pp.99-106.
- Mendoza-de Gyves, E., Roupael, Y., Cristofori, V. and Rosana Mira, F., 2007. A non-destructive, simple and accurate model for estimating the individual leaf area of kiwi (*Actinidia deliciosa*). *Fruits*, 62(3), pp.171-176.
- Mohammad, N.I., Farzad, P., Mohsen, Z., Mohammad, R.A. and Ali, K., 2011. Prediction model of leaf area in soybean (*Glycine max* L.). *American Journal of Agricultural and Biological Sciences*, 6(1), pp.110-113.
- Nyakwende, E., Paull, C.J. and Atherton, J.G., 1997. Nondestructive determination of leaf area in tomato plants using image processing. *Journal of Horticultural Science*, 72(2), pp.255-262.
- Olfati, J.A., Peyvast, G., Shabani, H. and Nosratie-Rad, N., 2010. An estimation of individual leaf area in cabbage and broccoli using non-destructive methods. *J. Agr. Sci. Tech.*, 12(Supplementary issue), pp.627-632.
- Olosunde, M.A., Dauda, T.O. and Aiyelaagbe, I.O., 2010. Rapid leaf area estimation of *Crytorchid monteiroae*. *Journal of American Science*, 6(12), pp.1549-1553.
- Pandey, S.K. and Singh, H., 2011. A simple, cost-effective method for leaf area estimation. *Journal of Botany*. 6 pages. Doi: 10.1155/2011/658240
- Peksen, E., 2007. Non-destructive leaf area estimation model for faba bean (*Vicia faba* L.). *Sci. Hort.*, 113(4), pp.322-328.
- Rasul, T.N., Abbas, A.S. and Abdul, K.S., 1986. *333 Question and Answer about Ornamental Plants, Fruits and Vegetative under Iraqi Environment Conditions*. Mosul University. Iraq. Directorate of Dar Al-Kutob for printing and publication.
- Reza, A.H., 2006. *Design of Experiments for Agriculture and the Natural Sciences*. New York, Chapman & Hall.
- Rivera, C.M., Roupael, Y., Cardarelli, M. and Colla, G., 2007. A simple and accurate equation for estimating individual leaf area of eggplant from linear measurements. *European Journal of Horticultural Science*, 72(5), pp.228-230.
- Rosatia, A., Badeck, F.W. and Dejong, T.M., 2001. Estimating canopy light interception and absorption using leaf mass per unit leaf area in *Solanum melongena*. *Annals of Botany*, 88(1), pp.101-109.
- Salerno, A., Rivera, C.M., Roupael, Y., Colla, G., Cardarelli, M., Pierandrei, F., Rea, E. and Saccardo, F., 2005. Leaf area estimation of radish from linear measurements. *Adv. Hort. Sci.*, 19, pp. 213-215.
- Schwarz, D. and Klaring, H.P., 2001. Allometry to estimate leaf area of tomato. *Journal of Plant Nutrition*, 24(8), pp.1291-1309.
- Srikrishnah, S., Peiris, S.E. and Sutharsan, S., 2012. Effect of shade levels on leaf area and biomass production of three varieties of *Dracaena sanderiana* L. in the dry zone of Sri Lanka. *Tropical Agricultural Research*, 23(2), pp.142-151.
- Williams, L. and Martinson, T.E., 2003. Non-destructive leaf area estimation of 'Niagara' and 'DeChawnac' grape-vines. *Scientia Horticulturae*, 98(4), pp.493-498.
- Zhang, L. and Liu, X., 2010. Non-destructive leaf area estimation for *Bergenia purpuracense* across timberline ecotone, south east Tibet. *Ann. Bot. Fennici.*, 47(5), pp.346-352.

Taguchi Method for Investigating the Performance Parameters and Exergy of a Diesel Engine Using Four Types of Diesel Fuels

Dara K. Khidir¹ and Soorkeu A. Atrooshi²

¹Koya University

Daniel Mitterrand Boulevard, Koya KOY45, Kurdistan Region – F.R. Iraq

²Department of Mechanical Engineering, Salahaddin University
Erbil Kirkuk Road, Erbil, Kurdistan Region – F.R. Iraq

Abstract—The effects of changes in engine operating parameters, i.e., engine speed, throttle and water temperature, for four types of diesel fuel (A, B, C and D) of different specific gravities, as supplied from local market and refineries, were studied and simultaneously optimized. The experiment design was based on Taguchi's "L' 16" orthogonal table, and the engine was put to test at different engine speeds, throttling opening percentages and water temperatures, using different fuels. The data were analyzed using S/N (signal to noise ratio) for each factor. The obtained results show that the optimum operating conditions for minimum BSFC (brake specific fuel consumption) are achieved when the engine speed is 2500 rpm, the throttle is placed at 75% of full throttling, the water temperature is 80 °C and the engine is using fuel type D. Also, results of S/N ratio reveal that the throttle has significant influence on brake thermal and exergic efficiencies. Water temperature is the second most effective factor and then comes the influence of engine speed. The least effective factor among the studied parameters for the types of fuel considered in this experiment is the fuel type.

Index Terms—Compression ignition engines, exergy, Taguchi, performance.

I. INTRODUCTION

A charge of compressed air and a diffused spray of liquid fuel operate the compression ignition engine. The combustion pressure in the cylinder of a diesel engine is the result of a larger compression ratio which, combined with better combustion efficiency, gives it a higher indicated thermal

efficiency when compared to spark ignition engine. The diesel engine is still recognized as a promising power train for the foreseeable future due to superior thermal efficiency and reliability (Xin, 2011).

This work is based on experimental observations to improve our understanding of the parameters affecting the performance of a diesel engine. To select the range of parameters to work with, it was necessary to run a review over the working parameters and check their effect on the performance of the compression ignition test rig.

Engine characteristics such as; engine speed, reduction in intake throttle pumping loss, equivalence ratio balance and its effect on leaner mixture of air and fuel, and higher compression ratio, prove that the diesel engine can run at a higher brake thermal efficiency than its gasoline engine counterpart (Xin, 2011; Mollenhauer and Tschoeke, 2010; Doe, 1993).

It is estimated that for diesel engine, the specific fuel consumption is about 80% of that of petrol engine. The lowest specific fuel consumption of compression ignition engine is attained as the fuel-air ratio approaches the stoichiometric ratio and a speed at which volumetric efficiency is at the optimum. It is also estimated that the highest thermal efficiency and lowest fuel consumption of diesel engines occur at approximately 50-85% of maximum brake mean effective pressure (Garrett, 2001; Rajput, 2008).

To improve our understanding of the significance of diesel fuels and their influence on the engine itself, it is important to have a basic understanding of fuel characteristics, properties and contaminants that impact the operation of such an engine. The quality of fuel plays an important role in diesel engine performance. It also affects the durability of operation and maintenance intervals. A fuel property is considered to be a characteristic occurring in the fuel carried over from its crude source or the result of the refining processes by which it was produced. Fuel characteristics are affected by fuel delivery temperatures and excessive evaporation of fuel during its transport to the combustion chamber can disturb the performance of the fuel injectors.

ARO-The Scientific Journal of Koya University
Volume IV, No 1(2016), Article ID: ARO.10101, 08 pages
DOI: 10.14500/aro.10101

Received 28 July 2015; Accepted 30 March 2016

Regular research paper: Published 17 May 2016

Corresponding author's e-mail: dara.khalid@koyauniversity.org

Copyright © 2016 Dara K. Khidir and Soorkeu A. Atrooshi. This is an open access article distributed under the Creative Commons Attribution License.



Cooling systems are designed to maintain engines at optimum temperatures, allowing the design of components that expand on heating to form very tight fits and running tolerances. The calibration of ignition and fuel settings is balanced against the operating temperature imposed for the clean and efficient combustion of fuel. Temperatures inside the combustion chamber of an engine, during combustion, reach the order of 2427 °C and up (Pulkrabek, 2004). Engine components may not be able to tolerate this kind of temperature and can fail if proper heat transfer does not occur. Cooling the combustion chamber is highly critical in keeping an engine and engine lubricant from thermal failure. This is balanced against the principle that it is desirable to operate an engine as hot as possible to maximize thermal efficiency (Pulkrabek, 2004; Denton, 2011).

Many researchers studied the performance of CI engines, using Taguchi method. An experimental study has been carried out by Nataraj, Arunachalam and Dhandapani (2005), to simultaneously optimize several diesel engine designs and operating parameters for low exhaust emissions using, Taguchi method. Kanog˘lu, Isık, and Abuşog˘lu (2005) studied the characteristics and performance parameters of the internal combustion engines of the power plant. The mass, energy and exergy balances are verified for each flow stream in the power plant. The work and heat interactions, the exergy losses and the efficiencies of various components based on both energy and exergy concepts are evaluated and the thermal and the exergy efficiencies of the plant are determined. Tamilvendhan, et al. (2011) based their experiment on diesel fuel blends and studied fuel replacing ability, performance and emission behavior with respect to blend proportions, injection timing and pressure, using Taguchi's nine trials for optimization. The trials were based on studying the main effect of each of the above three parameters. The measured performance figures from these trials were used to analyze the effect of the studied factors. The results indicated improved brake thermal efficiency without excessive deterioration of the exhaust emission.

Wu and Wu (2013) used Taguchi method to determine the optimal concentration of diesel/biodiesel blend using cooled exhaust gas recirculation (EGR) at the inlet port. They researched the optimal operating factors for achieving good combustion performance and low emissions at various engine loads and 1500 rpm.

Sekmen and Yılbaşı (2010) conducted experimental investigation of diesel engine performance including, specific fuel consumption and brake horse power, based on energy and a number of exergy balances such as; exergy destruction and exergetic efficiency, with different fuel. They arrived at the conclusion that a combined energy and exergy analysis provides a much better and more realistic answer.

ANOVA (analysis of variance) is an approach based on analysis related to sums of squares for each effective factor to express dispersion of characteristics, (Lee, et al., 2013). It finds the factors with significantly effective impact, when compared to the others. This helps in reducing the number of considered parameters.

Xiao, et al. (2014) conducted a simulation investigation using, CFD (computation fluid dynamics) with Taguchi method and ANOVA to understand the combined effect of a number of combustion parameters such as EGR (exhaust gas recirculation), fuel quality and injection timing on NOx (oxides of nitrogen). They concluded that EGR is the most effective factor in estimation of the amount of produced NOx.

There are a large number of parameters to be considered for every experimental investigation. An approach based on Taguchi method is adopted in this work with the aim of optimizing the experimental parameters with a reduced number of attempts. Larger number of parameters leads to larger number of trials and consumes more time to complete the experiment.

Taguchi method depends on orthogonal arrays, which are statistically analyzed, leading to a thorough investigation of the results. Based on this approach the considered data is assessed and optimized taking into account a more universal view when considering the mean and the variation through signal to noise ratio. The strength of the influence of parameters is based on the outcome of signal to noise ratio evaluation.

The concept of signal (product quality) to noise (uncontrollable factors) ratio are log functions based on Larger the better, Smaller the better and Nominal the better.

In this work the effective parameters to be investigated are pre-defined as engine speed, throttle position, cooling water temperature and the fuel type. ANOVA was not applied to optimize the selection process due to limited number of considered parameters. At one stage, Taguchi method is applied to indicate the order of significance of these parameters.

II. THEORETICAL APPROACH

A. Fuel Consumption

Specific fuel consumption is defined as the amount of fuel consumed for each unit of brake power developed per hour. It is a clear indication of the efficiency with which the engine develops power from fuel, (Rajput, 2008).

$$BSFC = 3600 m_f BP \quad (1)$$

B. Volumetric Efficiency

This is equal to the ratio of mass of air, which enters or is forced into the cylinder in intake stroke, to the mass of air equivalent to the piston displacement at intake temperature and pressure conditions, (Rajput, 2008).

$$\eta_v = m_a / m_f \quad (2)$$

Air volumetric flow-rate is measured with air box manometer head by the relation, (Cussons Technology Ltd, 1989):

$$V_{actual} = 0.1244 d^2 (hh/\rho_{air})^{0.5} \quad (3)$$

C. Energy Analysis of Diesel Engine

Most transient-flow processes can be modeled as uniform flow. The following assumptions were made to simplify the first law calculation; the engine operates at steady state and the whole engine, including the dynamometer, is selected as a control volume. This excludes the work transfer between the engine and the dynamometer. Also the combustion air and the exhaust gas each form ideal gas mixtures and potential and kinetic energy effects of the incoming and outgoing fluid streams are ignored.

Fuel energy rate to the control volume is given by Equation:

$$Q_f = \dot{m}_f LHV \quad (4)$$

Brake power of the engine is determined by:

$$P_b = T_r \cdot \omega = 2\pi N T_r / 60 \quad (5)$$

Brake thermal efficiency of the control volume (η_b) is usually determined as the ratio of the power output (net work) to the fuel energy input and is represented by:

$$BTE = P_b / Q_f = P_b / (\dot{m}_f LHV) \quad (6)$$

D. Exergy Analysis

Exergy is the maximum theoretical work obtainable from an overall system consisting of a system and the environment as the system comes into equilibrium with the environment. The order of exergy destruction and losses in the processes and components of a thermal system can be revealed by the exergy analysis of the system. The results of exergy analysis can be used for identifying certain processes in a thermal system, on which further studies must be conducted to achieve better energy source utilization. The specific chemical exergies of liquid fuels can be evaluated from the following expression on a unit mass basis (Sayin, 2006; Rakopoulos, 2004).

$$a_{fch} = LHV (1.04224 + 0.011925 m_1/m_2 - 0.042 m_2) \quad (7)$$

On the other hand, assuming the ideal solution assumption is valid; the specific chemical exergy for a multi component stream can be calculated as:

$$e_{ch} = R T_o \sum_{i=1}^n a_i \ln(y_i/y_{io}) \quad (8)$$

When R is gas constant (kJ/(kmol.K)) and T_o is the ambient temperature as indicated in the nomenclature.

Diesel fuel can be modeled as $C_{14.4}H_{24.9}$ (Rakopoulos, 2004). When computing the rate of exergy transfer accompanying heat transfer, it was assumed that Q_{cv} is rejected into the ambient air from the boundary having the same temperature as the engine coolant circulating in the engine block. Inserting values for the exergy transfer accompanying heat, mass flow, and power transfers, used in calculation of fuel and work exergies, the rate of exergy destruction in the

engine can be determined by (12), indicated below. Exergetic efficiencies also can be used to evaluate the effectiveness of engineering measures taken to improve the performance of a thermal system. Finally, the exergetic efficiency of the engine (13) can be evaluated from the ratio of the power output to the fuel exergy input. Exergy destruction can be calculated from the difference between the exergy input and the net work produced. If the proportion of exergy destruction to the entered fuel exergy decreased, then the exergetic efficiency is increased. The relevant exergy relations are defined below (Sorathia and Yadav, 2012):

$$\text{Fuel Exergy: } E_f = \dot{m}_f e_{ch} \quad (9)$$

$$\text{Heat Exergy: } E_Q = \sum_s (1 - T_o/T) \quad (10)$$

$$\text{Work Exergy: } E_w = W = P_b \quad (11)$$

$$\text{Destroyed Exergy: } E_d = E_f - E_w \quad (12)$$

$$\text{Exergetic Efficiency: } \eta_{II} = E_w/E_f = 1 - E_d/E_f \quad (13)$$

III. EXPERIMENTAL WORK

In this study the experimental set up consists of a compression ignition engine test bed connected directly to an eddy current dynamometer as indicated in Fig. 1.

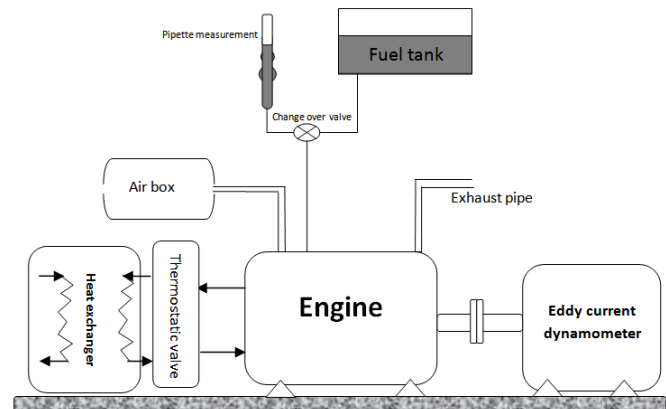


Fig. 1. Test rig schematic

For this layout the specifications are shown below:
 Engine type: Ford XLD 416, four stroke, water cooled, indirect injection compression ignition engine, 1.6 liter engine.
 Number of cylinders: 4 in-Line, Bore: 80 mm and stroke: 80 mm.
 Compression ratio: 21.5:1.
 Dynamometer: Froude EC38 TD eddy current dynamometer.
 The rig is used for testing, based on Taguchi's (L'16) table, with four types of locally available fuels with the specifications shown in Table I. The fuel types shown in this table represent four types of fuel available in the region.

TABLE I
PROPERTIES OF FOUR TYPES OF DIESEL FUELS

Type	SG AT 15.5 °C	LHV (MJ/Kg)
A	0.8118	43.188
B	0.8318	43.154
C	0.8284	43.265
D	0.8322	43.364

The succession of tests is listed in Table II. This table shows throttle openings of (55%, 65%, 75% and 85%), engine speed variations of (2000 rpm, 2250 rpm, 2500 rpm and 2750 rpm) and water temperatures of (65 °C, 70 °C, 75 °C and 80 °C) for four fuel types.

TABLE II
TEST ARRANGEMENTS

L'16 ORTHOGONAL ARRAY						Obtained Data	
Experiment no.	Fuel Type	Engine Speed (rpm)	Throttle (%)	Water Temperature (°C)	Torque	Head of Air Box Manometer (mm) [converted to air flow rate (l/min)]	Time for Fuel Consumption (sec) [converted to fuel flow rate (g/sec)]
1	A	2000	55	65	40.1	7.75 [1183.15]	29.1 [0.821]
2	A	2250	65	70	53	9.75 [1327.062]	22.05 [1.083]
3	A	2500	75	75	65.3	12.25 [1487.5]	19.55 [1.221]
4	A	2750	85	80	72.4	14 [1590.204]	15.25 [1.566]
5	B	2000	55	65	37.9	7.5 [1163.91]	32.1 [0.752]
6	B	2250	65	70	59.9	9.5 [1309.938]	22.6 [1.069]
7	B	2500	75	75	63.9	12.75 [1517.554]	18.08 [1.336]
8	B	2750	85	80	72.1	14.25 [1604.34]	15.1 [1.599]
9	C	2000	55	65	31.2	7.5 [1163.91]	33.03 [0.738]
10	C	2250	65	70	44.6	9.75 [1327.062]	24.23 [1.005]
11	C	2500	75	75	73	12.25 [1487.5]	20.33 [1.198]
12	C	2750	85	80	73	14.25 [1604.34]	18.332 [1.33]
13	D	2000	55	65	22.6	7.5 [1163.91]	37.98 [0.644]
14	D	2250	65	70	51.7	10 [1343.968]	24.3 [1.006]
15	D	2500	75	75	72.2	12 [1472.243]	20.29 [1.205]
16	D	2750	85	80	74	14 [1590.204]	19.11 [1.279]

All data are taken after the engine coolant temperature, coming out of the engine, reached the desired temperature. The results of the experimental layout of L'16 orthogonal array were calculated. The data is analyzed with Minitab 16 software, which simplifies the Taguchi procedure and results and S/N ratios are calculated. The software was checked for accuracy using stepwise hand calculations. S/N ratio represents the transformation of repetition data to measure of present variation. There are several S/N ratios available depending on the type of characteristic, the equations for calculating S/N ratios give negative values as is indicated from the format of these equations (Ross, 1996):

- Lower is better:

$$s/N_{LB} = -10 \text{ LOG}(1/n \sum_{i=1}^n Y_i^2) \quad (14)$$

- Higher is better:

$$s/N_{HB} = -10 \text{ LOG}(1/n \sum_{i=1}^n 1/Y_i^2) \quad (15)$$

IV. RESULTS AND DISCUSSION

The present work uses four factors at four levels. Hence, an L'16 orthogonal array, Table II, with four columns and sixteen rows were used to design Taguchi's experiment with Minitab 16 software. The factors considered for experiment and levels are shown in Table II. Sixteen independent experiments were conducted in an attempt to obtain high accuracy and research quality results. All the parametric variations were done on the same fuel to avoid mixing between the fuels during experimentations. To ensure the correct throttle position, the gap between the throttle lever and its stop was measured with a set of spacers for each similar throttle positions.

- Nominal is better:

$$s/N_{nominal} = -10 \text{ LOG}(1/n \sum_{i=1}^n Y_i - Y_m) \quad (16)$$

Once the experimental design was determined and the trials were carried out, the measured performance characteristic from each trial was used to analyze the relative effect of the different parameters.

Fig. 2 and Fig. 3 show the obtained graphs of Taguchi experiments for the value of the means and the mean of S/N ratios, ranging from smaller is better for SFC (Fig. 2) which explains the opposite projection of the graph of mean of means, which is an engine characteristic that is optimum when smallest to larger is better for volumetric efficiency (Fig. 3) which is best when largest and is projected comparably by mean of means graphs. They were used for selecting the optimum level of the parameters.

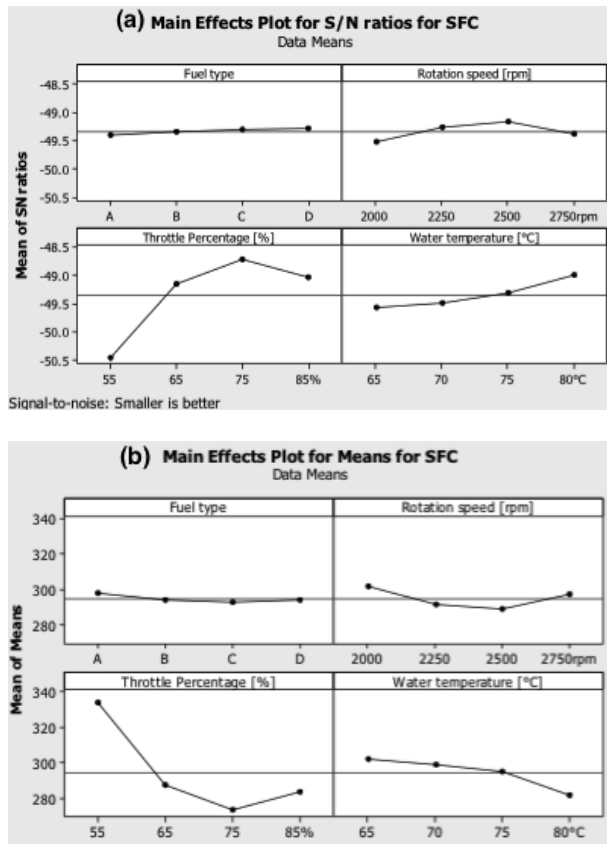


Fig. 2. Main effects plot of the S/N ratios and means for BSFC.

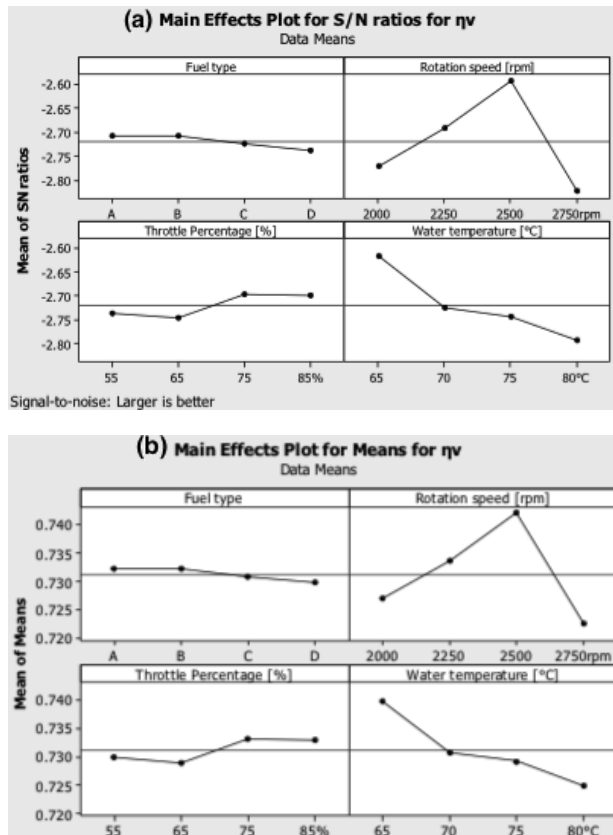


Fig. 3. Main effects plot of the S/N ratios and means for volumetric efficiency.

The peak value of each graph is considered as the optimum point, as these points are offering highest S/N ratios. The horizontal line in the middle of each figure indicates the mean of the projected values. The mean of means indicates the average of the highest and lowest averages for each factor and the graphs are limited in presentation by the software mini tab (5) grapher and this has partially affected the presentation of the throttle contribution as the highest value of the graph falls outside the y-axis limit.

The confirmation tests were later conducted with the optimum combination of results showing that the obtained parameters have prime values compared to the other tested experiments. The obtained results are discussed below:

A. Brake Specific Fuel Consumption (BSFC)

Results reveal that the specific fuel consumption is strongly affected by the throttle position because of the highest range between maximum to minimum S/N ratio. Fig. 2 shows that the minimum point of consumption occurs at %75 of the full throttle. The second most effective factor is the water temperature of the engine. The plot profile reveals that BSFC decreases as the water temperature is increased, reaching the minimum at a water temperature of 80°C. The third effective factor over the output of BSFC characteristic is rotation speed of the engine. The minimum fuel consumption is achieved at an engine speed of 2500 rpm. And it is at this speed that the engine attains maximum volumetric efficiency. The contours of the diesel fuel type curves are almost unremitting. The results reveal approximated output. As specific gravity (SG) is increased, BSFC is slightly decreased and it indicates the minimum value with diesel fuel type (D), which has the highest specific gravity ($SG_{15.5} = 0.833$). If BSFC is expressed in [liter/kW.hr], the consumption differences become more observable.

B. Volumetric Efficiency

The engine speed (N) has a major effect on volumetric efficiency. Fig. 3 shows that (η_v) has maximum value at an engine speed of 2500 rpm. The temperature of water is the second most effective factor on the volumetric efficiency. As the temperature is increased, the volumetric efficiency is decreased as a result of the decreasing density of the air entering the combustion chamber. It is concluded that the volumetric efficiency reaches the maximum value at a temperature of (65°C).

As normally aspirated diesel engines receive almost equal amounts of air and the power is controlled by the injection pulses and duration, then the throttle has no significant effect on the volumetric efficiency and the indicated differences are related to errors in the precision of the measurement of the manometer inside the air box. The fuel type has no substantial effect on the volumetric efficiency because the mixing of fuel and air takes place inside the cylinder and there is no visible influence for the evaporation of fuel after injection, on the induction of air.

C. Brake Thermal Efficiency (BTE)

The energy converted into power output was measured by the dynamometer. The dynamometer was also used to keep the engine speed at a constant value.

The torque was measured from the force imposed by the dynamometer. The recorded engine speed and the measured torque lead to the calculation of the output power, (5). To measure the energy transferred from the fuel to the engine, the mass flow rate of fuel was calculated, the net heating value (LHV) was obtained from an empirical relation (Mollenhauer and Tschoeke, 2010):

$LHV = 46.22 - 9.13 \times (SG)^2 + 3.68 \times (SG)$, and then (BTE) was found. In order to efficiently study the factors and find their optimum impact point, Taguchi techniques are employed. Results reveal that the throttle has a significant effect on the brake thermal efficiency (BTE) and Fig. 4 shows that (BTE) reaches its optimum point at 75% of the maximum throttle. The second significant factor affecting (BTE) is the water temperature. Within the operating range, (BTE) is directly increased as the water temperature is increased. From the test it is established that η_b has the optimum point at 80°C. The engine speed is the third effective factor on (BTE). (BTE) reaches the optimum point at an engine speed of 2500 rpm. Diesel fuel type has a minor effect on (BTE). However, increasing the specific gravity (SG) of the diesel fuel slightly increases (BTE). From the experiments, it is concluded that (BTE) is optimum for the diesel fuel type D which has $SG_{15.5^\circ C} = 0.833$.

The optimal values are obtained from using Taguchi method on the samples of test results for the variables indicated above as shown in Fig. 4. After conducting the confirmation test with the optimum combination (water temperature = 80 °C, throttle = 75%, N = 2500 rpm, fuel type (D)), the results show a value of 0.331 for (BTE). This value, which is obtained with the optimal data, as explained above, represents the maximum value which is confirmed though using only the optimized values of above mentioned parameters and it is the maximum value when compared to the other experiments. Therefore, the validity of this value is confirmed using Taguchi method, which is the case for this work.

D. Exergetic Efficiency

Since the exergetic efficiency takes into account not only the first but also the second law of thermodynamics, it provides a better measure of the performance for a thermal system. The fuel exergy (based on chemical exergy), expressed in (7), (8) and (9) for the four fuel types is calculated with procedures involving lower heating value (LHV). Exergetic efficiency (η_{II}) and S/N ratios for all experiments are calculated and the effects of factors are investigated as shown in Fig. 5. The throttle has a significant effect on the exergetic efficiency (η_{II}) and it has the optimum value at %75 of full throttle. Temperature of water is the second significant factor for (η_{II}). The pattern of the curve of (η_{II}) is increased as the temperature is increased and it has a maximum value at 80 °C.

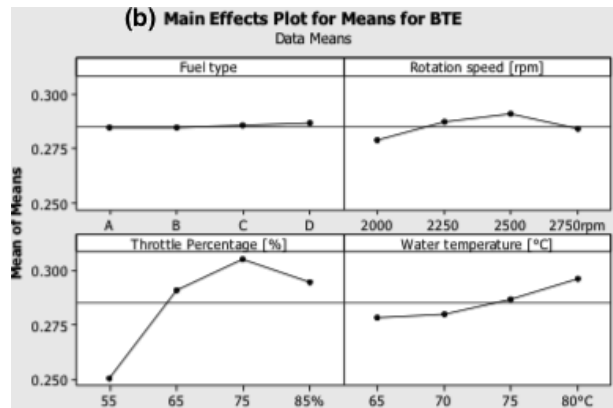
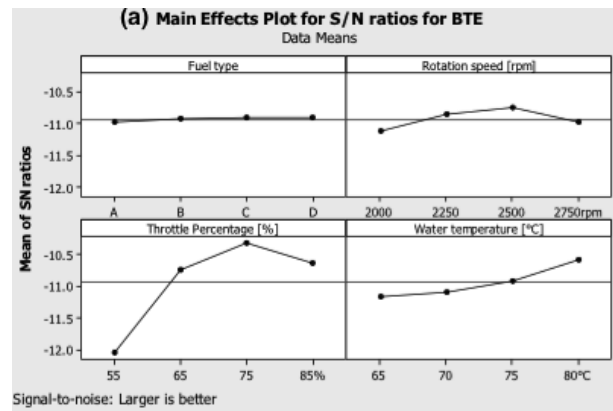


Fig. 4. Main effects plot of the S/N ratios and means for (η_b).

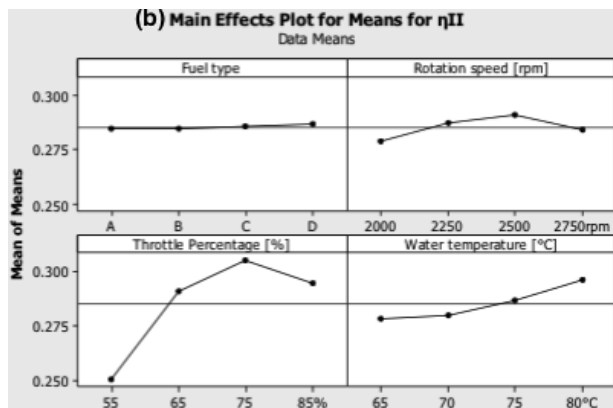
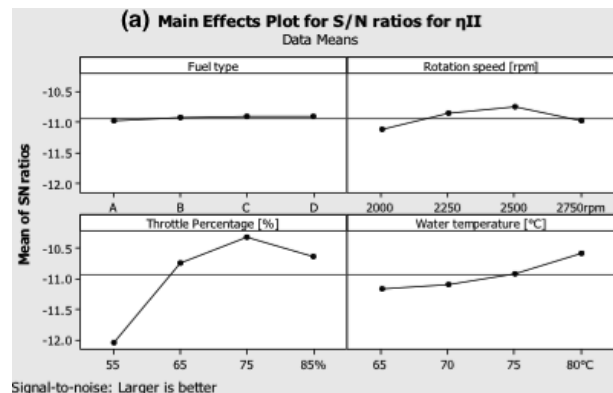


Fig. 5. Main effects plot of the S/N ratios and means for the exergetic efficiency.

Engine speed is the third effective factor for (η_{II}) and it has the peak value at 2500 rpm. Diesel fuel type has a minor effect on (η_{II}). However fuel type D achieves the optimum value of (η_{II}). Due to the fact that both exergetic efficiency and BTE are inherently expressing deviation from the ideal performance, their trends are also similar. However, the exergetic efficiencies are lower than the corresponding (BTE) because a higher amount of deviations are expressed in fuel exergy, compared to the fuel energy.

V. CONCLUSION

- a) The effectiveness of Taguchi methodology is underlined by replacing the required ($4^4 = 256$) tests, needed to decide the effect of parameters: engine speed, throttle and water temperature for four types of fuel by only 16 deciding experiments as indicated in Table II.
- b) The throttle has a proportional relation to break mean effective pressure as a result of the increase in the quantity of injected fuel. The best operating point was accomplished at 75% of full throttle.
- c) Throttle position has no effect on volumetric efficiency of test engine.
- d) Water temperature is second most effective parameter on engine operation for minimum BSFC. The optimum temperature for improved brake thermal and exergetic efficiencies is found to be 80°C.
- e) As the water temperature was increased the volumetric efficiency dropped. During the experiments, the maximum volumetric efficiency was recorded at a water temperature of 65°C.
- f) The optimum engine speed for the test engine, based on maximum volumetric efficiency, minimum BSFC and improved values of thermal and exergetic efficiencies was 2500 rpm.
- g) Fuel specific gravity has a limited effect on BSFC. It is shown from the results that the reduction in power caused by the reduction in volumetric flow rate is compensated by increasing the fuel density.

Future work can focus on applying a similar procedure to a direct injection diesel test rig, which is more susceptible to variation in diesel engine fuel type.

NOMENCLATURE

Symbol	Definition	Unit
A_i	Coefficient of the component i in the reaction equation	-
a_{fch}	Specific chemical exergy	kJ/kg
BSFC	Brake specific fuel consumption	g/kW.hr
BP	Brake power	kW
D	Orifice diameter	mm
E_d	Destroyed exergy	kJ
E_f	Fuel exergy	kJ
E_Q	Heat exergy	kJ
E_w	Work exergy	kJ

E_{ch}	Specific chemical exergy for a multicomponent stream	kJ/kg
h_e	Exit enthalpy	kJ/kg
h_i	Inlet enthalpy	kJ/kg
Hh	Manometer reading	mm
LHV	Lower heating value	kJ/kg
m_e	Exit mass flow rate	kg/sec
m_i	Inlet mass flow rate	kg/sec
N	Number of tests in a trial	-
N	Engine speed	Rpm
Q	Heat rate	Watt
Q_{cv}	Heat rejection	Watt
Q^o_f	Fuel energy rate	Watt
P_b	Brake power	Watt
R	Gas constant	kJ/kmole.K
SG	Specific gravity	-
S/N	Signal to noise ratio	-
T	Temperature	°C
T_o	Ambient temperature	°C
Tr	Torque	N.m
V^o	Volumetric flow rate	m ³ /sec
W^o	Rate of work	Watt
y_i	Molar ratio of i^{th} component in exhaust	-
y_i^o	Molar ratio of i^{th} component in the environment	-
Y_i	Value of the performance characteristic for a given experiment	-
Y_m	Nominal value of results	-
Greek letters		
η_b	Brake thermal efficiency	-
η_{II}	Exergetic efficiency	-
η_v	Volumetric efficiency	-
ρ	Density	kg/m ³
ω	Angular velocity	rad/sec
π	3.14	-

REFERENCES

Cussons, *Diesel Multi-cylinder Engine Test Bed Instructions Manual*, 1989 Cussons Technology Ltd.

Denton, T., 2011. *Automobile mechanical and electrical systems*, Butterworth-Heinemann, Elsevier.

Doe, 1993. *Fundamentals handbook of mechanical science*, 1, U.S. Department of Energy.

Garrett, T.K., 2001. *The motor vehicle* thirteenth edition, Butterworth Heinemann.

Lee, D.H., 2013. Development of a highly efficient low-emission diesel engine-power co-generation system and its optimization using Taguchi method. *Applied Thermal Engineering*, 50(2013), pp.491-495.

Kanog`lu, M., Isik, S.K. and Abuşog`lu, A., 2005. Performance characteristics of a diesel engine power plant. *Energy Conversion and Management*, 46(11-12), pp.1692-1702.

Mollenhauer, K., and H. Tschoeke, 2010. *Handbook of diesel engines*, Springer.

Nataraj, M., Arunachalam, V.P. and Dhandapani, N., 2005. Optimizing diesel engine parameters for low emissions using Taguchi method: variation risk analysis approach-Part I. *Indian Journal of Engineering & Materials Sciences*, 12(3), pp.169-181.

- Pulkrabek, W.W., 2004. *Engineering fundamentals of the internal combustion engine*, 2nd ed. Pearson Educational International.
- Rajput, R.K., 2008. *A text book of internal combustion engine*, 2nd Edition, Laxmi Publications.
- Rakopoulos, C.D., 2004. Availability analysis of a turbocharged diesel engine operating under transient load conditions, *Energy*, 29(8), pp.1085-1104.
- Ross, P., 1996. *Taguchi techniques for quality engineering*, 2nd ed. McGraw-Hill Book Company.
- Sayin, C., 2006. *Energy and exergy analyses of a gasoline engine*, Wiley Inter-Science, John Wiley & Sons, Ltd.
- Sekmen, P. and Yılbaşı, Z., 2010, Application of energy and exergy analyses to a CI engine using biodiesel fuel, *Mathematical and Computational Applications*, 16(4), pp.797-808.
- Sorathia, H.S. and Yadav, H.J., 2012. Energy analyses to a CI engine using diesel and bio-gas dual fuel; A review study. *International Journal of Advanced Engineering Research and Studies (IJAERS)*, 1(2), pp.212-217.
- Tamilvendhan, D., Ilangovan, V. and Karthikeyan, R., 2011. Optimization of engine operating parameters for eucalyptus oil mixed diesel fueled DI diesel engine using Taguchi method. *Journal of Engineering and Applied Sciences (ARPN)*, 6(6), pp.14-22.
- Wu, H-W., and Wu, Z-Y, 2013. Using Taguchi method on combustion performance of a diesel engine with diesel/biodiesel blend and port-inducting H₂. *Applied Energy*, 104, pp.326-370.
- Xiao, S., Sun, W., Du, J. and Li, G., 2014. Application of CFD, Taguchi method and ANOVA technique to optimize combustion and emissions in light duty diesel engine. *Mathematical Problems in Engineering*, Article ID 502902, 9 pages, doi:10.1155/2014/502902.
- Xin, Q., 2011. *Diesel Engine System Design*, Wood Head Publishing Limited.

Tissue-like P System for Segmentation of 2D Hexagonal Images

Rafaa I. Yahya^{1,2,3}, Siti Mariyam Shamsuddin^{1,2}, Shafaatunnur Hasan^{1,2} and Salah I. Yahya^{1,4}

¹UTM Big Data Center, Ibnu Sina Institute for Scientific and Industrial Research
Universiti Teknologi Malaysia, UTM Skudai, 81310 Johor, Malaysia

²Faculty of Computing, Universiti Teknologi Malaysia
UTM Skudai, 81310 Johor, Malaysia

³Department of Computer, Collage of science, University of Al-Mustansiriyah
Baghdad – F.R. Iraq

⁴Department of Software Engineering, Faculty of Engineering, Koya University
University Park, Danielle Mitterrand Boulevard, Koya KOY45, Kurdistan Region - F.R. Iraq

Abstract—Membrane computing, which is a new computational model inspired by the structure and functioning of biological cells and by the way the cells are organized in tissues. MC has been adopted in many real world applications including image segmentation. In contrast to the traditional square grid for representing and sampling digital images, hexagonal grid is an alternative efficient mechanism which can better represents and visualizes the curved objects. In this paper, a tissue-like P system with region-based and edge-based segmentations is used to segment two dimensional hexagonal images, wherein P-Lingua programming language is used to implement and validate the proposed system. The achieved experimental results clearly demonstrated the effectiveness of using hexagonal connectivity to segment two dimensional images in a less number of rules and computational steps. Moreover, the results reveal that this approach has the potential of segmenting large images in little number of steps.

Index Terms—Membrane computing, edge-based image segmentation, P-Lingua, region-based image segmentation, Tissue-like P system.

I. INTRODUCTION

Membrane Computing (MC) is a recent and fast growing branch of natural computing which is inspired by the structure and functioning of the living cell aiming to build computational models (Dang, et al., 2005). It takes its inspiration from the way that the living biological cells

employ to process chemical compounds in their compartmental structures.

Hence, in P systems (the computational models of MC), regions which are described by a membrane structure consist of objects evolving which based on specific evolution rules. Those objects can be represented by symbols or alternatively by strings of symbols, wherein multisets of objects are placed inside regions delimited by membranes.

Venn diagram and a tree-like structure are two different organizations of membranes where one membrane may contain other membranes inside it. The transaction from one configuration to another configuration can be accomplished by using the evolution rules in a non-deterministic and maximally parallel way. A series of transitions reveals how the P system is evolving. Different procedures of how to control the communication of objects from a region to another and how to apply the rules as well as membrane desolation, division or creation have been investigated widely in the literature (Păun, 2002).

As stated previously, MC gets the ideas of the cell aiming to learn mechanisms that could be useful from the perspective of computer science, but the research also takes into consideration how the cells are organized in tissues, as well as, the arrangement of neurons in the human brain. Based on this formalization, there are three basic variants of P systems, namely; (i) cell-like P system, (ii) tissue-like P system, and (iii) neural-like P system (Ibarra and Paun, 2006).

Different types of computing models known as P systems were proposed, motivated by biological related facts or inspired from mathematical or computer science perspectives. A vast number of applications were proposed in the past few decades in different domains – biology, bio-medicine, linguistics, computer graphics, economics, approximate optimization, cryptography and image processing (Paun, 2007).

In image processing, segmentation is the process of partitioning a digital image into separate regions, with the aim



of simplifying or modifying its representation to be more meaningful and easier to understand. Basically, image segmentation is used to find objects and boundaries (lines, curves and etc.) in digital images. Moreover, image segmentation is the method of giving labels to every pixel in an image,; in a way that pixels having same label have similar visual features (Shapiro and Stockman, 2001). The main objective of any image segmentation method is to perform segmentations in a sense that there is a high correlation between the entities of the real world objects and the regions of the segmentation (Kohler, 1981).

This paper is organized as follows: Section II provides a comprehensive summary of related works pertaining to image segmentation using P systems. A basic definition of tissue-like P systems is presented in Section III. Section IV describes the use of tissue-like P system for segmenting hexagonal images, region-based and edge-based segmentation. Section V presents the methodology of segmentation with membrane computing using P-Lingua programming language. The experimental results and comparison are presented in Section VI. Finally, Section VII concludes the paper and suggests some directions for the future work.

II. RELATED WORKS

MC possesses several interesting features including the encapsulation of data, a trivial way of representing information as well as the maximal parallelism, all of which are most proper when handling digital images.

Most recently, a number of research trends have been using MC approaches for solving problems pertaining to digital image processing. In a work relating to segmentation problems, Christinal, et al. (2009) have designed a family of tissue-like P system using communication and evolution rules to get edge-based segmentation of 2D image using 4-adjacency and 3D image using 26-adjacency. Their results have been obtained in a constant number of steps where the system has been implemented by tissue simulator software to check its validity and effectiveness. Christinal, et al. (2010) proposed a membrane computing approach to solve the threshold problem by using cell-like P system rules where the massive parallelism feature of MC has helped the solution to be reached in linear time which depends on the size of the input image.

Carnero, et al. (2010) have proposed a new hardware tool including a Field-Programmable Gate Array unit (FPGA) to perform segmentation of digital images for solving edge-based detection and noise removal problem. Their system uses MC method as well as a hardware programming (VHDL) language to propose an ad-hoc processor. In the same context, Reina-Molina, et al. (2010) have developed a new version of tissue-like P system by replacing the concept of one cell with the use of multiple auxiliary cells to deal with segmentation problem to get all the potential parallelization. In another work, Díaz-Pernil, et al. (2010) have proposed a new software tool for segmenting 2D digital images on the basis of tissue-like P system, wherein the object oriented C++ programming

language has been used in the implementation part. However, they did not provide a clear explanation regarding the technical aspects of developing the proposed tool.

Christinal, et al. (2011) have proposed a tissue-like P system (using communication rules) to perform a region-based segmentation in nine computational steps. In their work, 4-adjacency pixels neighborhood has been used to segment 2D digital images, whereas 26-adjacency has been employed for 3D digital images. A bio-inspired MC software has been proposed by Peña-Cantillana, et al. (2011) to solve the threshold problem and it has been implemented by an innovative device architecture called Compute Unified Device Architecture (CUDA™). Carnero, et al. (2011) have presented the use of the FPGA to implement tissue-like P system rules for solving segmentation problems. Sheeba, et al. (2011) have proposed tissue-like P system to segment medical image, nuclei of the white blood cells (WBCs) of the peripheral blood smear images in morphology segmentation technique. Their algorithm has been implemented using MATLAB software.

Similarly, Zhang and Peng (2012) have proposed novel infrared object segmentation based on thresholding method using cell-like P system to get the best set of parameters quickly. Christinal, et al. (2012) have proposed a variant of P system (tissue-like P system) using the rules to perform a parallel color segmentation of 2d images based on a threshold method. Peng, et al. (2012) have developed a novel threshold segmentation method based on cell-like P system to improve the performance of the threshold segmentation. Similarly, Yang, et al. (2013) have proposed an image segmentation approach using tissue-like P system to develop conventional region-based image segmentation.

In the work of Díaz-Pernil, et al. (2013), a CUDA™ has been presented to implement tissue-like P system rules for segmenting images by the use of gradient-based edge detection to enhance the traditional methods of segmenting digital images. Peng, et al. (2014) have proposed a novel segmentation by improving the traditional region-based colour image segmentation method using tissue-like P systems. Isawasan, et al. (2014) used tissue-like P system rules to perform region-based segmentation of 2D hexagonal images where the segmentation steps has been done in 7 steps, but they did not illustrate how they used P-Lingua to perform the segmentation. Peng, et al. (2015) have proposed a new method using cell-like P system to solve the optimal multi-level thresholding problem. Yahya, et al. (2015) have presented a traditional region-based segmentation with tissue-like P system rules. In their proposed work, a simple artificial image has been used to give a more detailed illustration of the basic idea of how P system works. Furthermore, various colour relations have been investigated to illustrate the effect of colors on the segmentation results.

As can be depicted from the literature review presented above, only one work has implemented the region-based segmentation in 6-adjacency of hexagonal image (Isawasan, et al., 2014). However, Isawasan, et al., did not clearly illustrate how their approach has been implemented in P-Lingua programming language. Hence, in this paper tissue-like P

system has been used to segment two dimensional hexagonal artificial images by employing both of edge-based segmentation and region-based segmentation, simultaneously, and illustrate the implementation of hexagonal segmentation in P-Lingua with more details.

Hexagonal grid is an efficient pixel tessellation scheme different from the traditional square grid for modelling and representing digital images. In contrast to square images, the pixels of the hexagonal images are much closer to each other which make the edges more clear and sharp. The main reasons to use hexagonal image processing are:

- 1) To improve the performance of the image recognition algorithms.
- 2) To minimize the computational complexity of processing the image and make it much faster.
- 3) By using this approach, image features can be detected more precisely (He and Jia, 2005).

In this paper, we comprehensively illustrate the idea of 2D image segmentation using hexagonal connectivity based on tissue-like P system. P-Lingua programming language has been used to perform segmentation and to check the validity of the proposed approach. For illustration purpose, a large artificial image with three colors is used to test the effectiveness of the system, as will be shown in Section V.

III. DEFINITION OF TISSUE-LIKE P SYSTEMS

Tissue-like P system, a variant of membrane computing models, was proposed by Martine vide (2003). The structure of tissue-like P systems is arranged as a graph having two biological inspirations, namely intercellular communications that represent all communication channels available between the cells as well as the communication between cells and environment. The second motivation pertaining to this model is the cooperation between neurons. Tissue-like P system has a distinguishing feature from the computational point of view which is cells do not have electrical charges (Păun, 2010).

Formally, a family of a tissue-like P system with input of degree q , 1 is a tuple (Pan and Pérez-Jiménez, 2010):

$$\Pi(n, m) = (\Gamma, \Sigma, w_1, \dots, w_q, R, i\Pi, o\Pi)$$

Where the components are defined as follows:

- 1) $\Gamma = \Sigma \cup \mathcal{E}$ is a finite alphabet where each symbol working is called object that is placed in a cell or surrounding the cell (in the environment).
- 2) $\Sigma \subseteq \Gamma$ is the input alphabet (the objects inside the cell)
- 3) $\mathcal{E} \subseteq \Gamma$ is an infinite set of objects that are available in the environment with arbitrary large amount of copies.
- 4) The multi-sets w_1, \dots, w_q represent the objects placed in the cells at the beginning of the computation.
- 5) R is the finite set of communication rules in the following form
 $(i, u/v, j)$ for $i, j \in \{0, 1, 2, \dots, q\}, i \neq j, u, v \in \Gamma$
- 6) $i\Pi \in \{1 \dots q\}$ refers to the input cell.
- 7) $o\Pi \in \{0, 1 \dots q\}$ refers to the output of the cell.

In the typical framework of MC, each cell is viewed as a computing unit working in a maximally parallel and non-deterministic manner. The configuration is an instantaneous description of the P system at a particular time, where a sequence of computation steps can be applied in a parallel way to get a new configuration. A computation is said to be successful if it halts, reaching a specific configuration where no more rules can be further applied to the current objects. With a halting computation, the associated output can be codified by the content of the output membrane.

IV. SEGMENTATION-BASED ON TISSUE-LIKE P SYSTEM OF 2D HEXAGONAL IMAGE

As can be depicted from the literature review presented previously, only one work has implemented the segmentation of hexagonal (6-adjacent) image (Isawasan, et al., 2014). The majority of the work reviewed was implemented using 4-adjacent. Isawasan, et al. (2014) have proposed the 6 adjacent in P-Lingua programming platform to obtain region-based segmentation, but they have not provide a comprehensive illustration of how to use P-Lingua or refer to the computational time of segmentation. Hence, this paper adopts the work of (Isawasan, et al., 2014) and obtains edge-based segmentation with region-based segmentation and presents in more details the implementation of P-Lingua as long as showing the time of execution by using a large artificial apple image.

We define a family of tissue-like P system to perform region-based segmentation for 2HD image as follows:

$$\Pi(n, m) = (\Gamma, \Sigma, w_1, w_2, R, i\Pi, o\Pi)$$

Where the components are defined as follows:

- 1) Finite all alphabets that working in the system is $\Gamma = \Sigma \cup \mathcal{E}$
- 2) The input is $\Sigma \subseteq \Gamma, \Sigma = \{a_{ij} : a \in C \wedge 1 \leq i \leq n \wedge 1 \leq j\}$
- 3) The object of environment is $\mathcal{E} \subseteq \Gamma$, where
 $\mathcal{E} = \{\bar{a}_{ij} : a \in C \wedge 1 \leq i \leq n \wedge 1 \leq j \leq m\} \cup \{Z_i : 1 \leq i \leq 7\}$
- 4) The multisets (objects placed in the cell1 and cell2) w_1, \dots, w_2 is
 $w_1 = z_1^{\lfloor r_1^{1/2^5} \rfloor}, 2 = \emptyset$, where $r_1 = \max(n, m)$
- 5) R represents the set of communication rules:

Type 1 rules:

$$(1, Z_i/Z_{i+1}^2)$$
 for $i = 1, \dots, 7$.

These communication rules make the counter Z_i be duplicated in each step.

Type 2 rules:

$$(1, a_{ij} b_{kl}/\bar{a}_{ij} b_{kl}, 0)$$
 for $a, b \in C, a < b, 1 \leq i, k \leq n$ and $1 \leq j, l \leq m$.

The type 2 of the rules is basically applied when two adjacent pixels having different colors, those pixels are called border pixels. For instance, the two adjacent pixels with different colours are shown in Fig. 1. The pixel which has small associated color will be marked, for example, if the system learned that Red colour is greater than Green then the green pixel (G) will be marked and brought from the environment the marked green pixel (Gx) instead of Green pixel for any of the possible directions as shown in Fig. 2.

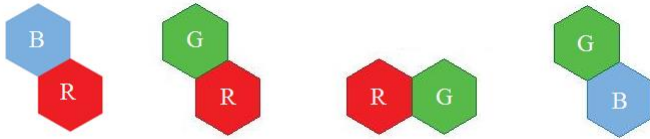


Fig. 1. Two adjacent pixels with different colors.



Fig. 2. Marked adjacent pixels using type 2 rules.

Type 3 rules:

$(1, Z_7 \bar{a}_{ij} / \lambda, 2)$ for $1 \leq i \leq n, 1 \leq j \leq m$.

These communication rules will take the marked pixel and send them to cell 2, where the marked pixel will be disappeared

- 1) The input of the cell is $i\pi = 1$.
- 2) The output of the cell
 - $o\pi = 1$ if we need to obtain the region based segmentation.
 - $o\pi = 2$ if we need to obtain the edge-based segmentation.

V. P-LINGUA FOR SEGMENTATION OF 2HD IMAGES

P-Lingua is considered as the standard and official programming language of MC (Díaz-Pernil, et al., 2009). This language is created to include all P systems variants (cell-like P systems (García-Quismondo, et al., 2009), tissue-like P system (Perez-Hurtado, et al., 2014) and neural-like P system (Macías-Ramos, et al., 2012)). The principal component in P-Lingua is a PLinguaCore Java library. PLinguaCore Java library accepts as input all text files, XML or P-Lingua format (.PLI), which describe the P system model. Furthermore, P-Lingua includes parsers to handle input files and built-in simulators to produce P system computations. It can export several output file formats to represent P systems. It is an open source product since expert developers with good knowledge

of Java can contribute and add new components to enlarge the library (García-Quismondo, et al., 2010).

In this paper, the tissue-like P system is used along with the PLinguaCore4 java library to implement the segmentation of the hexagonal artificial image as shown below in Fig. 3 which describes the methodology of segmentation implemented in P-Lingua platform.

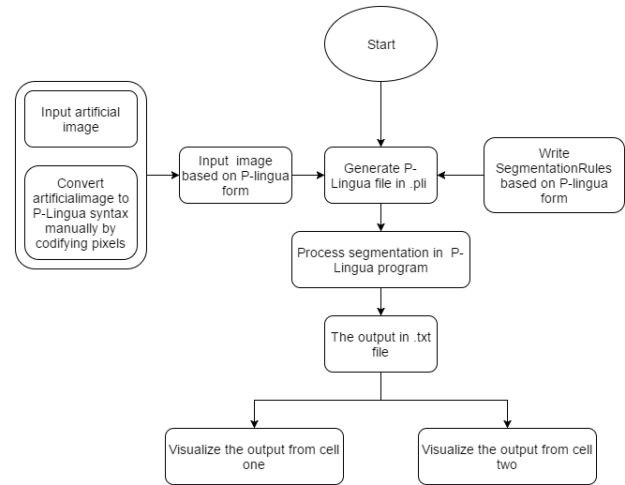


Fig. 3. Methodology of 2DH image segmentation.

A. Generating P-Lingua File in pli Format

The pixels of the artificial image along with the rules of segmentation of hexagonal 2D image (2DH) is written and placed together in one text file (.txt) and saved as P-Lingua file.Pli. Thus, the basic steps of generating P-Lingua file are explained in detail as shown below.

Input image based on P-Lingua form

The artificial apple image will be analyzed and codified manually as an input in a text file according to the standard syntax of P-Lingua.

1) Input artificial image

The image has hexagonal pixels that are manually codified and inserted into the system as an input image according to the standard syntax of P-Lingua. In tissue-like P system, the image is considered as a cell and the pixels of the image are represented as objects in the cell. Specifically, every pixel (object) has the color and coordinates (x, y) . In this paper, the artificial image used is a simple apple image with three colors (Red, Blue and Green) which has been drawn manually with size (13×13) as shown in Fig. 4.

2) Convert Image to P-Lingua Syntax

The pixels should have color and coordinates as mentioned earlier to match the syntax of P-Lingua. Basically, the color and the coordinates of each pixel will be read and converted to P-Lingua syntax. The standard syntax is to put the color of the

pixel followed by curly bracket that contain the coordinate of the associated pixel which in turn will be written in text files. For example, $R\{x, y\}$, where x and y are the coordinates of the red pixel in the image as shown below in Fig. 5. All pixels are converted to the syntax of P-Lingua by following this procedure.

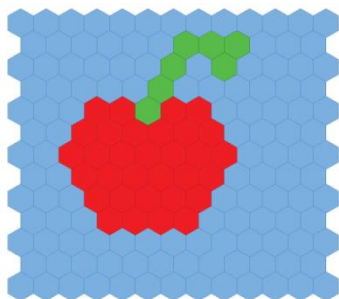


Fig. 4. Simple artificial apple image (size of 13x13).

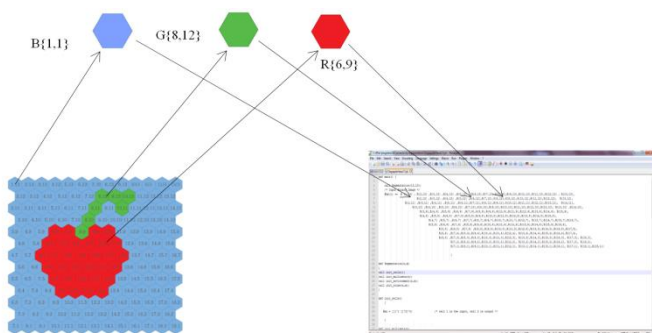


Fig. 5. Artificial apple image of (size 13x13) in P-Lingua syntax.

Writing the rules of segmentation based on P-Lingua form

In this paper, the segmentation rules is based on the rules of membrane computing for 2HD image segmentation method employed in (Isawasan, et al., 2014) . The rules are written in the P-Lingua format with input image and saved in a text file, but with (.Pli) extension. This file is now ready to be executed as shown in Appendix I.

Technically speaking, a 2D digital image can be represented by a matrix where each pixel in the image is an element of the matrix. Basically, in this paper, the 6-adjacent connectivity of neighborhoods surrounding a pixel is considered. The hexagonal pixels are:

$$\{(x, y + 1), (x, y - 1), (x + 1, y), (x - 1, y), (x - 1, y + 1), (x + 1, y - 1)\}$$

which contains 6 directions from the central pixel as demonstrated in Fig. 6.

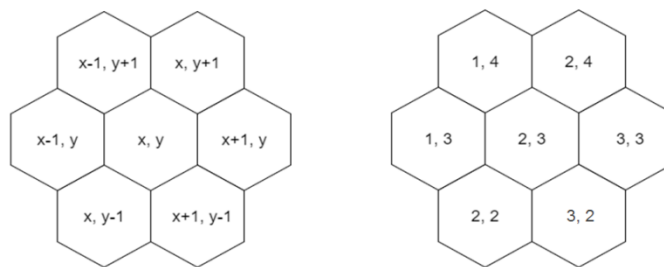


Fig. 6. Illustration of the 6-adjacent (hexagonal) neighborhoods.

When the image contains two different colors, namely Red and Blue, then if the six- adjacency (hexagonal) is considered, the segmentation rules will be as the following:

$$\begin{aligned} [B \{i, j\}, R \{i, j + 1\}]'1 &< \text{---} > [Bx \{i, j\}, R\{i, j + 1\}]'0; \\ [B \{i, j\}, R \{i, j - 1\}]'1 &< \text{---} > [Bx \{i, j\}, R\{i, j - 1\}]'0; \\ [B \{i, j\}, R \{i + 1, j\}]'1 &< \text{---} > [Bx \{i, j\}, R\{i + 1, j\}]'0; \\ [B \{i, j\}, R \{i - 1, j\}]'1 &< \text{---} > [Bx \{i, j\}, R\{i - 1, j\}]'0; \\ [B \{i, j\}, R \{i - 1, j + 1\}]'1 &< \text{---} > [Bx \{i, j\}, R\{i - 1, j + 1\}]'0; \\ [B \{i, j\}, R \{i + 1, j - 1\}]'1 &< \text{---} > [Bx \{i, j\}, R\{i + 1, j - 1\}]'0; \end{aligned}$$

B. Process segmentation in P-Lingua program

The PLinguaCore4 java library will simulate the P-Lingua rules to implement the segmentation of the artificial image. All the steps above are to prepare the P-Lingua file (image and rules of segmentation) for simulation by PLinguaCore4 Java library.

C. Output of segmentation in file.txt

The final result of the segmentation process is available in the file that is generated after segmentation (.txt). This file contains the details of every step of segmentation; it contains information like the configuration, input of the cell, the output of cell, the environment, the time of every step, memory used and final time of execution.

Once the image has been segmented using MC, bearing in mind that our model contains two different cells, the output can be read from any of these cells as needed. In the first case, if the output is being read from cell two, then edge-based segmentation will be obtained and visualized. It is worth mentioning that cell two contains the border and edge pixels, that is why edge-based segmentation can be obtained from this particular cell as shown in Fig. 7. Otherwise, in the second case if the output is being read from cell one, then, region-based segmentation will be obtained as shown in Fig. 8. More specifically, there are two types of segmentation strategies which can be obtained regarding the philosophy of reading the output from the chosen cell.

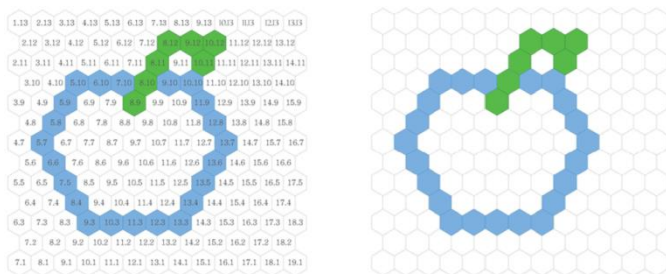


Fig. 7. Output of segmentation from cell 2 (edge-based).

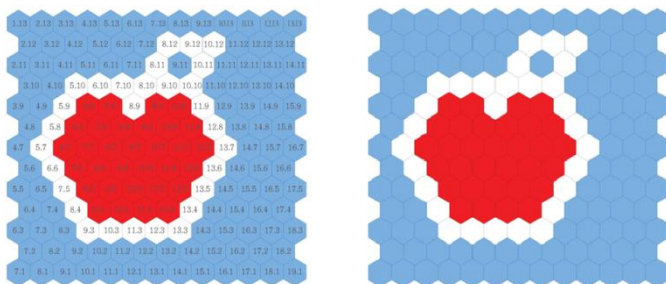


Fig. 8. Output of segmentation from cell 1 (region-based).

VI. EXPERIMENTAL RESULTS

According to the literature review, the majority of the works on image segmentation have used 4-adjacency to perform segmentation. Yahya, et al., (2015) presented the segmentation of an artificial apple image with size of 13×13 and three colours (Red, Blue and green) using 4-adjacency connectivity. The time of segmentation was not considered because the segmentation was achieved by implementing a tissue simulator. The same artificial apple image of (Yahya, et al., 2015) was used in this paper, and the total time needed for segmentation using 4 and 6-adjacency connectivity was achieved for the sake of comparison. The results are presented in Table I.

TABLE I
COMPARISON BETWEEN DIFFERENT TYPES OF CONNECTIVITY

Type of adjacency	Input image	Size of image	Time	Memory usage	No. of Configuration steps
4-adjacency	Apple	13×13	2.136 s	310272 kb	9
6-adjacency	Apple	13×13	1.327 s	178688 kb	7

It is obvious that using 6-adjacency is more efficient and the processing time is much faster than the 4-adjacency. Moreover, the number of computational steps has been reduced from 9 to 7 steps. The reason of the better performance of 6-adjacency connectivity, as compared with the 4-adjacency, is attributed to the fact that the computational

requirement for processing a hexagonally connected image is less than that for square sampled images due to the compact and circular nature of the hexagonal connectivity. There are many conclusions can be drawn from the results in Table I. However, the main conclusion is; the number of edge pixels using both 4 and 6-adjacency were roughly the same but the edge detected of hexagonal-image appears to be qualitatively better. This stems from the consistent connectivity of the pixels in hexagonal-images which aids image segmentation. The hardware platform that used to achieve the results of this paper is a PC with an Intel® Core™ i5-M430 processor running at 2.27 GHz and 4 GB of memory.

VII. CONCLUSION

In this paper, tissue-like P system, a variant of MC, is used to segment two dimensional hexagonal artificial images by employing edge-based segmentation and region-based segmentation. P-Lingua programming language is used to implement and validate the proposed P system. The experimental results have shown that the use of the hexagonal connectivity is more efficient than the four connectivities where the number of rules and computational steps have been reduced from 9 steps to 7 steps. Finally, we can conclude that the use of hexagonal-images rather than the classical square-images for image segmentation has several advantages as demonstrated in this paper. These are due mainly to the connectivity of the individual hexagonal pixels generating more consistent contours. The proposed framework of segmentation offers an added advantage in using hexagonal-images for image segmentation, namely, great computational savings. This makes a strong case for hexagonal-based image segmentation and seems to reinforce the point that hexagonal-image processing has the potential to be a viable alternative to square-image processing in the future. However, the major limitation of the proposed approach is that the images are codified manually in the system. The reason for that is the hard processing of hexagonal images compared with the traditional square image. In our future work, we aim to find an automatic solution to enter the hexagonal-image in the system.

ACKNOWLEDGMENT

This work is partially supported by The Malaysian Ministry of Higher Education under the fundamental research grant scheme (4F802 and 4F786). The authors would like to thank the Research Management Centre (RMC), Universiti Teknologi Malaysia (UTM) for the support in R&D. The first author is grateful to the Iraqi Ministry of Higher Education for sponsoring her Ph.D. study.

REFERENCES

- Carnero, J., Diaz-Pernil, D. and Gutierrez-Naranjo, M.A., 2011. Designing tissue-like P systems for image segmentation on parallel architectures. *Ninth Brainstorming Week on Membrane Computing*, pp.43-62.

- Carnero, J., Diaz-Pernil, D., Molina-Abril, H. and Real, P., 2010. Image segmentation inspired by cellular models using hardware programming. *3rd International Workshop on Computational Topology in Image Context, 2010*. pp.143-150.
- Christinal, H.A., Diaz-Pernil, D., Gutierrez-Naranjo, M.A. and Perez-Jimenez, M.J., 2010. Thresholding of 2D images with cell-like P systems. *Romanian Journal of Information Science and Technology (ROMJIST)*, 13, pp.131-140.
- Christinal, H.A., Diaz-Pernil, D. and Jurado, P.R., 2009. Segmentation in 2D and 3D image using tissue-like P system. *Progress in Pattern Recognition, Image Analysis, Computer Vision, and Applications*, 5856, pp.169-176.
- Christinal, H.A., Diaz-Pernil, D. and Jurado, P.R. and Selvan, S.E., 2012. Color Segmentation of 2D Images with Thresholding. *Eco-friendly Computing and Communication Systems*, 305, pp.162-169.
- Christinal, H.A., Diaz-Pernil, D. and Real, P., 2011. Region-based segmentation of 2D and 3D images with tissue-like P systems. *Pattern Recognition Letters*, 32(16), pp.2206-2212.
- Dang, Z., Ibarra, O.H., LI, C. and Xie, G., 2005. On model-checking of P systems. *Unconventional Computation*, 8340, pp.151-172.
- Diaz-Pernil, D., Berciano, A., Pena-Cantillana, F. and Gutierrez-Naranjo, M.A., 2013. Segmenting images with gradient-based edge detection using Membrane Computing. *Pattern Recognition Letters*, 34(8), pp.846-855.
- Diaz-Pernil, D., Molina-Abril, H., Real, P. and Gutierrez-Naranjo, M.A., 2010. bio-inspired software for segmenting digital images. Bio-Inspired Computing: Theories and Applications (BIC-TA). In: *IEEE Fifth International Conference, 2010*, IEEE, pp.1377-1381.
- Diaz-Pernil, D., Perez-Hurtado, I., Perez-Jimenez, M.J. and Riscos-Nunez, A., 2009. A P-lingua programming environment for membrane computing. *Membrane Computing*, 5391, pp.187-203.
- Garcia-Quismondo, M., Gutierrez-Escudero, R., Martinez-Del-Amor, M.A., Orejuela-Pinedo, E. and Perez-Hurtado, I., 2009. P-Lingua 2.0: A software framework for cell-like P systems. *Int J Comput Commun Control*, 4(3), pp.234-43.
- Garcia-Quismondo, M., Gutierrez-Escudero, R., Perez-Hurtado, I., Perez-Jimenez, M.J. and Riscos-Nunez, A. 2010. An overview of P-Lingua 2.0. *Membrane Computing*, 5957, pp.264-288.
- HE, X. and Jia, W., 2005. Hexagonal structure for intelligent vision. Information and Communication Technologies. In: *First International Conference on ICICT 2005*, IEEE, pp.52-64.
- Ibarra, O.H. and Paun, G., 2006. Membrane computing: A general view. *Ann Eur Acad Sci. EAS Publishing House, Liege*, pp.83-101.
- Isawasan, P., Venkat, I., Subramanian, K., Khader, A., Osman, O. and Christinal, H., 2014. Region-based segmentation of Hexagonal digital images using membrane computing. In: *Asian Conference on Membrane Computing (ACMC), 2014*. IEEE, pp.1-4.
- Kohler, R. 1981. A segmentation system based on thresholding. *Computer Graphics and Image Processing*, 1594, pp.319-338.
- Macias-Ramos, L.F., Perez-Hurtado, I., Garcia-Quismondo, M., Valencia-Cabrera, L., Perez-Jimenez, M. J. and Riscos-Nunez, A., 2012. A P-Lingua Based Simulator for Spiking Neural P Systems. *Membrane Computing*, 7184, pp.257-281.
- Martin-Vide, C., Pazos, J., Paun, G. and Rodriguez-Paton, A., 2002. A new class of symbolic abstract neural nets: Tissue P systems. *Computing and Combinatorics*. 2387, pp.290-299.
- Pan, L. and Perez-Jimenez, M.J., 2010. Computational complexity of tissue-like P systems. *Journal of Complexity*, 26(3), pp.296-315.
- Paun, G., 2007. Tracing some open problems in membrane computing. *Romanian Journal of Information Science and Technology*, 10(4), pp.303-314.
- Paun, G., 2002. Introduction: Membrane Computing—What It Is and What It Is Not. *Membrane Computing*. pp.1-6.
- Paun, G., 2010. A quick introduction to membrane computing. *The Journal of Logic and Algebraic Programming*, 79(6), pp.291-294.
- Pena-Cantillana, F., Diaz-Pernil, D., Berciano, A. and Gutierrez-Naranjo, M. A., 2011. A parallel implementation of the thresholding problem by using tissue-like P systems. *Computer Analysis of Images and Patterns, Computer Analysis of Images and Patterns - 14th International Conference, CAIP 2011*, August pp.29-31, 2011, Seville, Spain.
- Peng, H., Shao, J., LI, B., Wang, J., Perez-Jimenez, M. J., Jiang, Y. and Yang, Y., 2012. Image thresholding with cell-like P systems. In: *Proceedings of the Tenth Brainstorming Week on Membrane Computing*, 2.
- Peng, H., Wang, J. and Perez-Jimenez, M.J., 2015. Optimal multi-level thresholding with membrane computing. *Digital Signal Processing*, 37, pp.53-64.
- Peng, H., Yang, Y., Zhang, J., Huang, X. and Wang, J., 2014. A Region-based Color Image Segmentation Method Based on P Systems. *Science and Technology*, 17(1), 63-75.
- Perez-Hurtado, I., Valencia-Cabrera, L., Chacon, J.M., Riscos-Nunez, A. and Perez-Jimenez, M. J., 2014. A P-Lingua based Simulator for Tissue P Systems with Cell Separation. *Science and Technology*, 17(1), pp.89-102.
- Reina-Molina, R., Carnero, J. and Diaz-Pernil, D., 2010. Image segmentation using tissue-like P systems with multiple auxiliary cells. *Image-A*, 1, pp.143-150.
- Shapiro, L. and Stockman, G.C., 2001. *Computer Vision*. 1st ed. Prentice Hall.
- Sheeba, F., Thaburaj, R., Nagar, A.K. and Mammen, J.J., 2011. Segmentation of peripheral blood smear images using tissue-like P systems. Bio-Inspired Computing: Theories and Applications (BIC-TA), *2011 Sixth International Conference on*, IEEE, pp.257-261.
- Yahya, R.I., Hasan, S., George, L.E. and Alsalibi, B., 2015. Membrane Computing for 2D Image Segmentation. *Int. J. Advance Soft Compu. Appl*, 7(1), pp.35-50.
- Yang, Y., Peng, H., Jiang, Y., Huang, X. and Zhang, J., 2013. A region-based image segmentation method under P systems. *J. Inf. Comput. Sci*, 10(10), pp.2943-2950.
- Zhang, Z. and Peng, H., 2012. Object segmentation with membrane computing. *Journal of Information & Computational Science*, 9, pp.5417-5424.

APPENDIX I

Rules of Segmentation Using six Adjacency in P-Lingua Syntax

```

def init_cells()
{
  @mu = [[ ]'1 [ ]'2]0;          /* cell 1 is the input, cell 2 is output */
}
def init_multisets(n)           /* define the initial multisets*/
{
  @ms(1) += z{1} ;
}
def init_environment(n,m)      /*define the environment */
{
  @ms(0) += z{i}: 1<=i<=7;      /*define the Z counter */
  @ms(0) += Gx {i,j},Bx {i,j},R {i,j} ,B {i,j},G {i,j}: 1<=i<=n ,1<=j<=m;
}
/* ***** Rules ***** */
def init_rules(n,m)
{
  /****** Type 1 rules ***** */
  /* Type one the rule is used to increment the counter z after each
  configuration duplicating the number of copies in each step */
  /*R1*/ [z{i}]'1 <-> [z{i+1}]'2]0 : 1 <= i <= 7;
  {
    /****** Type 2 rules ***** */

    /* ***** G<B ***** */
    /*Type two the rules are used when the image has two adjacent pixels with
    different colours, so it will mark the pixel with the less associated colour.
    Pixel Gx will be marked because it is less than B. */
    /*R2,1*/ [G {i,j} , B {i,j+1}]'1 <-> [Gx {i,j} , B {i,j+1}]'0;
  }
}

```

```

/*R2,2*/ [G {i,j} , B {i,j-1}]'1 <--> [Gx {i,j} , B{i,j-1}]'0;
/*R2,3*/ [G {i,j} , B {i+1,j}]'1 <--> [Gx {i,j} , B{i+1,j}]'0;
/*R2,4*/ [G {i,j} , B {i-1,j}]'1 <--> [Gx {i,j} , B{i-1,j}]'0;
/*R2,5*/ [G {i,j} , B {i-1,j+1}]'1 <--> [Gx {i,j} , B{i-1,j+1}]'0;
/*R2,6*/ [G {i,j} , B {i+1,j-1}]'1 <--> [Gx {i,j} , B{i+1,j-1}]'0;
      }; 1 <= i <= n , 1 <= j <= m;
      {

```

```

/* ***** B<R ***** */

```

```

/*Type two the rules are used when the image has two adjacent pixels with
different colours, so it will mark the pixel with the less associated colour.
Pixel Bx will be marked because it is less than R. */

```

```

/*R2,1*/ [B {i,j} , R {i,j+1}]'1 <--> [Bx {i,j} , R{i,j+1}]'0;
/*R2,2*/ [B {i,j} , R {i,j-1}]'1 <--> [Bx {i,j} , R{i,j-1}]'0;
/*R2,3*/ [B {i,j} , R {i+1,j}]'1 <--> [Bx {i,j} , R{i+1,j}]'0;
/*R2,4*/ [B {i,j} , R {i-1,j}]'1 <--> [Bx {i,j} , R{i-1,j}]'0;
/*R2,5*/ [B {i,j} , R {i-1,j+1}]'1 <--> [Bx {i,j} , R{i-1,j+1}]'0;
/*R2,6*/ [B {i,j} , R {i+1,j-1}]'1 <--> [Bx {i,j} , R{i+1,j-1}]'0;
      }; 1 <= i <= n , 1 <= j <= m;
      {

```

```

/* ***** G<R ***** */

```

```

/*Type two the rules are used when the image has two adjacent pixels with
different colours, so it will mark the pixel with the less associated colour.
Pixel Gx will be marked because it is less than R. */

```

```

/*R2,1*/ [G {i,j} , R {i,j+1}]'1 <--> [Gx {i,j} , R{i,j+1}]'0;
/*R2,2*/ [G {i,j} , R {i,j-1}]'1 <--> [Gx {i,j} , R{i,j-1}]'0;
/*R2,3*/ [G {i,j} , R {i+1,j}]'1 <--> [Gx {i,j} , R{i+1,j}]'0;
/*R2,4*/ [G {i,j} , R {i-1,j}]'1 <--> [Gx {i,j} , R{i-1,j}]'0;
/*R2,5*/ [G {i,j} , R {i-1,j+1}]'1 <--> [Gx {i,j} , R{i-1,j+1}]'0;
/*R2,6*/ [G {i,j} , R {i+1,j-1}]'1 <--> [Gx {i,j} , R{i+1,j-1}]'0;
      }; 1 <= i <= n , 1 <= j <= m;

```

```

/* ***** Type 3 ***** */

```

```

/* Type three the rules are used to send the marked pixels to the environment
using counter z*/

```

```

/*R3*/ [z{7},Gx {i,j}]'1 <--> [#]2 : 1 <= i <= n , 1 <= j <= m;
/*R3*/ [z{7},Bx {i,j}]'1 <--> [#]2 : 1 <= i <= n , 1 <= j <= m;
      }

```

Hemodynamic, Thyroid and Immunomodulatory Effects of Heroin in Rats

Ismail M. Maulood

Department of Biology, College of Science, Salahaddin University
Kurdistan Region – F.R. Iraq

Abstract—Diacetylmorphine (heroin) has many effects on the body system; it exerts effects on cardiovascular, immune and endocrine systems. The aim of this study is to investigate the short-term effects of low and high doses of heroin on systolic blood pressure (SBP), thyroid hormones and monocyte chemoattractant protein-1 (MCP-1). The experimental rats were divided into three groups, each with six individuals and the treatments were continued for seven days. SBP significantly reduced by heroin administration in the second dose as compared with the control group. A marked decrease in the serum NO level was also noticed after first (low) and second (high) dose of administration as compared with control group. The present results also revealed that serum MCP-1 was statistically increased in the second dose of heroin group. Statistical analysis showed that both serum T3 and T4 levels were reduced significantly by heroin administration. In conclusions, for the first time, our findings suggested that diacetylmorphine could affect immune system through MCP-1 elevation. As well as heroin may affect cardiac and liver functions via increasing troponin-T and bilirubin levels.

Index Terms—Blood pressure, Heroin, MCP-1, Thyroxine, Troponin-T.

I. INTRODUCTION

Heroin (diacetylmorphine) is an opioid analgesic synthesized adding two acetyl groups to morphine molecule. Morphine affects some physiological functions like hemodynamics, gastrointestinal function, respiration, and immunoregulation (Xu, et al., 1997), they also demonstrated that intravenous morphine enhances the NO levels through cholinergic and adrenergic mechanism. Furthermore, (Fonarow, 2002) resulted that may induce hypotension, bradycardia, regulation of sympathetic and parasympathetic nerve system through venodilation mechanism. Long term

administration of morphine alters immune system (Szabo, et al., 1993) demonstrating that macrophages may be attenuate after morphine exposure. Strong evidence has been established in the modulation of the immune system by morphine administration. (Wetzel, et al., 2000) indicated that μ -opioid may change produce MCP-1, which has an important role in proinflammatory reactions and cell-mediated immune responses.

On the other hand, heroin may alter some endocrine glands. Recently, (Bhoir, et al., 2009) reported that heroin caused necrosis in the follicular epithelial cells of the thyroid gland. Furthermore, most recent data showed that addiction of opium could cause elevation of thyroid stimulating hormone (TSH) and reduction of T4 hormone. Besides those above effects of heroin, the wide spectrum of kidney alteration was found among heroin users (Cunningham, et al., 1984). Also, (Dettmeyer, et al., 2005) revealed that heroin is highly associated with nephropathy. The effects of diacetylmorphine on hemodynamics, immune system, and thyroid hormone are largely unknown. Accordingly, the aim of the current study was to investigate the short-term effects of a low and high dose of heroin on blood pressure, troponin-T (a marker for acute myocardial infarction), thyroid hormones and MCP-1 as a marker in proinflammatory reactions and cell-mediated immune responses.

II. MATERIALS AND METHODS

A. Morphine (Heroin) Preparation

An adequate amount of diacetylmorphine or diamorphine or heroin was obtained by Narcotics Control Directorate in Erbil province-Iraq. For laboratory preparation, 250 mg of diamorphine powder was mixed with 25 mg of citric acid, then the mixture was dissolved in 0.8ml of D.W at 40 °C, they mixed well by using tip of needle, then the solution was heated over a flame until observing bubbles and the remaining solution was taken by 1ml then it diluted to 5mg/ml. One ml was injected to 1kg body weight (b.w.) of rats (5mg Heroin/kg b.w. rats), while another dilution was taken for the second dose by suspending the stock solution in sterilized distilled water.

ARO-The Scientific Journal of Koya University
Volume IV, No 1(2016), Article ID: ARO.10097, 05 pages
DOI: 10.14500/aro.10097

Received 17 July 2015; Accepted 02 March 2016

Regular research paper: Published 18 May 2016

Corresponding author's e-mail: ismail.maulood@su.edu.krd

Copyright © 2016 Ismail M. Maulood. This is an open access article distributed under the Creative Commons Attribution License.



B. Animals and Housing

Eighteen adult female albino rats were involved in this study. All rats were weighing about (250 - 290 grams) at the time when the injection started. Rats were housed in standard plastic cages and they bedded with wooden chips. They were housed under normal laboratory conditions like 12:12 dark / light photoperiod at 23 ± 2 °C. The rats were given standard pellets and tap water *ad libitum*.

C. Experimental Design

The current experiment was designed to study the impacts of two doses of heroin on blood pressure, thyroid and renal function measurements. The experimental rats were divided into three groups, each with six individuals and the treatment injections were continued for seven days as the following:

Group 1: Control. The animals were injected with normal saline and the rats were given standard rat chow. Group 2: Dose 1. The rats were given standard rat chow and they were injected with diacetylmorphine (1 mg/kg) intraperitoneal. Group 3: The rats were given standard rat chow and the animals were injected with diacetylmorphine (5 mg/kg) intraperitoneal.

D. Collection of Blood Samples

At the end of the experiment, the animals were anesthetized by 50 mg/kg of ketamine.

The sample of blood were taken by cardiac puncture into plastic tubes and centrifuged at 3000 rpm for 20 minutes. The sera were stored at -80 °C until use.

E. Blood Pressure and Heart Rate Measurements

Measurements of SBP and heart rate were measured by the tail-cuff method in all groups using power Lab. (AD Instruments, power lab 2/25). The rats were placed in a special rat restrain chamber and they warmed up to about 37 °C. Five readings were taken for each rat, and the highest and lowest values were neglected. The average was taken of the remaining readings.

F. Biochemical Determination

Serum Total Nitric Oxide Measurement

Serum total NO was determined by NO non -enzymatic assay kit (US Biological, USA).

Determination of Serum T_3 , T_4 and Troponin-T

Serum T_3 , T_4 and Troponin-T were determined by electrochemiluminescence immunoassay "ECLIA" using Elecsy and Cobas immunoassay analyzers.

Determination of serum creatinine level

Creatinine level was determined by colorimetric method kit (BIOLABO. SA, France). Creatinine in alkaline picric acid solution, forms a color complex in which the absorbance was measured at 490 nm using spectrophotometer.

Determination of serum urea

Urea was determined by enzymatic test kit (BIOLABO. SA, France). The color intensity was measured at 600 nm.

Determination of serum total protein

Serum total protein was determined by biuret method, using colorimetric test kit (Biolab, France).

Determination of Serum Albumin

Serum albumin was determined by BCG method, using colorimetric test kit (Biolab, France).

Determination of Serum Total Bilirubin

Serum total bilirubin was determined by sulfanilic acid method ((BIOLABO. SA, France).

Determination of Serum Sodium, Potassium and Chloride Ion Concentrations

Serum Na^+ , K^+ and Cl^- ion concentrations were determined by using automated electrolyte analyzer (ELITE, USA).

Serum total calcium ion determination

Ca^{2+} -Kit enables colorimetric determination of total calcium without deproteinization. In serum, the calcium kit reacts with methylthymol blue indicator (MTB) in an alkaline medium. The color intensity of the Ca^{2+} -MTB complex, measured at 612 nm, is proportional to the quantity of calcium present in the sample. The kit was obtained from (BIOLABO.SA, France).

Determination of serum inorganic phosphate

Serum inorganic phosphate was determined by the ultra violet method. The absorbance measured at 340 nm is proportional to phosphate ions in the specimen (BIOLABO . SA, France).

G. Statistical Analysis

The obtained data were expressed as means \pm standard error (SE) and statistical analysis was performed using statistical programmed for social science (SPSS version 15). Analysis of data was made by one-way analysis of variance (ANOVA). Then the comparisons between groups were done using Duncan post hoc analysis. P values <0.05 are considered as statistical significant.

III. RESULTS

As shown in Fig. 1, SBP significantly reduced by heroin administration in the second dose (108.66 ± 4.200 mm Hg) as compared with the control group(123.66 ± 5.841 mmHg). On the other hand, H.R was lowered by heroin in the first dose of it administration (Fig. 2). A marked decrease in the serum NO level was also noticed after the first and second dose of administration as compared with control group (Fig. 3).

Table I shows that serum Na^+ concentration tended to decrease significantly in the second dose while no significant differs were observed in serum PO_4 , K^+ and Cl^- concentrations. Diacetylmorphine administration significantly decreased serum ionized Ca^{2+} from 1.270 ± 0.109 mmol/L in control rats to 0.876 ± 0.0242 mmol/L in heroin group.

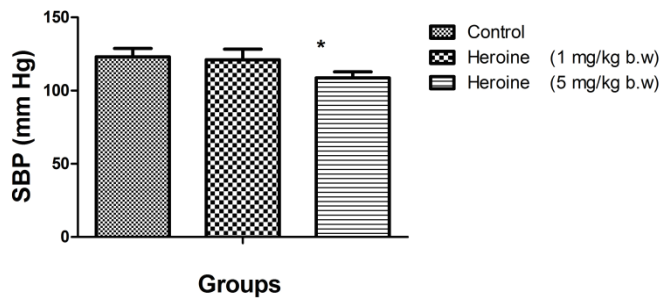


Fig. 1. Effects of heroin on SBP in rats.

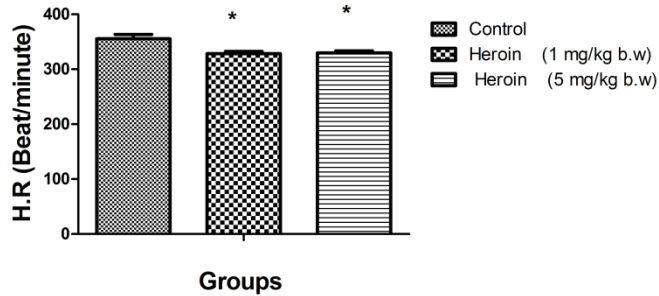


Fig. 2. Effects of heroin on H.R in rats.

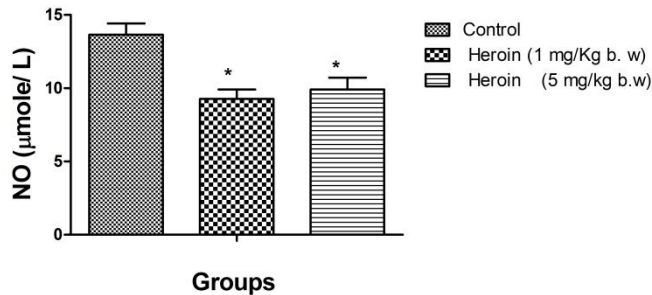


Fig. 3. Effects of heroin on serum NO in rats.

Table I shows that serum Na⁺ concentration tended to decrease significantly in the second dose while no significant differs were observed in serum PO₄⁻, K⁺ and Cl⁻ concentrations. Diacetylmorphine administration significantly decreased serum ionized Ca⁺² from 1.270 ± 0.109 mmol/L in control rats to 0.876 ± 0.0242 mmol/L in heroin group.

In Fig. 4, the results reveal that serum MCP-1 was statistically increased in the second dose of heroin group (22.70 ± 4.736 ng/ml) as compared with control rats (7.857 ± 1.208 ng/ml)

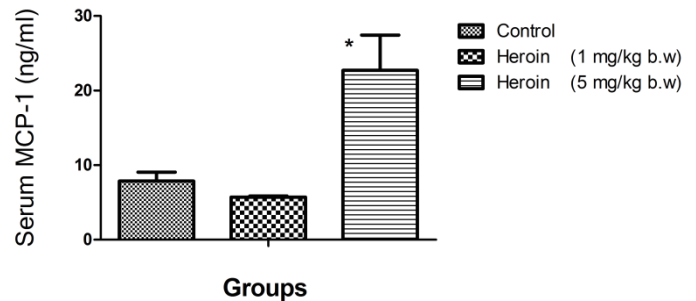


Fig. 4. Effects of heroin on serum MCP-1 in rats.

Statistical analysis also revealed both serum T₃ and T₄ levels was reduced significantly by heroin administration. Table II shows some liver and renal function test parameters; here only serum total bilirubin and serum urea were increased, whereas, serum total protein, serum albumin and serum creatinine did not statistically differ among the studied groups.

Serum troponin-T did not significantly alter in the first dose (Table II), while second dose caused a marked decrease in troponin-T concentration (0.3517 ± 0.0878) as compared with control group (1.652 ± 0.760).

TABLE I
EFFECTS OF HEROIN ON SERUM T₃, T₄, ELECTROLYTES, CALICUM AND PHOSPHATE IN ALBINO RATS.

Groups Parameter	Control	Heroin (1 mg/Kg b.w)	Heroin (5mg/Kg b.w)
T ₃ (nmol/L)*	1.4360±0.0271 ^a	1.3200±0.0255 ^{ab}	1.0967±0.1330 ^b
T ₄ (nmol/L)*	55.798±5.0165 ^a	54.768±3.5061 ^a	38.455±4.8212 ^b
Serum Na ⁺ *(meq/L)	167.40±2.2494 ^a	164.40±2.2045 ^a	142.20±6.7852 ^b
Serum K ⁺ *(meq/L)	4.9400±0.1326 ^a	4.8200±0.1462 ^a	4.6200±0.1496 ^a
Serum Cl ⁻ *(meq/L)	122.00±4.3703 ^{ab}	125.20±1.5297 ^b	110.60±5.3254 ^a
Serum Ca ⁺² *(mg/dL)	1.2700±0.1090 ^a	1.1800±0.0406 ^a	0.8760±0.0242 ^b
Serum PO ₄ ⁻ *(mg/dL)	9.0930±1.4398 ^a	9.5543±1.10899 ^a	10.6008±1.1806 ^a

TABLE II
EFFECTS OF HEROIN ON SERUM TROPONIN-T, SOME LIVER AND RENAL FUNCTION TEST PARAMETERS IN ALBINO RATS

Groups Parameter	Control	Heroin (1 mg/Kg b.w)	Heroin (5 mg/Kg b.w)
Serum troponin-T *	1.6520±0.7601 ^a	1.8267±0.3414 ^{ab}	0.3517±0.0878 ^b
Serum total protein (gm/dL)	8.8000±0.4131 ^a	8.9333±0.5529 ^a	9.4000±0.2250 ^a
Serum bilirubin (mg/dL)*	0.1345±0.0150 ^a	0.1960±0.0066 ^b	0.2713±0.0166 ^c
Serum creatinine (mg/dL)	0.5351±0.080 ^a	0.393±0.1139 ^a	0.807±0.2733 ^a
Serum urea (mg/dL)*	20.60±3.2749 ^a	22.72±3.9487 ^a	80.60±19.84 ^b
Serum uric acid (mg/dL)*	13.055±1.0243 ^a	11.111±0.7657 ^{ab}	9.1667±1.4433 ^b

The data is expressed as mean \pm S.E. The same letters mean no significant differences. The different letters mean significant differences * $P < 0.05$ and according to 1 way ANOVA followed by Duncan post hoc test.

IV. DISCUSSION

As shown in Fig. 1, statistical analysis revealed that SBP was significantly decreased in heroin administered rats as compared with control. The possible mechanism of BP reduction would be through direct inhibition of the sympathetic nervous system (Fonarow, 2002; Mori, et al., 1998). On the other hand, Chang, et al. (2012) reported that diacetylmorphine users show decreased cardiac vagal activity. The reduction in heart rate (H.R) as obtained by the present result (Fig. 2) also may be involve in decreasing blood pressure (BP) which is consistent with (Newby, et al., 2007) showing that heroin administration is promptly induced marked bradycardia (and a concomitant reduction in cardiac output. Interestingly, the result of the present study illustrated in Table II, showed that heroin administration for seven days had a reduction effect on serum troponin-T. Liu, et al. (2011) resulted that heroin significantly can ameliorate hemodynamic parameters and reduce serum troponin I concentration. Calcium ions may also participate in such reduction of BP, as seen in Table I, heroin administration caused a significant decrease in serum ionized Ca^{+2} . It has also been reported that serum

Ca^{+2} concentrations of diacetylmorphine addicts shows a significant decrease compared to that of the control group (Li, et al., 2011). In our finding, however, serum NO level was significantly reduced by heroin administration as compared with control group (Fig. 3). (Habibey, et al., 2010) also resulted that morphine significantly could decrease plasma NO levels in rats. Such results may be due to the compensatory mechanism for decreased BP. Also, (Rezazadeh, et al., 2014) resulted that morphine significantly attenuate systolic blood pressure, diastolic blood pressure, and mean arterial pressure in the 2K1C animals; they also showed that serum concentrations of nitric oxide were decreased. It has also been suggested that intravenous morphine increases release of NO from spinal cord by α - adrenergic and cholinergic mechanism (Xu, et al., 1997). Another possible mechanism for antihypertensive effects of heroin may be associated with sodium homeostasis, because there is now well established that sodium ions has a major role for depolarizing membranes, hence producing vasoconstriction, sympathetic activation and hypertension (Barrett, et al., 2010). Although, little is known about the effect of diacetylmorphine on serum sodium, but according to the present result shown in Table II, serum urea as indicator for renal functions was significantly elevated and this is may be due its enhancement of kidney injury (Dettmeyer, et al., 2005) reporting that heroin associated with nephropathy. Although, recent studies observed that heroin significantly increase creatinine clearance (Javadian, et al., 2013). The present results also showed that diacetylmorphine

could affect liver tissues. It markedly elevated serum total bilirubin (Table II). Researches on the effects of diacetylmorphine in renal diseases are also very limited. Morphine-induced renal function in terms of serum urea and creatinine level was reported by (Sumathi, Niranjali and Devaraj, 2009).

Interestingly, and for the first time, we found that diacetylmorphine administration caused a significant elevation in serum MCP-1 levels. It is a potent chemoattractant, which has ability to promote monocyte recruitment as well as activates macrophages and monocytes. (Fuentes, et al., 1995). However little are known about the relation of diacetylmorphine and immunomodulation, although the present finding of MCP-1 elevation (Fig. 4) supports this modulation of immunity. According to our knowledge, this is the first study shows the beneficial effects of diacetylmorphine in immunomodulation through MCP-1 elevation. However, it has been postulated that μ -Opioids are capable of altering inflammatory response and the release of cytokines (Wetzel, et al., 2000). Also (Hatsukari, et al., 2005) reported that morphine-induced modulation of macrophage acts as immunosuppressive due to the requirement of macrophage recruitment. As shown in Table I, heroin administered rats reduced serum T3 and T4 significantly. The rational reason for these reductions may be through thyroids stimulating hormone (TSH) inhibition (Moshtaghi-Kashanian, et al., 2005). However, further studies need to explain the exact mechanism by which heroin reduces thyroid hormones.

V. CONCLUSION

The results suggested that heroin may have beneficial effects in modulating BP, thyroid hormones and immune system, but it also alters liver and kidney functions, the results also suggest that the hypotensive effects of heroin may be returned to its nitric oxide and potassium modulation. For the first time, the present results recorded that heroin could affect immune system through macrophage stimulation to release MCP-1 into the blood. As well as heroin affects cardiac and liver functions via increasing troponin-T and bilirubin levels.

REFERENCES

- Barrett, K.E., Barman, S.M., Boitano, S. and Brooks, H.L., 2010. *Ganong's review of medical physiology*. 23rd ed. Lange Basic Science
- Bhoir, K.K., Suryawanshi, S.A. and Pandey, A.K., 2009. Effects of sub-lethal heroin administration on thyroid stimulating hormone (TSH), thyroid hormones (T3, T4) and thyroid gland of *Mus norvegicus*. *J Environ Biol*, 30(6), pp.989-94.
- Chang, L.R., Lin, Y.H., Kuo, T.B., Ho, Y.C., Chen, S.H., Wu Chang, H.C., Liu, C.M. and Yang, C.C., 2012. Cardiac autonomic modulation during methadone therapy among heroin users: a pilot study. *Prog Neuropsychopharmacol Biol Psychiatry*, 37(1), pp.188-193.
- Cunningham, E.E., Venuto, R.C. and Zielesny, M.A., 1984. Adulterants in heroin/cocaine: implications concerning heroin-associated nephropathy. *Drug Alcohol Depend*, 14(1), pp.19-22.
- Dettmeyer, R.B., Preuss, J., Wollersen, H. and Madea, B., 2005. Heroin-associated nephropathy. *Expert Opin Drug Saf* 4(1), pp.19-28.

- Fonarow, G.C., 2002. Pharmacologic therapies for acutely decompensated heart failure. *Rev Cardiovasc Med*, 3(4), pp.18-27.
- Fuentes, M.E., Durham, S.K., Swerdel, M.R., Lewin, A.C., Barton, D.S., Megill, J.R., Bravo, R. and Lira, S.A., 1995. Controlled recruitment of monocytes and macrophages to specific organs through transgenic expression of monocyte chemoattractant protein-1. *J Immunol*, 155(12), pp.5769-5776.
- Habibey, R., Ajami, M., Ebrahimi, S.A., Hesami, A., Babakoochi, S. and Pazoki-Toroudi, H., 2010. Nitric oxide and renal protection in morphine-dependent rats. *Free Radic Biol Med*, 49(6), pp.1109-1118.
- Hatsukari, I., Hitosugi, N., Dinda, A., R. Maddula, R., Tan, R. and Singhal, P.C., 2005. Morphine modulates monocyte-macrophage conversion phase: implications in obstructive nephropathy. *Journal of Leukocyte Biology*, 78, pp.1-10.
- Javadian, P., Salமான, B., Javadi-Paydar, M. Shamsheersaz, A.A., Ejtemaei Mehr, S., Gharedaghi, M.H. and Dehpour, A.R., 2013. Effect of morphine on the reduced uteroplacental perfusion model of pre-eclampsia in rats. *Eur J Obstet Gynecol Reprod Biol*, 168(2), pp.161-6.
- Li, K., He, H.T., Li, H.M., Liu, J.K., Fu, H.Y. and Hong, M., 2011. Heroin affects purine nucleotides metabolism in rat brain. *Neurochem Int*, 59(8), pp.1104-1108.
- Liu, C., Dai, R., Yu, R. and Xu, J., 2011. Morphine preconditioning, cardioprotection and left ventricular remodelling in rabbits. *Acta Cardiol*, 66(3), pp.341-348.
- Mori, T., Nishikawa, K., Terai, T., Yukioka, H. and Asada, A., 1998. The effects of epidural morphine on cardiac and renal sympathetic nerve activity in alpha-chloralose-anesthetized cats. *Anesthesiology*, 88(6), pp.1558-1565.
- Moshlaghi-Kashanian, G.R., Esmaeeli, F. and Dabiri, S., 2005. Enhanced prolactin levels in opium smokers. *Addict Biol*, 10(4), pp.345-349.
- Newby, N.C., Gamperl, A.K. and Stevens, E.D., 2007. Cardiorespiratory effects and efficacy of morphine sulfate in winter flounder (*Pseudopleuronectes americanus*). *Am J Vet Res*, 68(6), pp.592-597.
- Rezazadeh, H., Hosseini Kahnouei, M., Hassanshahi, G., Allahtavakoli, M., Shamsizadeh, A., Roohbakhsh, A., Fatemi, I., Zarisfi, M. and Pourshanazari, A.A., 2014. Regulatory effects of chronic low-dose morphine on nitric oxide level along with baroreflex sensitivity in two-kidney one-clip hypertensive rats. *Iran J Kidney Dis*, 8(3), pp.194-200.
- Sumathi, T. and Niranjali Devaraj, S., 2009. Effect of Bacopa monniera on liver and kidney toxicity in chronic use of opioids. *Phytomedicine*, 16(10), pp.897-903.
- Szabo, I., Rojavin, M., Bussiere, J.L., Eisenstein, T.K., Adler, M.W. and Rogers, T.J., 1993. Suppression of peritoneal macrophage phagocytosis of *Candida albicans* by opioids. *J Pharmacol Exp Ther*, 267(2), pp.703-706.
- Wetzel, M.A., Steele, A.D., Eisenstein, T.K., Adler, M.W., Henderson, E.E. and Rogers, T.J., 2000. Mu-opioid induction of monocyte chemoattractant protein-1, RANTES, and IFN-gamma-inducible protein-10 expression in human peripheral blood mononuclear cells. *J Immunol*, 165(11), pp.6519-6524.
- Xu, Z., Tong, C., Pan, H.L., Cerda S.E. and Eisenach, J.C., 1997. Intravenous morphine increases release of nitric oxide from spinal cord by an alpha-adrenergic and cholinergic mechanism. *J Neurophysiol*, 78(4), pp.2072-2078.

General Information

Aro's Mission: Aro seeks to publish those papers that are most influential in their fields or across fields and that will significantly advance scientific understanding. Selected papers should present novel and broadly important data, syntheses, or concepts. They should merit the recognition by the scientific community and general public provided by publication in Aro, beyond that provided by specialty journals.

We welcome submissions from all fields of natural science and technology, and from any source. We are committed to the prompt evaluation and publication of submitted papers. Aro is published biannually; selected papers are published online ahead of print.

Submission

Manuscripts should be submitted by the correspondent authors of the manuscript via the on-line submission page. Regardless of the source of the word-processing tool, only electronic Word (.doc, .docx, .rtf) files can be submitted on-line. There is no page limit. Only online submissions are accepted to facilitate rapid publication and minimize administrative costs. Submissions by any other one but the authors will not be accepted. The submitting author takes responsibility for the paper during submission and peer review. If for some technical reason submission through the email is not possible, the author can contact aro.journal@koyauniversity.org for support. Before submitting please check Aro's guide to authors thoroughly to avoid any delay in the review and publication process.

Authors are explicitly responsible for the language of their texts. Paper should be submitted in a well written in understandable English. Authors should not expect the editor or editorial board to rewrite their paper. Prior to submission, authors should have their paper proofread by a possible academic native speaker of English.

- Submit the Article with contact Information
- File name should be your article title
- Don't submit your article in multiple journal, we are taking only minimum time for review process. please don't waste our time
- Once the paper is accepted, it can't be withdrawn
- Please follow publication ethics and regulation
- Avoid plagiarism and copied material
- Strictly Follow Aro's Template

Terms of Submission

Papers must be submitted on the understanding that they have not been published elsewhere and are not currently under consideration by another journal or any other publisher. Aro accepts original articles with novel impacts only. Post conference papers are not accepted "as is", however, regular papers on the same topic but with a different title can be submitted. The new paper should contain significant improvements in terms of extended content, analysis, comparisons with popular methods, results, figures, comments, etc. Please do not forget that the publication of the same or similar material in Aro constitutes the grounds for filing of an (auto) plagiarism case.

The submitting author is responsible for ensuring that the article's publication has been approved by all the other co-authors. It is also the authors' responsibility to ensure that the articles emanating from a particular institution are submitted with the approval of the necessary institution. Only an acknowledgement from the editorial office officially establishes the date of receipt. Further correspondence and proofs will be sent to the author(s) before publication unless otherwise indicated. It is a condition of submission of a paper that the authors permit editing of the

paper for readability. All enquiries concerning the publication of accepted papers should be addressed to aro.journal@koyauniversity.org.

Peer Review

All manuscripts are subject to peer review and are expected to meet standards of academic excellence. Submissions will be considered by an editor and “if not rejected right away” by peer-reviewers, whose identities will remain anonymous to the authors.

Guide to Author

We welcome submissions from all fields of science and from any source. We are committed to the prompt evaluation and publication of submitted papers. Selected papers are published online ahead of print. Authors are encouraged to read the instructions below before submitting their manuscripts. This section arranged into an overview speedy guidelines below and more detailed at the bottom section of this page

Manuscript Preparation

Submitting your manuscript will be in two stages namely before final acceptance and after.

Stage one:

At the first stage manuscript needs to be prepared electronically and submitted online via the online submission page in a Word (.doc, .docx, .rtf) format of one column double-spaced page, Times New Roman font type, and 12 p font size. A pdf version of the submitted manuscript should be submitted too. All authors' names, affiliations, e-mail addresses, and mobile phone numbers should be typed on a cover page, indicating the correspondent author.

Stage two:

- File type: MS-Word version 2003 or later.
- Format: The preferred format of the manuscript two-column template with figures and captions included in the text. This template can be downloaded via the following link. Please follow instructions given in the template; <http://aro.koyauniversity.org/about/submissions#onlineSubmissions>
- Text: All text is in Times New Roman font. The main text is 10-point, abstract is 9-point font and tables, references and captions are 8-point font.
- Figures: Figures should be easily viewed on a computer screen.

Units of Measurement

Units of measurement should be presented simply and concisely using System International (SI) units.

Title and Authorship Information

The following information should be included;

- Paper title.
- Full author names.
- Affiliation.
- Email addresses.

Abstract

The manuscript should contain an abstract. The abstract should be self-contained and citation-free and should not exceed 200 words.

Introduction

This section should be succinct, with no subheadings.

Materials and Methods

This part should contain sufficient detail so that all procedures can be repeated. It can be divided into subsections if several methods are described.

Results and Discussion

This section may each be divided by subheadings or may be combined.

Conclusions

This should clearly explain the main conclusions of the work highlighting its importance and relevance.

Acknowledgements

All acknowledgements (if any) should be included at the very end of the paper before the references and may include supporting grants, presentations, and so forth.

References

References must be included in the manuscript and authors are responsible for the accuracy of references. Manuscripts without them will be returned. Aro is following Harvard System of Referencing. (Learn how to import and use Harvard Styling in your Microsoft Office by following this link:

<http://bibword.codeplex.com/releases/view/15852>)

Preparation of Figures

Upon submission of an article, authors are supposed to include all figures and tables in the PDF file of the manuscript. Figures and tables should be embedded in the manuscript. Figures should be supplied in either vector art formats (Illustrator, EPS, WMF, FreeHand, CorelDraw, PowerPoint, Excel, etc.) or bitmap formats (Photoshop, TIFF, GIF, JPEG, etc.). Bitmap images should be of 300 dpi resolution at least unless the resolution is intentionally set to a lower level for scientific reasons. If a bitmap image has labels, the image and labels should be embedded in separate layers.

Preparation of Tables

Tables should be cited consecutively in the text. Every table must have a descriptive title and if numerical measurements are given, the units should be included in the column heading. Vertical rules should not be used.

Copyright

Open Access authors retain the copyrights of their papers, and all open access articles are distributed under the terms of the Creative Commons Attribution License, which permits unrestricted use, distribution and reproduction in any medium, provided that the original work is properly cited.

The use of general descriptive names, trade names, trademarks, and so forth in this publication, even if not specifically identified, does not imply that these names are not protected by the relevant laws and regulations.

While the advice and information in this journal are believed to be true and accurate on the date of its going to press, neither the authors, the editors, nor the publisher can accept any legal responsibility for any errors or omissions that may be made. The publisher makes no warranty, express or implied, with respect to the material contained herein.

ARO Reviewer/Associate Editor Application Form

Aro is a scientific journal of Koya University (p-ISSN: 2410-9355, e-ISSN: 2307-549X) which aims to offer a novel contribution to the study of Science. The purpose of Aro is twofold: first, it will aim to become an ongoing forum for debate and discussion across the sciences and Engineering. We hope to advance our problem solving capacity and deepen our knowledge regarding a comprehensive range of collective actions. Second, Aro accepts the challenges brought about by multidisciplinary scientific areas and aspires to expand the community of academics who are able to learn from and help to produce advances in a variety of different disciplines.

The Journal is seeking reviewers who can provide constructive analysis of papers thus enhancing overall reputation of the Journal. If any expert is interested in participating of the review process, we highly encourage you to sign up as a reviewer for our Journal and help us improve our presence in domain of your expertise. Appropriate selection of reviewers who have expertise and interest in the domain relevant to each manuscript are essential elements that ensure a timely, productive peer review process. We require proficiency in English.

How to apply

To apply for becoming a reviewer of Aro, please submit the application form by following the link:

<http://aro.koyauniversity.org/user/register>

To apply for becoming a member of the Editorial Board of Aro, please submit the application form by following the link: <http://aro.koyauniversity.org/pages/view/AEB>

Both Associate Editor and Reviewers should specify their areas of research and expertise. Applicants must have a doctorate (or an equivalent degree), and if Master degree they need to have significant publishing experience. Please note that;

- You will need to write your full official name.
- Please provide an email which reflects your official name, such as nameOne.NameTwo@... , or your institute's official email.
- All data need to be written in English.

Note: For more information, kindly visit the following websites:

1. aro.koyauniversity.org.
2. <http://libweb.anglia.ac.uk/referencing/harvard.htm>.
3. <http://bibword.codeplex.com/releases/view/15852>.

Koya University is a young university established in 2003 and it is located in the city of Koya (Koysinjaq), short distance to the East of regional capital city of Erbil (Arbil, Hewlér) in Kurdistan Region of Iraq. It is on the foothills of beautiful high mountain. Its campus has been carefully laid out to embrace the beautiful mountainous nature. The Koya University has a faculty systems which enhance the interactions between similar academic fields. Today the University has 4 faculties -Engineering, Sciences and Health, Humanities and Social Sciences, Education and a School of Medicine which consist of 25 departments in different fields, such as Petroleum Engineering, Geotechnical Engineering, Physics, Clinical Psychology, Social Science and Medical Microbiology as well as Sport Education.

Aro is a scientific journal published by the Koya University. Aro is a journal of original scientific research, global news, and commentary. The Aro Scientific Journal is a peer-reviewed, open access journal that publishes original research articles as well as review articles in all areas of Natural Science and Technology. Aro has been accepted for indexing in the Emerging Sources Citation Index (ESCI), a new edition of Web of Science™ as of Feb 2016.



ARO the Scientific Journal Office
Koya University Park
Danielle Mitterrand Boulevard
Koya KOY45
Kurdistan Region - F.R. Iraq

ISSN: 2410-9355 (print version),
ISSN: 2307-549X (electronic version), DOI: 10.14500/2307-549X